THESIS

EVALUATING FISH PASSAGE AT WHITEWATER PARKS USING A SPATIALLY

EXPLICIT 2D HYDRAULIC MODELING APPROACH

Submitted by

Travis L. Hardee

Department of Civil and Environmental Engineering

In partial fulfillment of the requirements

For the Degree of Master of Science

Colorado State University

Fort Collins, Colorado

Fall 2017

Master's Committee:

    Advisor: Peter A. Nelson

    Brian P. Bledsoe
    Christopher A. Myrick

ABSTRACT

EVALUATING FISH PASSAGE AT WHITEWATER PARKS USING A SPATIALLY

EXPLICIT 2D HYDRAULIC MODELING APPROACH

In-stream whitewater parks (WWPs) are increasingly popular recreational amenities that typically create waves by constricting flow through a chute to increase velocities and form a hydraulic jump. However, the hydraulic conditions these structures create can limit longitudinal habitat connectivity and potentially inhibit upstream fish migration. Recent work has shown that three-dimensional (3D) hydraulic models of flow over WWP structures can be used to accurately predict fish passage rates. Here, I explore the extent to which these methods can be extended to two-dimensional (2D) hydraulic models, which are much simpler and less computationally expensive and data-intensive than 3D models. This study uses a 2D model to calculate flows across several different WWP structures on North St. Vrain Creek at Lyons, Colorado. Potential fish swimming paths are extracted from the model results and evaluated for depth and velocity criteria for fish passage, ultimately yielding for each WWP structure, the fraction of potential passable flow paths for a given discharge. These results are paired with fish movement observations, and logistic regression is used to determine hydraulic variables that significantly contribute to passage success. In general, the 2D model predicts smaller fractions of impassable fish swimming paths than the 3D model. However, the 2D model achieves prediction accuracies greater than 82% for all WWP structures combined, with prediction accuracies at individual WWP structures of 85 to 92%, which equal or exceed the accuracy of the 3D model. These results suggest that 2D flow modeling can be used to evaluate complex flow at WWPs at scales relevant to upstream fish movement.

The 2D methods were also applied to new WWP structures to demonstrate the transferability of the methods and to analyze specific design features in terms of fish passage. The WWP structure design features included in this analysis are: chute slope, low flow fish channel, and sidewall terracing. Results showing the estimated fraction of passable flow paths and passable widths provided insight into the effects these design features have on fish passage. The results show that chute slope is an important factor in reducing the velocity barrier within the chute at low discharges. The inclusion of a low flow fish channel can potentially increase the number of upstream swimming paths available to a fish, especially at low discharges. Sidewall terracing can be used to alleviate the channelizing of flow and can be used to facilitate fish passage at larger discharges. Overall, these methods should be applicable to evaluating fish passage at other WWPs and other in-stream structures.

PREFACE

This thesis is organized as three chapters, each initially written as standalone documents. Chapter 1 compares 2D versus 3D methodology for predicting fish passage on three former WWP structures at Lyons, Colorado. The devastating floods along the Front Range of Colorado in September 2013 destroyed these former WWP structures. The structures were redesigned and construction on these new WWP structures was completed in 2016. Chapter 2 evaluates these new WWP structure designs at Lyons, Colorado using the methodology shown to be effective in Chapter 1. Chapter 3 is a user guide designed to aid practitioners through the process of evaluating WWP structures using the methodology from Chapters 1 and 2.

TABLE OF CONTENTS

CHAPTER 1: EVALUATION OF FISH PASSAGE AT WHITEWATER PARKS USING 2D AND 3D HYDRAULIC MODELING

1.1 Introduction

Whitewater parks (WWPs) are becoming increasingly popular recreational amenities installed in channels across Colorado and the United States. WWP structures are typically designed to create a wave by constricting the flow field to create shallow, high velocity conditions which induce a hydraulic jump. Such hydraulic conditions can potentially limit longitudinal habitat connectivity for aquatic organisms and exhibit lower species richness (Perkin and Gido, 2012). Lotic fishes rely on longitudinal connectivity in rivers to access a diverse range of habitats for feeding, refuge from harsh environmental conditions, and reproduction (Fausch et al., 2002; Poff et al., 1997; Schlosser and Angermeier, 1995).

Potential factors affecting the ability of fish to successfully move upstream past a WWP structure are fish swimming ability and the hydraulic conditions through the WWP structure. Such factors include flow depth (Dane, 1978), burst swimming speed (Castro-Santos et al., 2013; Haro et al., 2004; Peake et al., 1997), jumping ability (Brandt et al., 2005; Kondratieff and Myrick, 2006), and turbulence (Liao, 2007). Turbulence can both enhance fish swimming ability (Haro et al., 2004; Hinch and Rand, 2000; Lacey et al., 2012) and reduce swimming ability depending on the spatial and temporal scales of turbulent eddies (Lupandin, 2005; H. M. Tritico and Cotel, 2010). Typically, efforts to examine the effects of fish response and swimming ability to hydraulic conditions are limited by spatial scales from point measurements or constrained to laboratory settings. Similarly, the scales at which hydraulic conditions are analyzed have been shown to play a role in predicting the hydraulic conditions relevant to fish (Tullos et al., 2016). It

is important to analyze hydraulic conditions at scales relevant to fish movement and behavior (Williams et al., 2012).

Methods for evaluating fish passage at in-stream hydraulic structures (Kemp and O'Hanley, 2010) have already been developed. However, developing a tool for assessing impacts of in-stream structures prior to implementation is necessary for future projects. Recently, Kolden et al. (2016) showed that using 3D computational fluid dynamic (CFD) models at WWP structures can resolve complex hydrodynamics at spatial scales relevant to fish. Stephens et al. (2015), herein referred to as the "3D study," furthered the use of 3D CFD models by applying a spatially explicit analysis method to accurately predict fish passage success at the same WWP structures (upwards of 80% prediction accuracy).

However, 3D CFD models are computationally costly and thus are limited to small spatial and temporal scales. Depth-averaged 2D CFD models entail lower computational costs and there is myriad of free, open-source options available. 2D CFD models have been used extensively to assess habitat quality (Boavida et al., 2013; Branco et al., 2013; Lee et al., 2010; Waddle, 2010) and evaluate streamflow requirements for fish passage (Bonetti et al., 2016; Cowan et al., 2017; Grantham, 2013; Holmes et al., 2016; Reinfelds et al., 2010). Recently, Ryan (2015) mirrored the highly effective approach used in the 3D study by applying a 2D CFD model (River2D) and was able to show that a 2D approach to predicting fish passage is feasible. This led to the impetus of the present study to analyze all three WWP structures from the 3D study and improve upon the methods outlined in Ryan's (2015) analysis (Appendix A). Here I use an open-source, industry standard, 2D CFD model, NAYS2DH (Nelson et al., 2016; Takebayashi and Shimizu, 2014) to predict the hydraulic conditions at three WWP structures on North St. Vrain Creek in Lyons, Colorado. These hydraulic model results were evaluated by mirroring the highly

effective, spatially explicit approach (outlined in Appendix B) and obtaining the topographic and fish movement dataset used in the 3D study. I compare the predictive assessment ability of 2D versus 3D analyses to determine the feasibility of a simpler, more cost- and time-effective 2D approach.

1.2 Methods

1.2.1 Study Site

The WWP analyzed in this study was constructed in 2003 along an approximately 400 m section on the North St. Vrain Creek at Meadow Park in Lyons, Colorado, with 9 total structures. An extreme flood event in September 2013 destroyed the WWP used in this study and it has since been rebuilt. The North St. Vrain Creek drains approximately 310 square km upstream of the site and discharges east from the headwaters in the Rocky Mountains. The streamflow regime is snowmelt dominated with peak discharges in late May to early June, however monsoon events are geomorphically effective at this elevation. Colorado Division of Water Resources streamflow gage sites are located approximately 12 km upstream of the study site, below Button Rock (Ralph Price) Reservoir (NSVBBRCO) and on St. Vrain Creek approximately 300 m downstream of the confluence with the South St. Vrain Creek (SVCLYOCO). Therefore, to obtain accurate discharge estimates at the WWP, a local stage-discharge rating curve was developed (Fox et al., 2016).

Three of the nine structures were analyzed; each varied slightly in design specifications and thus contributed to distinct hydraulic conditions. WWP1, the downstream-most structure exhibited a drop-type design which consisted of large boulders creating a steep, short drop with the length of the chute of approximately 3 m. WWP2 and WWP3, the middle and upstream structures were designed with a long chute of approximately 5 m in length.

1.2.2 Fish Movement Data

Fish movement observations for a 14-month period between October 2011 and December 2012 were obtained from Fox et al. (2016). This study PIT-tagged and released 1639 fish of four species: brown trout (*Salmo trutta*), rainbow trout (wild *Oncorhynchus mykiss* and hatchery Hofer x Harrison strain), longnose dace (*Rhinichthys cataractae*) and longnose sucker (*Catostomus catostomus)*. Upstream movements were monitored using antenna arrays installed upstream and downstream of each WWP structure. There were insufficient movements of longnose dace and longnose suckers recorded, so the movement analysis focused on 536 brown trout and rainbow trout. Fish movement observations recorded the estimated discharge at which the movement occurred. The total lengths of the PIT-tagged fish ranged from 114 mm to 435 mm with a mean of 187 mm; fish lengths were grouped into 13 size classes from 100-124 mm to 400 mm and longer.

1.2.3 2D Hydraulic Modeling

Topographic data and field calibration measurements were obtained prior to the 3D modeling from Kolden et al. (2016). Topographic point data consisted of stereolithographic files of an approximately 50-meter reach surrounding each WWP structure. The 3D study identified an area of interest encompassing the main chute, which defined the region most critical to fish passage at each WWP structure. This area was defined by analyzing the Froude number calculated in the 3D model. Hydraulic modeling focused on the 50-m reach, and subsequent analyses were reduced to the area of interest.

Within the International River Interface Cooperative v2.3.9.6034 (iRIC) graphical user interface software package, I selected the NAYS2DH solver to develop a depth-averaged, hydrodynamic model of each WWP structure (Takebayashi and Shimizu, 2014). NAYS2DH solves the depth-

averaged equations of conservation of fluid mass and momentum in a general coordinate system. The cubic interpolated polynomial (CIP) is a high-order finite differencing method that was used to increase local precision, especially at areas of local unsteadiness and flow separation. While NAYS2DH also has morphodynamics capabilities, this feature was disabled for this study. Steady flow was assumed and four discharges, reflecting conditions during which most of fish movements occurred, were modeled (0.42, 0.85, 1.70, and 2.83 cms). A rectangular computational grid was automatically generated in iRIC and the overall mesh size was a uniform 0.05 m. Boundary conditions for upstream (discharge) and downstream (water surface elevation) were based on the previous 3D modeling (Kolden et al., 2016). Turbulence was modeled with the "zero-equation model": $v_t = \kappa/6\ A\ u_*h + B$, where v_t is the eddy viscosity, u_* is the shear velocity, h is the flow depth, κ is von Karman's constant, and A and B are user-defined coefficients, here set to the default values 1 and 0, respectively. Bed roughness is set using Manning's roughness coefficient (n) and friction along the bed is calculated using a coefficient of bed shear force, C_f, which accounts for varying depth as

$$C_f = \frac{gn^2}{h^{\frac{1}{3}}}$$

where h is depth and g is acceleration due to gravity.

Model calibration was evaluated for high and low discharges using measured water surface elevations (WSE) and depth-averaged point velocities. These values had been measured during the 3D study. The bed resistance (Manning n) was used to calibrate each simulation. For each simulation, the root mean squared (RSME) and mean absolute error (MAE) for depth and velocity were minimized to develop the most accurate model.

1.2.4   Streamline Development

To create a spatially explicit method for evaluating the flow field in a manner relevant to upstream fish movement, I generated streamlines using the modeled velocity vector field. Each streamline can be considered a potential flow path that a fish may follow in order to successfully swim upstream past a WWP structure. Hydraulic modeling results for each WWP structure were exported as unstructured grid files (.VTK) and imported into open-source data analysis and visualization software ParaView (Ayachit et al., 2015). Using the "Stream Tracer" filter in ParaView, two high-definition line sources (minimum 1000 seed points) were created – one upstream and one downstream of the area of interest. Streamlines were generated from each seed point towards the area of interest by integrating the velocity vector field via an adaptive Runge-Kutta method.

The points on each streamline were isolated and cropped to include only points within the analysis domain, the region most critical to fish passage which typically includes the upstream crest of the chute the downstream extent of the hydraulic jump, as defined in Stephens et al. (2015) using the Froude number. Complete streamlines are defined as those that cross both upstream and downstream boundaries. Incomplete streamlines are those that did not reach the opposite boundary, either stopping prematurely (velocity approached 0 m/s), recirculating back to the same boundary, or reaching the length limit. Incomplete streamlines that recirculated back to their original boundaries were split at the inflection point to create two separate incomplete streamlines. All incomplete streamlines were connected from the terminal point to the closest point of a complete streamline, provided that the distance between the terminal point and the closest complete streamline did not exceed 0.15 m. This process was conducted iteratively so that a newly connected streamline became a complete streamline to which an incomplete

streamline could be connected. Any incomplete streamlines that remained after this process were removed, so that only complete streamlines were used in this analysis.

1.2.5 Streamline Development

Modeled flow depth and velocity were analyzed at each point along each streamline to estimate the hydraulic conditions a fish would encounter on a given streamline. Streamlines were determined to be passable or impassable by comparing the modeled flow depth and velocity to fish swimming criteria. I computed streamline evaluation variables as the fraction of total streamlines determined to be impassable based on flow depth, velocity, or any combination of the two. The 2D and 3D methods were compared by subtracting the fraction of impassable streamlines for the 3D study from the fraction of impassable streamlines for the 2D study and evaluating the differences.

1.2.5.1 **Flow Depth**

Two minimum flow depth criteria (*MDC*) were used to evaluate each streamline as a potential swimming barrier. The 3D study used a *MDC* of 0.18 m ($MDC_{0.18}$) in their study. However, a preliminary assessment by Ryan (2015) showed that a flow depth of 0.11 m ($MDC_{0.11}$) was physically practical for the study fish population. The minimum depth ratios (*MDR*) were calculated as

$$MDR_{0.11} = \frac{h_{min}}{MDC_{0.11}}\,, \qquad MDR_{0.18} = \frac{h_{min}}{MDC_{0.18}}\,,$$

where h_{min} is the minimum flow depth at any point along a streamline. A streamline was considered impassable if the $MDR \leq 1$. The fractions of impassable streamlines based on $MDR_{0.11}$ and $MDR_{0.18}$ were computed for each simulated discharge.

For flow depth, five equally-spaced cross-sections were plotted within the analysis domain at each WWP structure. The intersections between cross sections and streamlines were then

colored green for intersecting with a passable streamline and yellow for intersecting with an impassable streamline. The distance between intersections of passable streamlines was calculated and considered consecutive if the distance was less than 0.1 m. The distance between all consecutive passable streamlines was summed to determine the passable width across each cross-section.

1.2.5.2 <u>Velocity</u>

The Nays2DH model's output provides water velocities as x-component, y-component. Direction of flow (positive downstream) was assigned by multiplying the velocity magnitude by the direction of the x-velocity component:

$$V = \sqrt{U^2 + V^2}\left(\frac{U}{|U|}\right)$$

For a fish to move upstream past a WWP structure, it must swim faster than the surrounding water velocity. Therefore, the maximum velocity ratio (*MVR*) is given as the ratio of maximum velocity (V_{max}) for each streamline to the burst swimming ability (V_{burst}):

$$MVR = \frac{V_{max}}{V_{burst}}$$

Typically, V_{burst} is calculated as a function of body lengths. Rainbow trout and brown trout have been recorded to reach burst swimming speeds of 10 and 25 body lengths per second (BL/s), respectively (Castro-Santos et al., 2013; Peake et al., 1997). Variability in swimming ability within species is known (Caudill et al., 2007; Williams et al., 2012) therefore using 10 BL/s and 25 BL/s should capture a wide range of swimming abilities for both species in this study. For all fish size classes and discharges, I calculated the fractions of streamlines were

determined to be impassable if the V_{max} exceeded 10 BL/s ($MVR_{10} \geq 1$) or 25 BL/s ($MVR_{25} \geq 1$).

1.2.5.3 <u>Combined Flow Depth and Velocity</u>

A streamline may be considered impassable if either $MDR \leq 1$ or $MVR \geq 1$ anywhere along the streamline. For example, at high discharges large minimum flow depths (suggesting a passable streamline, $MDR \geq 1$) along with high velocities (potentially impassable $MVR \geq 1$) might be observed along a streamline. To account for such conditions or the inverse of such conditions, streamlines were considered impassable streamlines when either $MDR \leq 1$ or $MVR \geq 1$, simultaneously. All four combinations of MDR ($MDR_{0.11}$ and $MDR_{0.18}$) and MVR (MVR_{10} and MVR_{25}) were used to create four additional, combined variables, denoted as: $D_{11}V_{10}$, $D_{11}V_{25}$, $D_{18}V_{10}$, and $D_{18}V_{25}$.

1.2.6 Statistical Analysis

Fish movement observations recorded the location (specific WWP structure), the estimated discharge at which the movement occurred, the length of fish associated with the movement, and whether the movement was successful or unsuccessful. Based on the estimated discharge at which the movement occurred, each fish movement observation was paired with the modeled hydraulic variables. Logistic regression was performed to determine the hydraulic variables that significantly contribute to passage success. Model significance was determined using the chi-square (χ^2) statistic. Stepwise forward and backward regressions, using the Akaike information criterion (AIC) and Bayesian information criterion (BIC), were employed to determine the hydraulic variables to be included in the model. Bivariate fits were examined to determine effects of collinearity, and variables were subsequently chosen manually. Several iterations were performed on all the variables to identify the most parsimonious model. The logistic regression

from the 3D study was updated to include evaluation of the $MDR_{0.11}$ variable which was not included in the original 3D study. Confusion matrices, used to examine performance measures between measured and predicted values, were created to examine fish passage predictive accuracy of various logistic regression models based on hydraulic variables from 2D models.

1.3 Results

1.3.1 2D Hydraulic Modeling

Recirculation zones observed in the field were accurately modeled at locations both upstream and downstream of the WWP structures (Table 1.1, Figure 1.1a, b), suggesting that the model was sufficiently able to model the complex flows at the WWP structures. Modeled depth and velocity are shown using streamlines created in Paraview (Appendix C).

Table 1.1 Summary of validation field measurements and model validation error analysis for the final models at the three WWP structures for low and high flows. Roughness values (Manning *n*) corresponding to final models shown were calibrated to minimize the error.

Struct.	Q (cms)	Validation Field Measurements # of values Depth	Vel.	Validation Error Analysis Depth RMSE (m)	MAE (m)	Vel. RMSE (m/s)	MAE (m/s)	Roughness Values Used (*n*) US	Chute	DS
WWP1	Low (0.42)	15	4	0.029	0.001	0.265	0.251	0.04	0.05	0.1
	High (4.56)	9	NA	0.036	0.025	-	-			
WWP2	Low (0.25)	25	19	0.057	0.048	0.323	0.229	0.07	0.07	0.07
	High (4.87)	15	NA	0.104	0.090	-	-			
WWP3	Low (0.79)	18	14	0.045	0.038	0.187	0.161	0.04	0.04	0.07
	High (4.79)	10	NA	0.054	0.033	-	-			
All	-	-	-	0.086	0.039	0.214	0.205	-	-	-

Comparing modeled to measured WSE illustrates that the 2D hydraulic model accurately represented WSE in the steep, complex flow through the chute of the structure. It also captured the hydraulic jump downstream of the chute (Figure 1.1c). The RMSE and MAE for the modeled depth versus measured depth (Figure 1.1d) were 0.086 m and 0.039 m, respectively. The RMSE and MAE for modeled velocity versus measured velocity were 0.214 and 0.205 m/s, respectively (Figure 1.1e). All velocity measurements were taken during low, shallow flows where
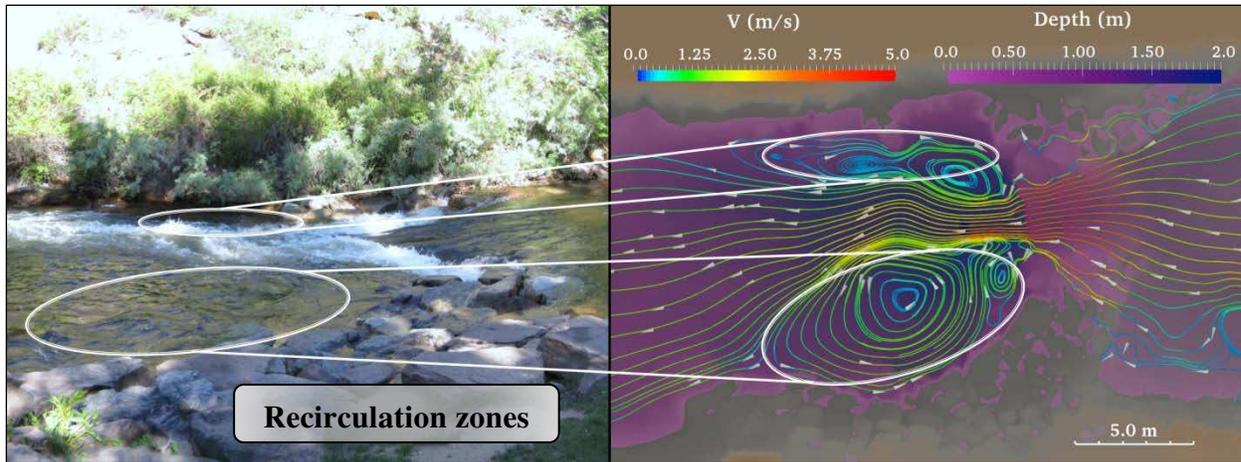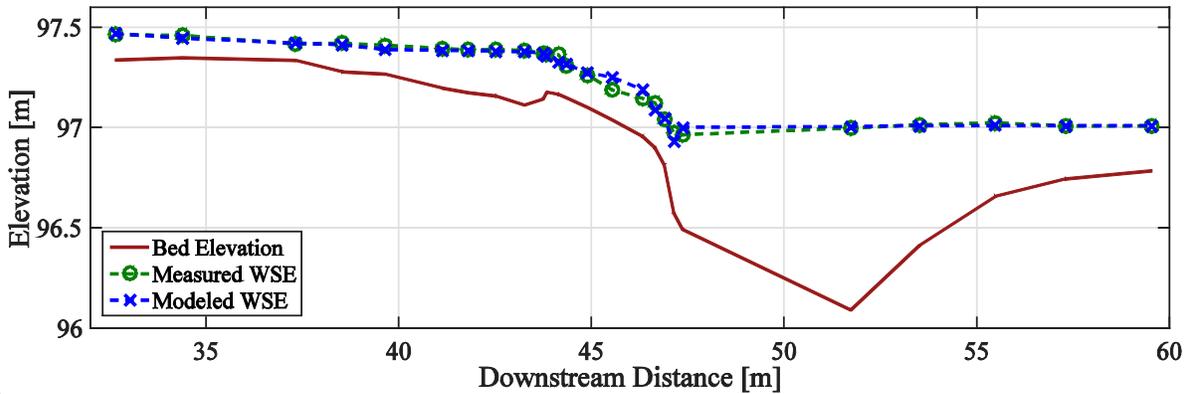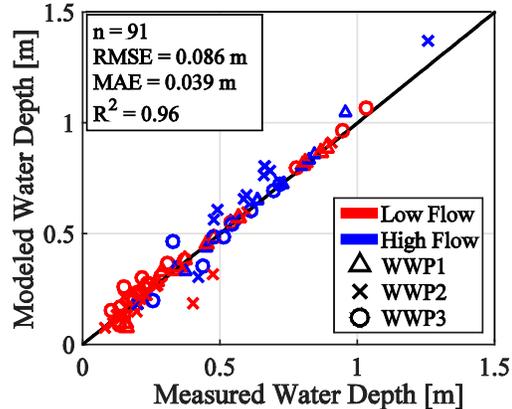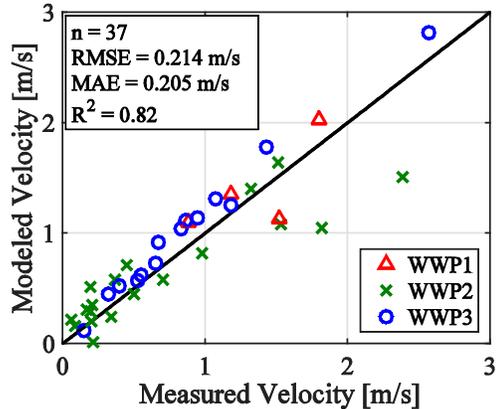
Figure 1.1 Model validation comparison showing recirculation zones in (a) photograph of WWP3 (Q = 4.79 cms) during which validation measurements were obtained. (b) Model results shown in Paraview with streamlines and flow depth shown to illustrate the size and location of major recirculation zones in downstream pool. (c) Example of modeled and measured WSE at WWP1 (Q = 0.42 cms). Modeled versus measured depth (d) and velocity (e) for all structures combined.

measurement errors were likely high due to turbulent variations. Similarly, many velocity

measurements were made in the chute where flow is constricted and the highest velocities were

measured. Further, at WWP2, validation measurements were obtained during very low flow

(0.25 cms), which likely contribute to prediction errors at this location. Overall, both WSE and

velocity validation results show the hydraulic results estimate hydraulic conditions with

acceptable accuracy.

1.3.2 Streamline Development

Streamlines were produced to estimate the hydraulic conditions across a nearly continuous

2D flow field. These streamlines represent all the possible swimming paths a fish may encounter

while attempting to swim upstream past a WWP structure (Figure 1.2). While the initial spacing

of 0.01 m between streamlines created in Paraview remained constant for all simulations, the

number of complete streamlines used in the analysis varied. This variation is a result of complex

hydraulic conditions outside the area of interest and through the process of developing complete

streamlines. An average of approximately 1,600 complete streamlines were created (minimum of

930) at each structure for all four simulated flows.
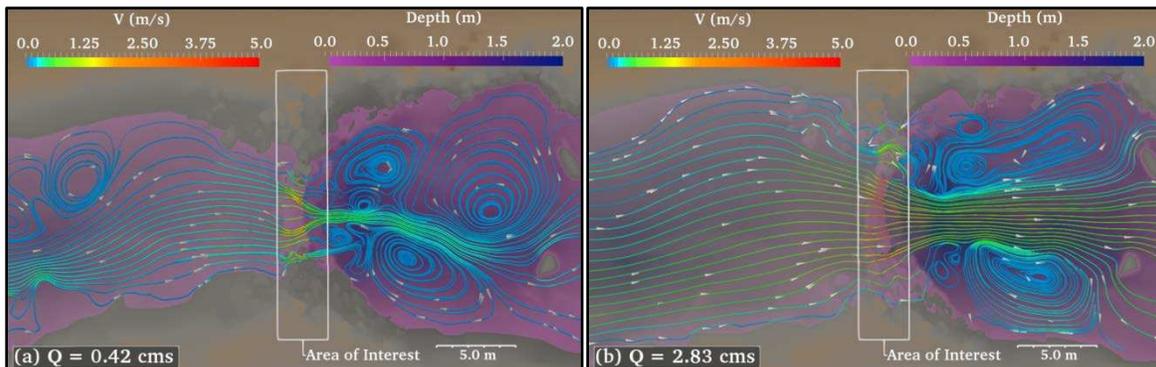
Figure 1.2. Example of streamlines at WWP1 showing modeled velocity at each point along the streamlines at (a) Q = 0.42 cms and (b) Q = 2.83 cms. Streamlines were clipped and analyzed between the white vertical lines representing the area of interest. Note: not all streamlines are shown here to aid in visualization of individual streamlines ($N_{used} \cong 1{,}500$, $N_{shown} = 90$).

1.3.3 Streamline Evaluation Using Hydraulic Variables

Results from the 2D hydraulic modeling were used to create and evaluate potential fish

swimming paths at each structure at the four simulated discharges. As reported in the 3D study,

nuanced differences between each structure were observed. Recall that the streamline evaluation variables are $MDR_{0.11}$, $MDR_{0.18}$, MVR_{10}, MVR_{25}, $D_{11}V_{10}$, $D_{11}V_{25}$, $D_{18}V_{10}$, and $D_{18}V_{25}$. The 2D results were analyzed for each streamline evaluation variable, fish size class and the fractions of impassable streamlines at each structure. These results were compared to those of the 3D study (Appendix D). The differences between the fractions for the 2D study and the 3D study were further analyzed to highlight distinctions between the two methods.

1.3.3.1 <u>Depth</u>

Figure 3 shows the relationship between the fraction of impassable streamlines and the rate of discharge. The red lines represent the 2D model and the blue lines are for the 3D model. For both the 2D and 3D models, the points representing $MDR_{0.11}$ (Minimum Depth Ratio using a depth criterion of 0.11 m) are below or equal the corresponding points for $MDR_{0.18}$. That happens because, in assuming fish need a depth of only 0.11 m versus 0.18 m, there must be fewer impassable routes.

Another feature of Figure 3 is that all the lines remain above 0.0. That is, both models (2D and 3D) predict that at least some of the flowlines will be impassable in every condition studied. Figure 1.3 shows a general downward slope (with exceptions) indicating that the fraction of impassable streamlines tends to decrease as the flow of water increases. Why should there be more potential swimming paths with sufficient depth as flow increases? The main effect that contributes to this is that increased flow is accompanied by an increase in the cross-sectional width of the stream, usually leading to greater width as well as depth.

There are exceptions to the downward trend. For example, at WWP2, the fraction of impassable streamlines increases significantly from 0.58 to 0.69 as discharge increases from 0.85 cms to 1.7 cms, counter to the overall trend observed. One possible explanation looks at the flow in these

structures in more detail. The depth-limited passable width tends to increase as discharge increases (Figure 1.4 and Appendix E). The passable width tends to decrease from XS1 to XS5 (upstream to downstream) while the number of passable streamlines remains constant. This suggests that passable streamlines become denser as the flow is constricted through the chute of the WWP structure. This constriction is a possible explanation for the cases in which the fraction of impassable streamlines increases with an increase in discharge.
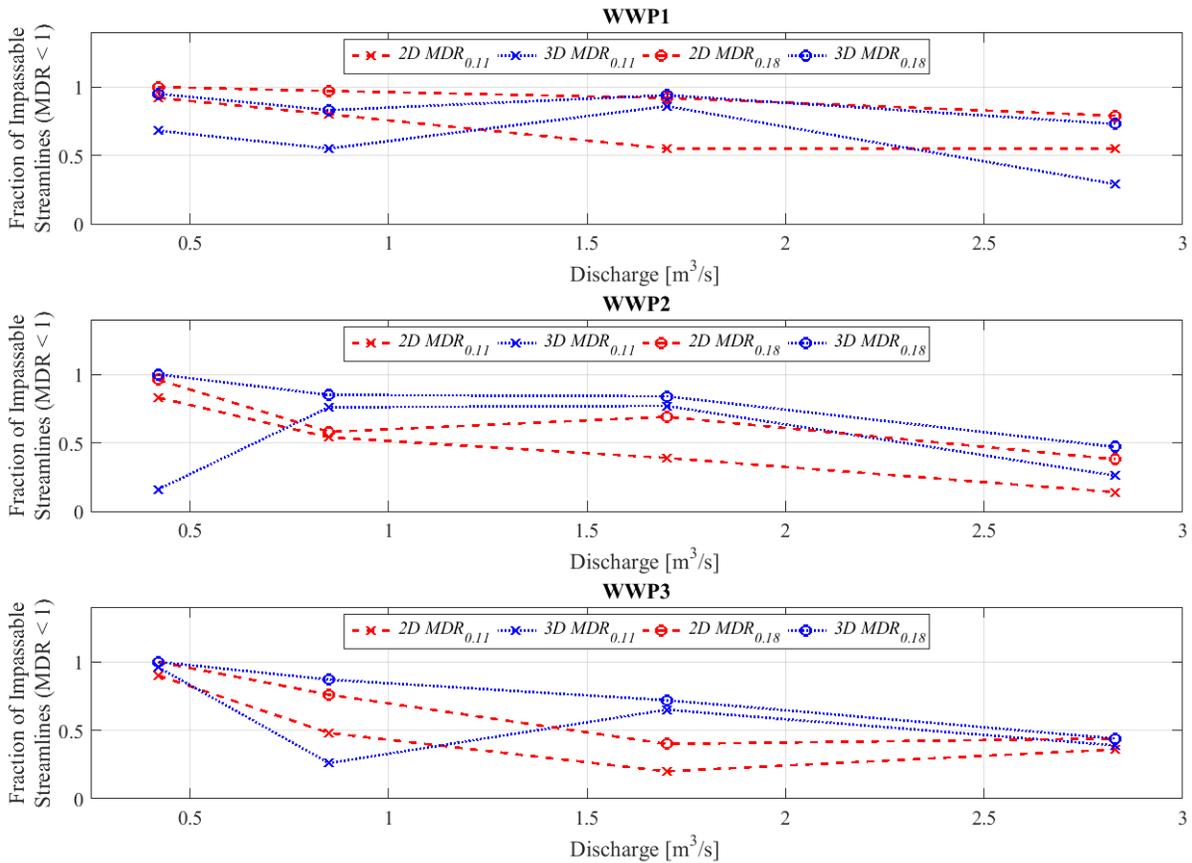
Figure 1.3. Fractions of impassable streamlines based on $MDR_{0.11}$ (values shown as X) and $MDR_{0.18}$ (values shown as circles) for the 2D (dashed, red lines) and 3D (dotted, blue lines) study analyses.

Figure 1.5 shows the distribution of differences between the fractions of impassable streamlines for the 2D model versus the 3D model. The large spread of $MDR_{0.11}$ differences is due to the unusually low 3D values computed at WWP2 for 0.42 cms. The spread in the difference values for $MDR_{0.18}$ shows a smaller maximum positive change than $MDR_{0.11}$. Both

14
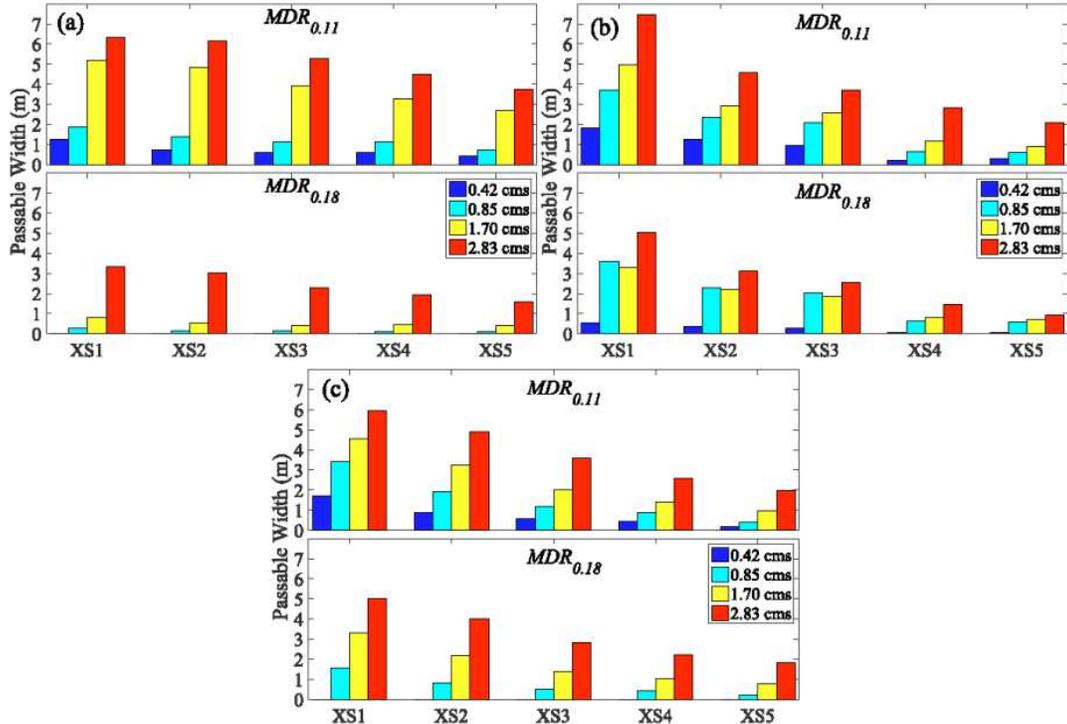
Figure 1.4. Passable widths from 2D study from at upstream extent (XS1) to downstream extent (XS5) of area of interest for all four modeled discharges for (a) WWP1, (b) WWP2, and (c) WWP3.
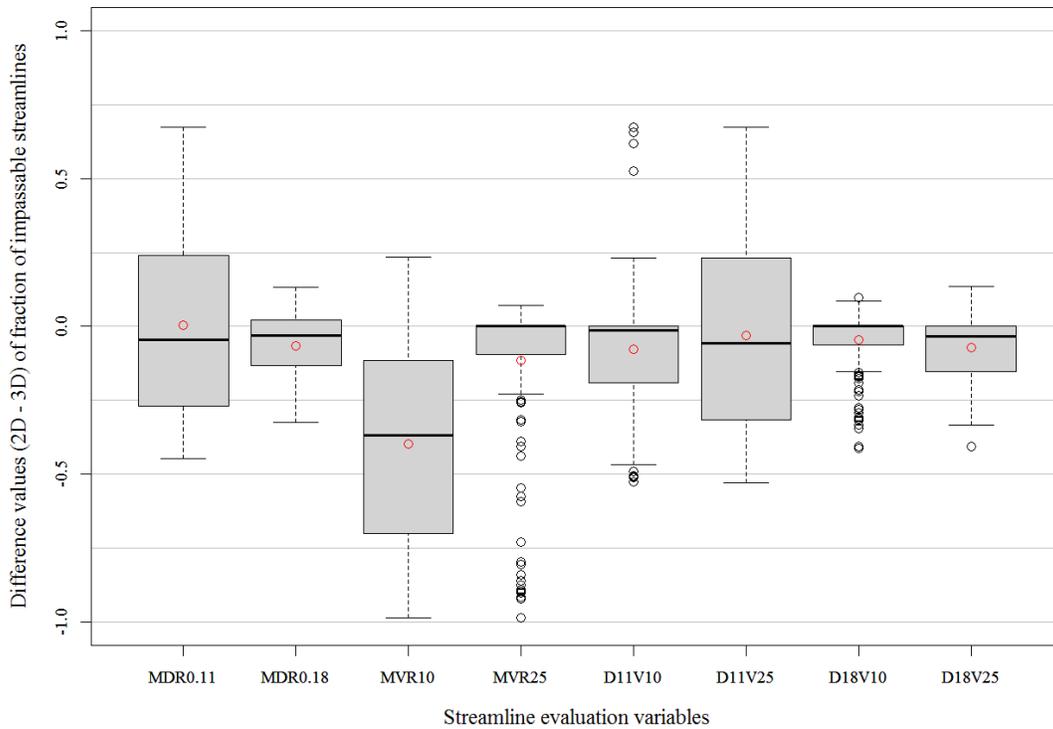
Figure 1.5. Distribution of differences between 2D and 3D fractions of impassable streamlines. The mean difference values are shown as red points. Difference values greater than zero indicate fractions that were larger in the 2D analysis than in the 3D analysis.

15

MDR$_{0.11}$ and *MDR$_{0.18}$* show median difference values of less than zero, suggesting that, in general, the 2D analysis predicts smaller fractions of depth-limited impassable streamlines.

1.3.3.2 <u>Velocity</u>

The velocity analyses are based on the Maximum Velocity Ratio (*MVR*) along each streamline. One expects that the maximum velocity along a streamline would be higher in conditions of higher stream flow. For example, in the 2D study, the fraction of impassable streamlines for *MVR$_{10}$* increases as discharge increases (Table D1 in Appendix D). Also, as expected, the fraction of impassable streamlines decreases with incremental increases in fish size class, since the criterion velocity is measured in fish body lengths per second.

Generally, smaller fractions of streamlines were determined to be impassable based on velocity criteria alone in the 2D study than in the 3D study. This can be seen in Figure 1.5, in which mean differences are below zero for both *MVR$_{10}$* and *MVR$_{25}$*. These results are shown in greater detail in Table D2 (Appendix D). First, consider the results for *MVR$_{10}$*. The 3D model predicts that almost all streamlines are impassable up to the 250 mm fish size class, thus suggesting that all three structures were potentially complete barriers for fish less than 250 mm in length. In contrast, the 2D model predicts a notably smaller fraction of impassable streamlines for almost all fish size classes. Turning now to the *MVR$_{25}$* criterion, both the 2D and the 3D results show relatively small fractions of impassable streamlines. Also for *MVR$_{25}$*, there were many outliers exhibiting difference values markedly smaller than the 3rd quartile (Figure 1.5). Overall, the difference values for both *MVR$_{10}$* and *MVR$_{25}$* criteria suggests that the 2D methods predicted smaller fractions of impassable streamlines than the 3D model.

1.3.3.3 <u>Combined Depth and Velocity</u>

The fraction of streamlines determined impassable due to *MDR* and/or *MVR* shows that depth is often either the dominant factor, or when the $MVR \geq 1$, the *MDR* is also ≤ 1. This is especially true at lower discharges, when flow depths are lowest and for larger fish size classes. The fractions of impassible streamlines using the $D_{11}V_{25}$ and $D_{18}V_{25}$ criteria greatly resemble those using the depth-only criteria MDR_{11} and MDR_{18}, respectively, indicating that depth is the dominant passage limiter in these structures at these flows. This is to be expected since the 2D analysis of MVR_{25} showed very few impassable streamlines. Comparison between the $D_{11}V_{10}$ versus $D_{18}V_{10}$ and $D_{11}V_{25}$ versus $D_{18}V_{25}$ again show that, as the velocity criterion is held constant, increasing the depth criterion results in a greater number of impassable streamlines (Tables D7-D18 in Appendix D).

The majority of difference values between the 2D and 3D analyses for the combined velocity and depth variables (Figure 1.5) are less than or equal to zero, indicating that the 2D model predicts fewer impassable streamlines than the 3D model. The upper range of difference values for $D_{11}V_{10}$ and $D_{11}V_{25}$ tend to reflect the $MDR_{0.11}$ difference values that further illustrate the anomaly at WWP2 (Q = 0.42 cms) described above.

1.3.4 *Statistical Analysis*

I performed an iterative logistic regression analysis to evaluate the significance of single variables ($MDR_{0.11}$, $MDR_{0.18}$, MVR_{10}, and MVR_{25}) separately from combined variables ($D_{11}V_{10}$, $D_{11}V_{25}$, $D_{18}V_{10}$, and $D_{18}V_{25}$) on fish passage success. Final logistic regression models for the updated 3D study (includes $MDR_{0.11}$) are presented as models 1 - 8 and compared to the logistic models from the 2D study, labeled as models 9 – 16 (Table 1.2). As expected, every model shows a decrease in predicted fish passage success for an increase in the fraction of

Table 1.2. Logistic regression analysis from 3D and 2D studies for single variables ($MDR_{0.11}$, $MDR_{0.18}$, MVR_{10}, MVR_{25}) and combined variables ($D_{11}V_{10}$, $D_{11}V_{25}$, $D_{18}V_{10}$, and $D_{18}V_{25}$)

Structure	Logit Model Variables Used	Model #	Predicted logit of (Passage Success) =	Likelihood Ratio Test (*p-value*)	Goodness-of-Fit Test (*p-value*)	Predictor	Predictor *p-value*	odds ratio (e^β)	Prediction Accuracy (%)
3D Study									
All Three	Single	1	$27.69 + (-2.422)* MVR_{10}$ $+ (-5.516)* MVR_{25}$ $+(-28.03)* MDR_{0.18}$	<0.0001	0.1222	MVR_{10} MVR_{25} $MDR_{0.18}$	0.0075 <0.0001 <0.0001	8.9E-02 8.1E-02 6.7E-13	87.5
	Combined	2	$24.67 + (-27.27)* D_{18}V_{25}$	<0.0001	<0.0001	$D_{18}V_{25}$	<0.0001	1.4E-12	87.5
WWP1		3	$31.98 + (-36.32)* MDR_{0.18}$	<0.0001	0.0068	$MDR_{0.18}$	<0.0001	1.7E-16	91.2
WWP2	Single	4	$29.72 + (-4.874)* MVR_{25}$ $+ (-31.74)* MDR_{0.18}$	<0.0001	0.9674	MVR_{25} $MDR_{0.18}$	0.0038 <0.0001	7.6E-03 1.6E-14	88.5
WWP3		5	$26.81 + (-3.248)* MVR_{10}$ $+ (-26.22)* MDR_{0.18}$	<0.0001	0.1389	MVR_{10} $MDR_{0.18}$	<0.0001 <0.0001	3.9E-02 4.1E-12	86.0
WWP1	Combined	6	$45.01 + (-49.73)* D_{18}V_{25}$	<0.0001	<0.0001	$D_{18}V_{25}$	<0.0001	2.5E-22	90.7
WWP2		7	$24.89 + (-27.00)* D_{18}V_{25}$	<0.0001	0.6235	$D_{18}V_{25}$	<0.0001	1.9E-12	87.5
WWP3		8	$20.42 + (-22.61)* D_{18}V_{10}$	<0.0001	0.9513	$D_{18}V_{10}$	<0.0001	1.5E-10	85.7
2D Study									
All Three	Single	9	$5.86 + (-8.75)* MDR_{0.11}$ $+ (30.30)* MVR_{25}$	<0.0001	<0.0001	$MDR_{0.11}$ MVR_{25}	<0.0001 0.011	1.6E-04 7.0E-14	83.3
	Combined	10	$5.64 + (-8.49)* D_{11}V_{25}$	<0.0001	0.84	$D_{11}V_{25}$	<0.0001	2.1E-04	82.7
WWP1		11	$31.88 + (-37.78)* MDR_{0.11}$	<0.0001	0.99	$MDR_{0.11}$	<0.0001	3.9E-17	92.2
WWP2	Single	12	$12.69 + (-16.45)* MDR_{0.11}$ $+ (-28.22)* MVR_{25}$ $+ (-4.35)* MVR_{10}$	<0.0001	0.68	$MDR_{0.11}$ MVR_{25} MVR_{10}	<0.0001 0.018 0.039	1.0E-05 3.8E-02 1.7E-02	89.1
WWP3		13	$15.88 + (-17.62)* MDR_{0.18}$ $+ (-2.65)* MVR_{10}$	<0.0001	0.51	$MDR_{0.18}$ MVR_{10}	<0.0001 0.092	2.2E-08 7.0E-02	85.3
WWP1		14	$31.89 + (-37.79)* D_{11}V_{25}$	<0.0001	0.99	$D_{11}V_{25}$	<0.0001	3.9E-17	92.2
WWP2	Combined	15	$7.88 + (-12.20)* D_{18}V_{25}$	<0.0001	0.21	$D_{18}V_{25}$	<0.0001	5.1E-06	89.1
		15a	$7.87 + (-12.19)* D_{11}V_{25}$	<0.0001	0.21	$D_{11}V_{25}$	<0.0001	5.1E-06	89.1
WWP3		16	$9.75 + (-11.94)* D_{18}V_{25}$	<0.0001	0.95	$D_{18}V_{25}$	<0.0001	6.6E-06	85.7
		16a	$3.98 + (-6.83)* D_{11}V_{25}$	<0.0001	0.65	$D_{11}V_{25}$	<0.0001	1.1E-03	85.7

impassable streamlines. Confusion matrices were recorded for all 2D models (Table 1.3) to show

model prediction accuracy. Overall, models better predicted unsuccessful fish movements

(average ~92% accuracy) compared to successful (average ~72% accuracy).

Table 1.3. Confusion matrices for 2D models showing observed and predicted movement outcomes and associated prediction accuracies

Model #	Observed Movement	Predicted Movement		TN/TP Accuracy (%)	Overall Accuracy (%)
		no pass	pass		
9	no pass	472	86	85%	83%
	pass	23	73	76%	
10	no pass	467	85	85%	83%
	pass	28	74	73%	
11	no pass	142	8	95%	92%
	pass	8	46	85%	
12	no pass	135	7	95%	89%
	pass	14	36	72%	
13	no pass	191	12	94%	85%
	pass	26	29	53%	
14	no pass	142	8	95%	92%
	pass	8	46	85%	
15	no pass	135	7	95%	89%
	pass	14	36	72%	
16	no pass	187	16	92%	86%
	pass	21	34	62%	
Average % Accuracy (true negative)				92%	
Average % Accuracy (true positive)				72%	

All three WWP fish movement observations were combined to determine significant

predictors across all three structures (models 9 and 10). The 2D study shows an overall

predictive accuracy of 83.3% for single variables and 82.7% for combined variables (Table 1.2).

These are slightly lower than the 87.5% predictive accuracy of the 3D study. The most

significant ($p < 0.0001$) single variables for the 2D study are $MDR_{0.11}$ and MVR_{25}, while $D_{11}V_{25}$

is the most significant combined variable. However, the goodness-of-fit test for model 9 ($p <$

0.0001) suggests additional variables would improve the model. The variables that are significant

differ between the 2D and 3D studies for all three structures.

The 2D analysis of individual structures for models 11 – 13 showed a range of statistically significant variables depending on the structure (Table 1.2). At WWP1, the 2D analysis suggests that $MDR_{0.11}$ was the only significant predictor of fish passage and was shown to predict fish passage with an overall prediction accuracy of 92.2%. The 3D study suggested the most significant variable for predicting fish passage was $MDR_{0.18}$; however, the overall predictive accuracy for the 2D study was slightly (0.5%) higher than for the 3D study. The final model for WWP2 using single variables suggests that $MDR_{0.11}$, MVR_{10}, and MVR_{25} are statistically significant with a predictive accuracy of 89.1%. In the 3D model at WWP2, the model suggests only $MDR_{0.18}$ and MVR_{25} are significant and again the 3D model shows slightly lower prediction accuracy (88.5%) than the 2D study. At WWP3, $MDR_{0.18}$ and MVR_{10} were shown to be significant for both the 2D and 3D studies; however, the 2D model was shown to be slightly less accurate (85.3%) than the 3D model (86%).

The 2D analysis of individual WWPs for combined variables ($D_{11}V_{10}$, $D_{11}V_{25}$, $D_{18}V_{10}$, and $D_{18}V_{25}$) suggests the significant predictors are $D_{11}V_{25}$ for WWP1 and $D_{18}V_{25}$ for WWP2 and WWP3. For the 2D study, goodness-of-fit (p > 0.05) suggests that additional variables would not significantly improve the models. The 3D study at WWP1, the goodness-of-fit (p < 0.05) suggests additional variables would improve the model.

In both the 2D and 3D studies, the logistic regression models for WWP1 differ in comparison to those for WWP2 and WWP3. For example, the predictor coefficients for models 15 and 16 (-12.20 and -11.94, respectively) are similar in magnitude to that of model 10 (-8.49), while the predictor coefficient for model 14 (-37.79) is much greater. The predictor for models 15 and 16 are $D_{18}V_{25}$, while the predictor for models 10 and 14 is $D_{11}V_{25}$. For direct comparison between all combined variable models, models 15a and 16a were included, using $D_{11}V_{25}$. The

results in Table 1.2 show that including the variable $D_{11}V_{25}$ in the models for WWP2 and WWP3 only marginally affects model significance statistics and does not affect prediction accuracies. The predictor coefficients for models 15a and 16a (-12.19 and -6.83) are similar in magnitude to model 10 and differ markedly compared to model 14. The logistic regression outcomes suggest WWP1 is unique in comparison to WWP2 and WWP3.

Logistic regression models for individual structures (models 14, 15, and 16) have greater prediction accuracies than the model for all three structures (model 10). Model 10 includes fish movement observations from each structure; 204 observations at WWP 1, 192 observations at WWP2, and 258 observations at WWP3. Prediction accuracies from model 10 were separated for each individual structure and compared to prediction accuracies from models 14, 15a, and 16a. The results (Table 1.4) show an almost 17% decrease in prediction accuracies at WWP1, while only 3% at WWP2 and < 1% at WWP3.

Table 1.4. Prediction accuracies for models 14, 15a, and 16a compared to prediction accuracies for model 10 at the corresponding WWP location.

	WWP1	WWP2	WWP3
Model 10	75.5%	86.5%	85.7%
Model 14	92.2%		
Model 15a		89.1%	
Model 16a			85.7%
Change	16.7%	2.6%	0.04%

1.4 Discussion

The comparison between the streamline evaluations of the 3D study and the 2D study show several interesting distinctions. Overall, the 3D analysis showed higher fractions of streamlines determined to be impassable than the 2D analysis for all the hydraulic variables; this suggests that the 3D analysis may be a more stringent evaluation. This is particularly evident from the smaller fractions of impassable streamlines using MVR_{10} and MVR_{25} criteria in the 2D study compared to 3D study. The depth-averaged velocity method of 2D CFD modeling

21

simplifies complex vertical velocity distributions into a single velocity value; this simplification likely leads to the prediction of fewer passable streamlines when compared to the 3D study.

Logistic regression shows that velocity and depth have a statistically significant influence on fish passage success at WWPs. With a 2D hydraulic model, I was able to predict fish passage success with ~83% accuracy using a single model for all structures. Using different models for each structure raised the accuracy to upwards of 85%. However, the relationship between velocity and depth on fish passage is complex, evidenced by the variety in predictors selected and the predictor coefficients of the final logistic regression models. This may be illustrated by two results. First, the final model for WWP1 is notably different from those of WWP2 and WWP3. Second, the single model for all three structures had substantially lower accuracy at WWP1 than at the other two structures. WWP1 is a steep, drop-type structure as opposed to the sloping, long chute-type structure of both WWP2 and WWP3. It is possible that these different structure types result in different effects of the hydrodynamic variables that I have considered.

This study ignores the complex hydraulic conditions that turbulence may have on upstream fish movement. Turbulent vortex systems have been shown to both aid swimming ability (Haro et al., 2004; Hinch and Rand, 2000; Lacey et al., 2012) and inhibit swimming ability (Lupandin, 2005; H. M. Tritico and Cotel, 2010), making these relationships difficult to quantify on a scale applicable to this spatially explicit approach. Furthermore, the distance a fish must travel upstream and the relative upstream speed (V_{max} minus v_{burst}) at which the fish may able to swim this distance may also be important factors in upstream fish movement. On the North St. Vrain Creek WWP, Stephens et al. (2015) found that measures of turbulence, vorticity, and a combined velocity and distance metric were not significant predictors of fish passage success.

Our results show that 2D modeling using depth and velocity criteria alone can accurately reproduce success or failure of fish passage.

Fish behavior plays a pivotal role in fish passage success and should be included in fishway design (Kemp et al., 2012; Santos et al., 2012). Physical variables that might influence fish behavior relevant to WWPs would include chute length and plunge pool depths for jumping ability (Kondratieff and Myrick, 2006), interstitial space width (Brandt et al., 2005) and spatial variability along potential swimming paths. Developing variables to account for these other factors could increase the accuracy of these methods.

The MVR_{25} streamline evaluation criterion showed almost no impassable streamlines for most fish size classes. By computing a range of values for the streamline evaluation criteria ($MDC_{0.11}$ versus $MDC_{0.18}$ and V_{burst} of 10 BL/s versus 25 BL/s), a diverse range of swimming abilities and flow conditions were captured. This is especially important when considering the variability in fish swimming abilities within species and between hatchery and wild fish (Duthie, 1987). However, distinctions between measuring fish swimming and jumping abilities in BL/s versus absolute speed (cm/s) have been observed. For example, while larger, older fish swim faster and jump farther, their swimming ability in BLs does not continue to increase (Blaxter and Dickson, 1959; Brandt et al., 2005; Kondratieff and Myrick, 2006).

This study focuses on two species: brown trout and rainbow trout. The 2D simplification may not adequately resolve the hydraulic conditions adequately for smaller fish. Applying these methods for swimming performance of smaller fishes or fishes with lesser swimming abilities (Ficke, 2015) may improve these methods for estimating fish passage of different fish species with varying swimming abilities. Additionally, future studies can help develop a more robust set

of fish swimming criteria by applying this method to and refining fish swimming evaluation criteria for a diverse range of species, including native fishes.

Further investigations at different WWP structure types and hydrologic conditions can help refine the results to produce a more robust set of criteria for future WWP projects. For instance, flow depth influenced fish passage significantly in this study, but at larger WWPs with higher discharges, MDR_{11} and MDR_{18} may not provide accurate results. Further, the implications of this study extend beyond just WWPs to include evaluation of engineered fishways of all sizes and designs. Typically, engineered fishways have been assessed using 3D CFD modeling or laboratory measurements, but this study suggests that 2D CFD models may be sufficient; thus, reducing fish passage evaluation durations and costs. While this study focuses on post-implementation effects, these results can also be applied to pre-implementation plans for future design guidance.

1.5   Conclusions

This study mirrored the spatially explicit methodology shown to be successful in Stephens et al. (2015) 3D study by applying a 2D CFD model to predict fish passage at three WWP structures at Lyons, Colorado. This study supports Ryan's (2015) results suggesting that 2D CFD modeling can be used to evaluate complex flow at WWPs at scales relevant to upstream fish movement, and can accurately predict fish passage (83% accuracy). Using a 2D model versus a 3D model reduces computational time and costs. This research can be applied to evaluate existing or proposed WWP structures of similar size and hydrologic regimes. Further research is necessary to apply these methods with fish movement data for fish of lesser swimming abilities, to expand criteria to include fish behavior and turbulence, and to define limitations to the 2D methods at a diverse range of structures and hydrologic regimes.

REFERENCES

Ayachit, U., Bauer, A., Chaudhary, A., DeMarle, D., Geveci, B., Jourdain, S., Lutz, K., Marion, P., Maynard, R., Shetty, N., Yuan, Y., 2015. The ParaView Guide. Kitware. Kitware Inc. doi:10.1017/CBO9781107415324.004

Boavida, I., Santos, J.M., Katopodis, C., Ferreira, M.T., Pinheiro, A., 2013. Uncertainty in predicting the fish-response to two-dimensional habitat modeling using field data. River Res. Appl. 29, 1164–1174. doi:10.1002/rra.2603

Bonetti, R.M., Reinfelds, I. V., Butler, G.L., Walsh, C.T., Broderick, T.J., Chisholm, L.A., 2016. A multi-scale GIS and hydrodynamic modelling approach to fish passage assessment: Clarence and Shoalhaven Rivers, NSW Australia. Geomorphology 260, 79–90. doi:10.1016/j.geomorph.2015.06.015

Branco, P., Boavida, I., Santos, J.M., Pinheiro, A., Ferreira, M.T., 2013. Boulders as building blocks: Improving habitat and river connectivity for stream fish. Ecohydrology 6. doi:10.1002/eco.1290

Brandt, M.M., Holloway, J.P., Myrick, C.A., Kondratieff, M.C., 2005. Effects of waterfall dimensions and light intensity on age-0 Brook Trout jumping performance. Trans. Am. Fish. Soc. 134, 496–502. doi:10.1577/T03-175.1

Castro-Santos, T., Sanz-Ronda, F.J., Ruiz-Legazpi, J., Jonsson, B., 2013. Breaking the speed limit — comparative sprinting performance of brook trout (*Salvelinus fontinalis*) and brown trout (*Salmo trutta*). Can. J. Fish. Aquat. Sci. 70, 280–293. doi:10.1139/cjfas-2012-0186

Caudill, C.C., Daigle, W.R., Keefer, M.L., Boggs, C.T., Jepson, M.A., Burke, B.J., Zabel, R.W., Bjornn, T.C., Peery, C.A., Caudill, C.C., Daigle, W.R., Keefer, M.L., Boggs, C.T., Jepson, M.A., Bjornn, T.C., Peery, C.A., Burke, B.J., Zabel, R.W., 2007. Slow dam passage in adult

Columbia River salmonids associated with unsuccessful migration: delayed negative effects of passage obstacles or condition-dependent mortality? Can. J. Fish Aquat. Sci 64, 979–995. doi:10.1139/F07-065

Cowan, W.R., Rankin, D.E., Gard, M., 2017. Evaluation of Central Valley spring-run Chinook Salmon passage through lower Butte Creek using hydraulic modelling techniques. River Res. Appl. 33, 328–340. doi:10.1002/rra.3098

Dane, B.G., 1978. A review and resolution of fish passage problems at culvert sites in British Columbia. Fisheries and Marine Service, Vancouver.

Duthie, G.G., 1987. Observations of poor swimming performance among hatchery-reared rainbow trout, *Salmo gairdneri*. Environ. Biol. Fishes 18, 309–311. doi:10.1007/BF00004884

Fausch, K.D.., Torgersen, C.E.., Baxter, C.V.., Li, H.W., 2002. Landscapes to Riverscapse: Bridging the Gap between Research and Conservation of Stream Fishes. Bioscience 52, 483–498.

Ficke, A.D., 2015. Mitigation measures for barriers to Great Plains fish migration. Colorado State University, Fort Collins, Colorado.

Fox, B.D., Bledsoe, B.P., Kolden, E., Kondratieff, M.C., Myrick, C.A., 2016. Eco-hydraulic evaluation of a whitewater park as a fish passage barrier. J. Am. Water Resour. Assoc. 52, 420–442. doi:10.1111/1752-1688.12397

Grantham, T.E., 2013. Use of hydraulic modelling to assess passage flow connectivity for salmon in streams. River Res. Appl. 29, 250–267. doi:10.1002/rra.1591

Haro, A., Castro-Santos, T., Noreika, J., Odeh, M., 2004. Swimming performance of upstream migrant fishes in open-channel flow: a new approach to predicting passage through velocity

barriers. Can. J. Fish. Aquat. Sci. 61, 1590–1601. doi:10.1139/f04-093

Hinch, S.G., Rand, P.S., 2000. Optimal swimming speeds and forward-assisted propulsion: energy-conserving behaviours of upriver-migrating adult salmon. Can. J. Fish. Aquat. Sci. 57, 2470–2478. doi:10.1139/f00-238

Holmes, R.W., Rankin, D.E., Ballard, E., Gard, M., 2016. Evaluation of Steelhead passage flows using hydraulic modeling on an unregulated coastal California river. River Res. Appl. 32, 697–710. doi:10.1002/rra.2884

Kemp, P.S., Anderson, J.J., Vowles, A.S., 2012. Quantifying behaviour of migratory fish: Application of signal detection theory to fisheries engineering. Ecol. Eng. 41, 22–31. doi:10.1016/j.ecoleng.2011.12.013

Kemp, P.S., O'Hanley, J.R., 2010. Procedures for evaluating and prioritizing the removal of fish passage barriers: A synthesis. Fish. Manag. Ecol. 17, 297–322. doi:10.1111/j.1365-2400.2010.00751.x

Kolden, E., Fox, B.D., Bledsoe, B.P., Kondratieff, M.C., 2016. Modeling whitewater park hydraulics and fish habitat in Colorado. River Res. Appl. 32, 1116–1127. doi:10.1002/rra.2931

Kondratieff, M.C., Myrick, C. a., 2006. How high can Brook Trout jump? A laboratory evaluation of Brook Trout jumping performance. Trans. Am. Fish. Soc. 135, 361–370. doi:10.1577/T04-210.1

Lacey, J.R.W., Neary, V.S., Liao, J.C., Enders, E.C., Tritico, H.M., 2012. The IPOS framework: linking fish swimming performance in altered flows from laboratory experiments to rivers. River Res. Appl. 28, 429–443. doi:10.1002/rra.1584

Lee, J.H., Kil, J.T., Jeong, S., 2010. Evaluation of physical fish habitat quality enhancement

designs in urban streams using a 2D hydrodynamic model. Ecol. Eng. 36, 1251–1259. doi:10.1016/j.ecoleng.2010.05.004

Liao, J.C., 2007. A review of fish swimming mechanics and behaviour in altered flows. Philos. Trans. R. Soc. Lond. B. Biol. Sci. 362, 1973–1993. doi:10.1098/rstb.2007.2082

Lupandin, A.I., 2005. Effect of flow turbulence on swimming speed of fish. Biol. Bull. 32, 461–466. doi:10.1007/s10525-005-0125-z

Nelson, J.M., Shimizu, Y., Abe, T., Asahi, K., Gamou, M., Inoue, T., Iwasaki, T., Kakinuma, T., Kawamura, S., Kimura, I., Kyuka, T., McDonald, R.R., Nabi, M., Nakatsugawa, M., Simoes, F.R., Takebayashi, H., Watanabe, Y., 2016. The international river interface cooperative: Public domain flow and morphodynamics software for education and applications. Adv. Water Resour. 93, 62–74. doi:10.1016/j.advwatres.2015.09.017

Peake, S., McKinley, R.S., Scruton, D. a, 1997. Swimming performance of various freshwater Newfoundland salmonids relative to habitat selection and fishway design. J. Fish Biol. 51, 710–723. doi:10.1006/jfbi.1997.0475

Perkin, J.S., Gido, K.B., 2012. Fragmentation alters stream fish community structure in dendritic ecological networks. Ecol. Appl. 22, 2176–2187. doi:10.1890/12-0318.1

Poff, N.L., Allan, J.D., Bain, M.B., Karr, J.R., Prestegaard, K.L., Richter, B.D., Sparks, R.E., Stromberg, J.C., 1997. The Natural flow regime. Bioscience 47, 769–784. doi:10.2307/1313099

Reinfelds, I. V., Lincoln-Smith, M., Haeusler, T., Ryan, D., Growns, I., 2010. Hydraulic assessment of environmental flow regimes to facilitate fish passage through natural riffles: Shoalhaven River below Tallowa Dam, New South Wales, Australia. River Res. Appl. 26, 589–604. doi:10.1002/rra.1262

Ryan, E.R., 2015. Effects of hydraulic structures on fish passage: an evaluation of 2d vs 3d hydraulic analysis methods. Colorado State University, Fort Collins, Colorado.

Santos, J.M., Silva, A., Katopodis, C., Pinheiro, P., Pinheiro, A., Bochechas, J., Ferreira, M.T., 2012. Ecohydraulics of pool-type fishways: Getting past the barriers. Ecol. Eng. 48, 38–50. doi:10.1016/j.ecoleng.2011.03.006

Schlosser, I.J., Angermeier, P.L., 1995. Spatial variation in demographic processes of lotic fishes: conceptual models, empirical evidence, and implications for conservation. Am. Fish. Soc. Symp. 17, 392–401.

Stephens, T.A., Bledsoe, B.P., Fox, B.D., Kolden, E., Kondratieff, M.C., 2015. Effects of whitewater parks on fish passage: A spatially explicit hydraulic analysis. Ecol. Eng. 83, 305–318. doi:10.1016/j.ecoleng.2015.06.032

Steffler, P., Blackburn, J., 2002. River2D Two-Dimensional Depth Averaged Model of River Hydrodynamics and Fish Habitat Introduction to Depth Averaged Modeling and User's Manual, University of Alberta, Edmonton, Alberta, Canada.

Takebayashi, H., Shimizu, Y., 2014. iRIC Software Nays2DH Solver Manual.

Tritico, H.M., Cotel, A.J., 2010. The effects of turbulent eddies on the stability and critical swimming speed of creek chub (*Semotilus atromaculatus*). J. Exp. Biol. 213, 2284–2293. doi:10.1242/jeb.041806

Tullos, D., Walter, C., Dunham, J., 2016. Does resolution of flow field observation influence apparent habitat use and energy expenditure in juvenile coho salmon? Water Resour. Res. 52, 1–13. doi:10.1002/2015WR018501

Waddle, T., 2010. Field evaluation of a two-dimensional hydrodynamic model near boulders for habitat calculation. River Res. Appl. 26, 730–741. doi:10.1002/rra.1278

Williams, J.G., Armstrong, G., Katopodis, C., Larinier, M., Travade, F., 2012. Thinking like a

    fish: a key ingredient for development of effective fish passage facilities at river

    obstructions. River Res. Appl. 28, 407–417. doi:10.1002/rra.1551

CHAPTER 2: APPLYING A SPATIALLY EXPLICIT TWO-DIMENSIONAL HYDRAULIC MODELING APPROACH TO EVALUATING WHITEWATER PARK DESIGN FOR FISH PASSAGE

2.1   Introduction

In-stream whitewater parks (WWPs) have been shown to partially impede upstream fish movement (Fox et al., 2016). WWP structures typically use sidewalls to constrict the channel into a narrow, steep chute which leads to a plunge pool. This constriction creates a hydraulic jump, or standing wave, used by boaters. However, the super-critical flow properties, namely high velocity and low flow depth, necessary to create a hydraulic jump can create a barrier to upstream fish movement and reduce longitudinal hydraulic connectivity. Longitudinal hydraulic connectivity is extremely important to anadromous fish (Fausch et al., 2002; Poff et al., 1997) which migrate upstream to spawn, and resident lotic fishes that require access to smaller scale lotic habitat features for feeding, refuge from harsh environmental conditions, and reproductive success (Schlosser and Angermeier, 1995).

3D and 2D computational fluid dynamics (CFD) models have been widely used to characterize habitat availability for fish species (Boavida et al., 2013; Branco et al., 2013; Lacey and Millar, 2004; Lee et al., 2010; Waddle, 2010). Only recently, however, have these models been applied to analyze upstream fish movement. The most common application has been of 2D CFD models to assess in-stream flow requirements for fish passage in natural channels (Bonetti et al., 2016; Grantham, 2013; Holmes et al., 2016; Reinfelds et al., 2010). Grantham et al. studied a least-cost-path of migration, which comprises only one continuous, depth-suitable potential fish swimming path. Recently, Stephens et al. (2015) developed a spatially explicit

approach to analyze 3D CFD modeling for WWP structures at individual points across all potential fish swimming paths. I adapted this approach for the same WWP structures to utilize the much more cost- and time-effective 2D CFD (Chapter 1). For these specific WWP structures, both the 2D and 3D approach accurately predicted fish passage. However, this spatially explicit approach has not yet been applied to a different set of WWP structures or used to explore WWP structure design characteristics.

The WWP structures on North St. Vrain Creek at Lyons, Colorado analyzed in Stephens et al. (2015) and in Chapter 1 were destroyed during the devastating 2013 flooding along the Colorado Front Range. These structures were recently redesigned and construction of a new WWP was completed in 2016. This chapter demonstrates the transferability of the 2D approach developed in Chapter 1 to these new WWP structures, and uses the methods to explore how WWP structure design characteristics and the associated hydraulic conditions may affect fish passage.

2.2 Methods

2.2.1 Study Site

The new WWP at what is now called Lavern M. Johnson Park in Lyons, Colorado comprises eight grouted-boulder, structures, four of which (Str1, Str5, Str6, and Str7) are studied here (Figure 2.1). Just upstream of Str7, a fraction of the flow from the main channel is split into a side channel (Split section). The Split section rejoins the main channel just upstream of Str6. Therefore, Str7 will have a lower flow rate than the rest of the WWP structures studied. While the side channel has its own structure adjacent to Str7, it was not included in this study.

The WWP structures included in this study employ a range of design configurations (Figure 2.2). Three design features are investigated in this study:
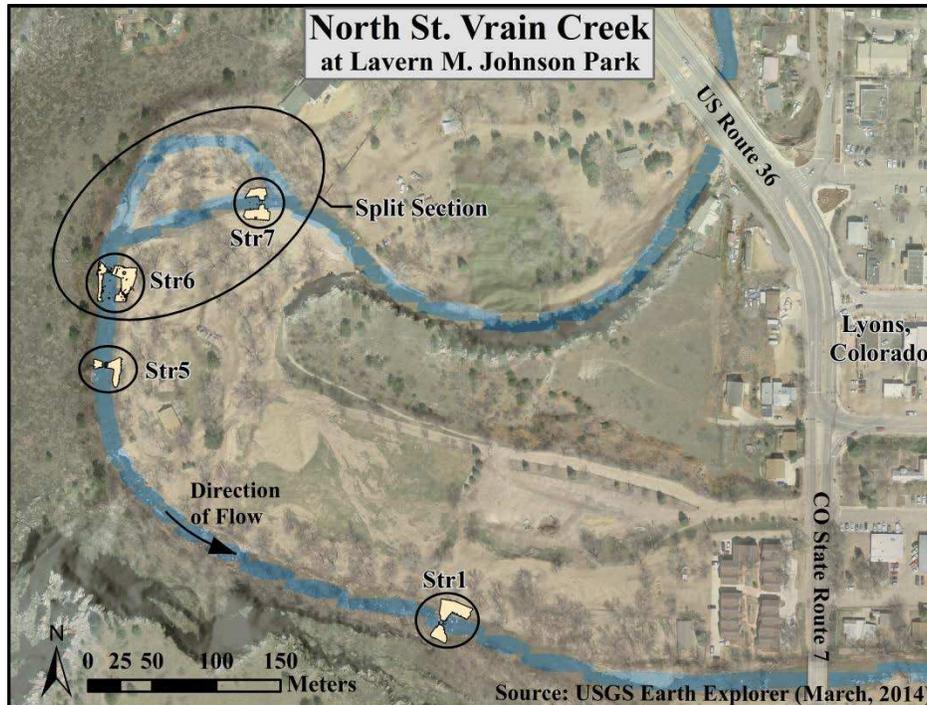
Figure 2.1. Site map showing the WWP on the North St. Vrain Creek at Lavern Johnson Park, west of Lyons, Colorado. The locations of the 4 structures analyzed in this study are circled. The Split section grouped Str6 and Str7 for 2D modeling purposes.

- **Chute Slope** – the main chute is typically designed with a steep slope that, in part, generates the high velocities and low flow depths that can potentially create a barrier to upstream fish movement. In theory, the steeper the slope of the structure, the more likely it is to become an upstream fish movement barrier.

- **Fish Channel** – a small, low elevation, low gradient throughway embedded within in the chute is designed to create a smaller, low flow channel to maintain adequate flow depth and velocity for fish passage even at low flows. The slope of the fish channel is designed with a lower slope than the slope of the surrounding chute – which could affect the velocity through the fish channel.

- **Sidewall Terrace** – the sidewalls were designed either as symmetrical or offset terraces. Symmetrical terrace sidewalls have the same elevation on both sides of the channel for a

33

given level (see Str1 in Figure 2.2). Offset terraces can include a terrace of higher elevation than the adjacent terrace on the opposite side of the channel (see Str5 in Figure 2.2).
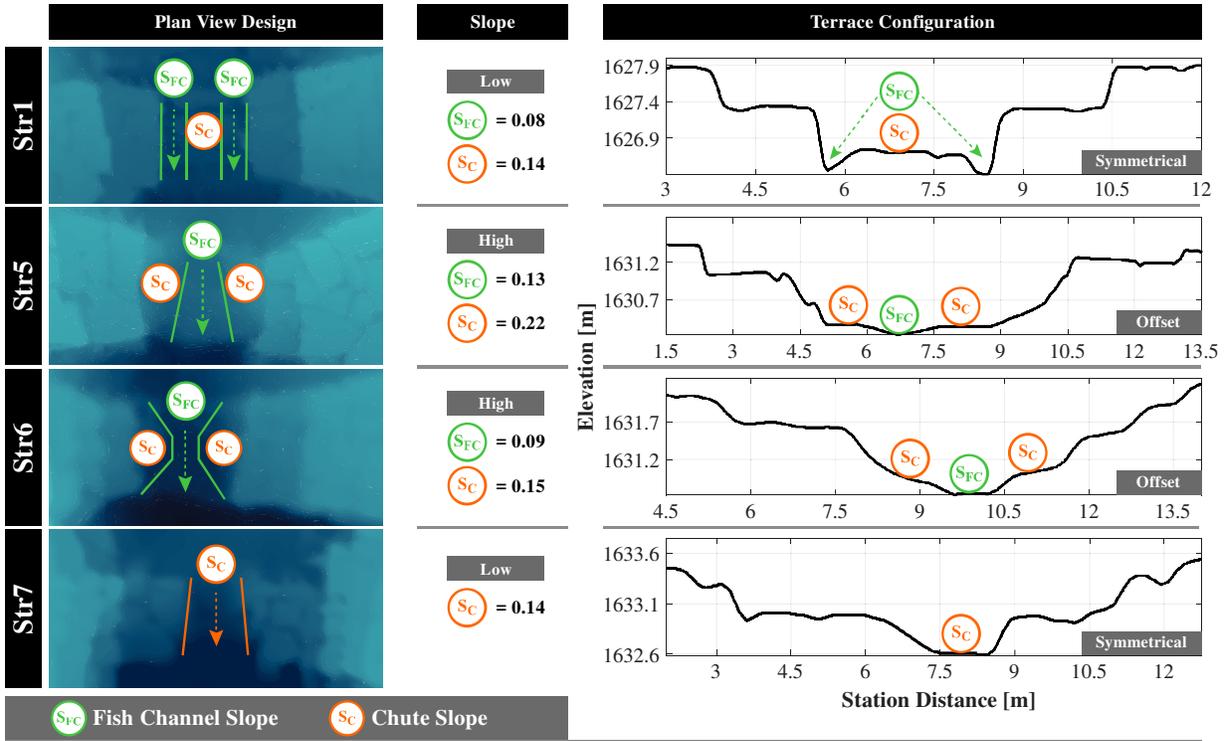
Figure 2.2. The design configurations at each WWP structure. The slope of the fish channel and the slope of the main chute are labeled in both the plan view and cross section terrace configuration. Station distance goes from left bank (0 m) to right bank.

The most downstream structure (Str1) has symmetrical sidewall terracing and a main chute with a slope of 0.14 surround by two fish channels of mild slope (0.09). Str5 is located approximately 350 m upstream of Str1. This structure exhibits the steepest main chute with a slope of 0.22. The fish channel at Str5 is narrow at the upstream end, widens at the downstream end, and has a steep slope of 0.13. The right bank at Str5 is confined by a hillslope. Hence, there is steep terracing on the right bank with more gradual, offset terracing on the left bank. Str6, less than 100 m upstream from Str5, is also confined by the hillslope on the right bank. Here, the sidewall terracing exhibits near-equal elevations, yet the right bank terraces are much less gradual than the left bank. The slope of the main chute and fish channel at Str6 are 0.15 and 0.09,

respectively. The furthest upstream structure studied (Str7) has no fish channel and a wide, uniform main chute with a slope of 0.14. The next highest terrace is at equal elevations on both sides with a fairly steep slope of 0.10, providing generally a symmetrical sidewall terrace design.

The different designs of the structures enable analysis of how each design feature can impact fish passage. Str1 and Str7 have gradual chute slopes compared to Str5 and Str6 and could lead to insights on how chute slope affects fish passage. Str1, Str5, and Str6 include variations of fish channel design that can be compared against Str7, which has no fish channel. The sidewall terrace designs of Str1 and Str7 are symmetrical and can be compared to Str5 and Str6, which both have offset sidewall terrace designs.

2.2.2 Data Collection

Topographic data were collected during low flow conditions using survey grade, real-time kinematic GPS (RTK-GPS) from a rod-mounted Topcon GR5 unit. Channel cross sections were measured starting approximately 30 m upstream and ending 30 m downstream of the WWP structures. Spacing between each point in a cross section was approximately 0.5 m near the WWP structure and 1.0 – 1.5 m towards the upstream and downstream extents. Measured cross sections were spaced approximately 0.5 m near the WWP structure and approximately 2.5 m towards the upstream and downstream extents. The average spacing in each reach was approximately 2 m. The WWP structures, in-channel boulders, large wood, and other abrupt changes in elevation were surveyed with the RTK-GPS in greater detail (4-19 points/m^2). All non-submerged areas were scanned using a high resolution terrestrial LiDAR (TLS) scanner, FARO® Focus. TLS data were processed to eliminate vegetation, water surface reflections, and noise, and subsampled to 0.02 m (average of approximately 80 points/m^2). TLS data were

combined with RTK-GPS data to create a final topographic surface for Str1, Str5, and the Split section (which includes both Str6 and Str7).

The Colorado Division of Water Resources operates streamflow gage sites located approximately 12 km upstream of the study site, below Button Rock (Ralph Price) Reservoir (NSVBBRCO) and on St. Vrain Creek approximately 300 m downstream of the confluence with the South St. Vrain Creek (SVCLYOCO), which are not representative of the discharge at the study reach. Therefore, discharge for model validation was measured using the velocity-area method on two separate site visits, once in July 2016 and once in February 2017. Downstream velocities were measured at 0.6 of the water depth with a Sontek FlowTracker acoustic doppler velocimeter. Hydraulic validation data (velocities and water surface elevations (WSE)) were collected during these site visits to capture low and moderate flows. The calculated discharge for February and July were 0.40 and 2.70 cms, respectively. WSE were measured at the edge of water using RTK-GPS for both discharges. In February, point velocity measurements at were collected at several locations surrounding each WWP structure for additional model validation.

2.2.3 *Hydraulic Modeling*

I used the Nays2DH solver within the graphical user interface software package from the International River Interface Cooperative (iRIC) to create a 2D, depth-averaged, hydrodynamic model of each WWP structure (Nelson et al., 2016; Takebayashi and Shimizu, 2014). NAYS2DH solves the depth-averaged equations of conservation of fluid mass and momentum in a general coordinate system. Topographic data were input into Nays2DH to create three separate models of Str1, Str5, and the Split section (Str6 and Str7). Uniform, rectangular (for Str1 and Str5) and curvilinear (for Split section) computational grids were automatically generated in Nays2DH. The mesh spacing was 0.05 m for Str1 and Str5 and 0.15 m for the Split section. I

developed models for seven, steady-state discharges: 0.4, 0.85, 1.7, 2.7, 5.0, 8.5, and 11.0 cms. As stated in Chapter 1, the range of discharges from 0.4 to 2.7 cms, herein referred to as fish flows, were chosen because almost all fish movements observed by Fox et al. (2016) occurred during this range. Discharges 5.0, 8.5, and 11.0 cms, herein referred to as terrace flows, were chosen to explore how the WWP structures affect fish passage at discharges large enough to access several levels of sidewall terraces.

Modeled and measured WSE for 0.40 and 2.7 cms and velocities for 0.40 cms were compared using the root mean square error (RMSE) and mean absolute error (MAE). For both 0.40 and 2.7 cms, I used the Manning n roughness parameter to calibrate each of the three models to result in the lowest RMSE and MAE. The optimal Manning's n roughness parameters were used for all the modeled discharges.

2.2.4 *Streamline Development and Evaluation*

Following the methodology developed by Stephens et al. (2015)and as adapted in Chapter 1, the entire depth-averaged flow field over the WWP structures was analyzed for fish passage using streamlines. This methodology uses streamlines as potential fish swimming paths and fish swimming criteria, based on depth and velocity, evaluated along the streamlines to determine whether the local hydraulics are conducive to upstream fish movement.

Streamlines were generated in the data analysis and visualization software ParaView by integrating the velocity vector field calculated in the 2D hydraulic model (Ayachit et al., 2015). The area of interest, or region in which streamlines are evaluated, was defined by identifying the streamwise extent of the region most critical to fish passage. The upstream and downstream extents were respectively marked by the rapid drop in the modeled WSE and the location downstream of the hydraulic jump where the slope of the WSE becomes gradual. In ParaView,

streamline sources are created from uniformly distributed points along and upstream and a downstream, user-defined line source with an initial spacing less than 0.01 m. The upstream line source integrates forward in time and the downstream line source integrates backward in time.

Streamlines were then processed to include only complete streamlines, that is, streamlines that cross both the upstream and downstream boundaries of the area of interest. Streamlines were separated between incomplete versus complete streamlines. If an incomplete streamline recirculated back to its original boundary, the streamline was clipped at the point it begins to recirculate to create two separate incomplete streamlines. All incomplete streamlines are connected to complete streamlines, provided the endpoint of the incomplete streamline was within 0.15 m of that complete streamline. This process was conducted iteratively so that newly connected streamlines were available to be connected to incomplete streamlines. Any incomplete streamlines at the end of the process were removed so that only complete streamlines were included in this analysis.

I used a minimum depth criterion of 0.11 m ($MDC_{0.11}$) and burst swimming speed of 10 BL/s to quantify fish passage success. These physical swimming criteria were developed based on brown trout (*Salmo trutta*) and rainbow trout (wild *Oncorhynchus mykiss* and hatchery Hofer x Harrison strain). Of the four criteria used in Chapter 1 these were selected because they were less conservative and would provide broader insight into how the WWPs perform under various flow conditions and for various design configurations. To simplify the analysis of the WWP structure designs, a single fish size was selected to be used in the analysis. Based on the size of fish found in the study reach (Fox et al., 2016), I used a fish length of 0.25 m, giving a burst swimming speed, V_{burst}, of 2.5 m/s. The minimum depth and maximum velocity are determined for each streamline. If the minimum depth is less than $MDC_{0.11}$, the maximum velocity is greater

than V_{burst}, the streamline is determined to be impassable. The fraction of impassable streamlines based on $MDC_{0.11}$, V_{burst}, or a combination of the two are defined as $MDR_{0.11}$, MVR_{10}, and $D_{11}V_{10}$, respectively, and were calculated at each WWP structure for all seven discharges.

The intersections between passable streamlines and five equally spaced cross sections were plotted within the area of interest. The passable width is the sum of the lateral distance between consecutive passable intersections. The passable widths for all three streamline evaluation variables at all seven flows were analyzed to compare the different structures.

2.3 Results

2.3.1 Hydraulic Modeling

Modeled versus measured WSE were within acceptable ranges of errors with the largest RMSE of 0.062 m (Figure 2.3). Modeled versus measured velocity values exhibit greater error than WSE, especially at Str5. Potential sources of these errors are measuring velocity at low discharges and the small range of measured values obtained. This is because even small errors can give large RMSE. I determined this to be acceptable because these values are typically not located within the area of interest. The models appear to under-predict velocity when compared with measured values, which may also be a factor of measuring velocity under low flow conditions. With low WSE errors, the models were determined to accurately resolve the flow conditions. The Manning n values used in the final, calibrated models were 0.06 for Str1 and Str5 and 0.03 for the Split section.

The model results were used to calculate discharge at cross sections downstream of Str6 and Str7 to estimate the fraction of flow diverted to the side channel. Str7 receives approximately 50% of the total discharge for low discharges, but this value increases steadily to 65% for high discharges.
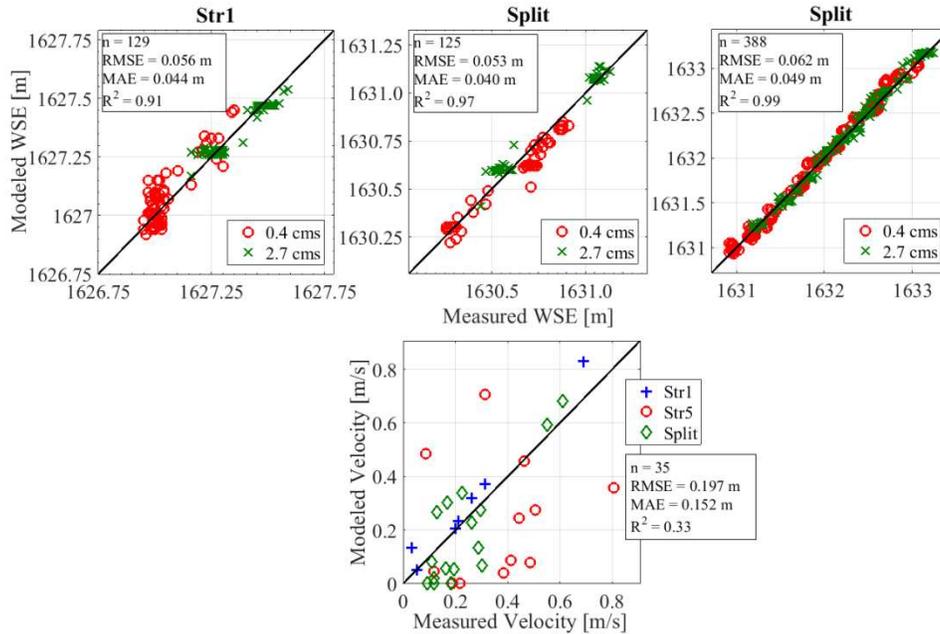
Figure 2.3. Hydraulic model validation plots showing modeled versus measured values for WSE (upper three plots). Validation plots are shown separately, by structure, for WSE. For WSE, values measured during 0.40 cms are shown as circles (red) and during 2.70 cms as X (green). Modeled versus measured velocity values, only measured at 0.40 cms, are shown in the lower plot. The number of validation data points (*n*), the RMSE, MAE, R^2 for WSE and velocity are also displayed.

Figure 2.4 plots hydraulic results for cross sections extracted from the center of each structure along with the WSE for all seven discharges. An increase in discharge will cause the flow field either to remain within a given terrace (depth of flow will increase) or activate a new terrace level (flow depth increases and the flow field spreads out laterally over the new terrace). The flow over a newly activated terrace is likely shallow and slow. At these structures, new terrace levels are activated at varying discharges for different structures, as indicated in Figure 2.4.

2.3.2   Streamline Analysis

For each of the seven modeled discharges, streamlines were determined to either meet fish swimming criteria (passable) or not meet fish swimming criteria (impassable). Appendix F presents plots of all passable and impassable streamlines for $MDR_{0.11}$, MVR_{10}, and $D_{11}V_{10}$.

Figure 2.5 summarizes the fractions of impassable streamlines for each structure and each discharge using the different fish passage metrics. If an increase in discharge causes the flow field to remain within a given terrace, $MDR_{0.11}$ tends to decrease and MVR_{10} tends to increase. If a new terrace is activated, the flow field spreads laterally resulting shallow, slow over the new terrace and the trend reverses: $MDR_{0.11}$ tends to increase and MVR_{10} tends to decrease. It can require more than one subsequent increase in discharge to fully develop the lateral extent of a terrace before the flow depth begins to increase more dramatically. For example, at Str1, a terrace is activated at 2.70 cms (Figure 2.4). Figure 2.5 shows the effect from activating this terrace because after a consistent decrease in $MDR_{0.11}$ from 0.40 cms to 1.70 cms there is a sharp increase in at 2.70. $MDR_{0.11}$ increases again at 5.0 cms as more streamlines cover the terrace.
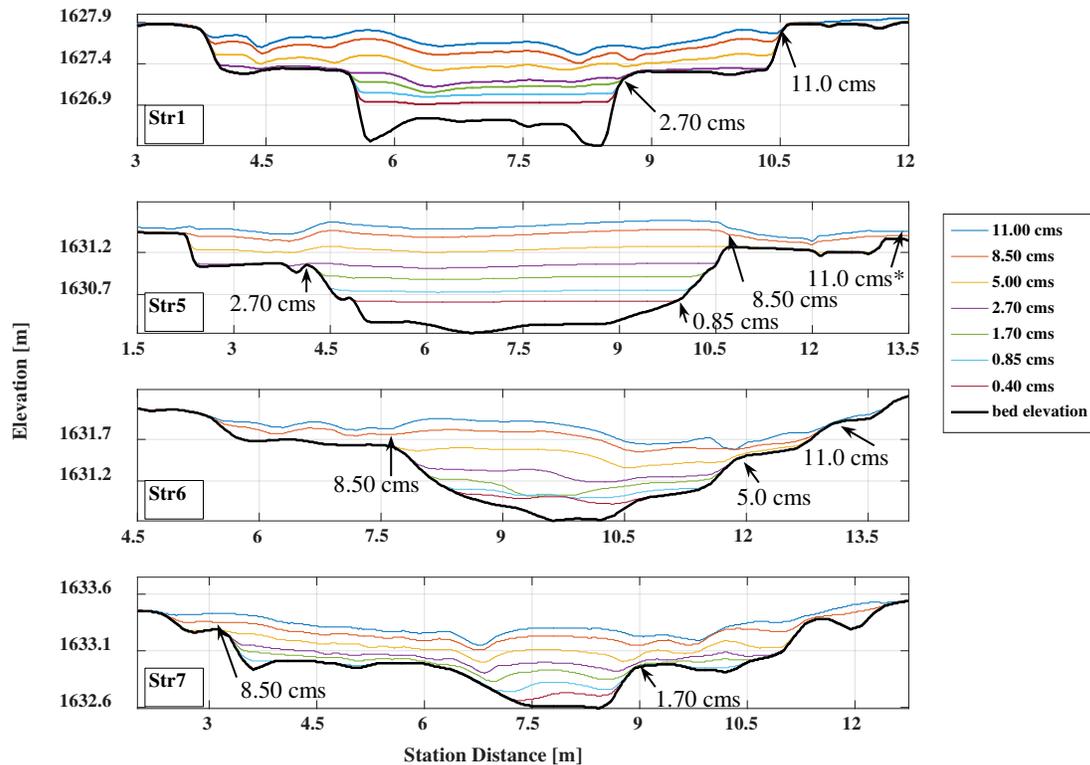
Figure 2.4. Cross section taken from the center of each structure showing the different terrace configurations with WSE plotted for each incremental increase in discharge. Flows at which terraces are activated are indicated with an arrow.

The fractions of impassable streamlines for $D_{11}V_{10}$ are a complex, spatially dependent interaction of $MDR_{0.11}$ and MVR_{10}. The $D_{11}V_{10}$ are smallest at low flows, yet are still large, ranging from nearly 0.80 to 1 for almost all discharges at all four structures. One exception to this occurs at Str1 where $D_{11}V_{10}$ are less than 0.50 for the lowest three discharges. At 2.7 cms, a new terrace is activated and an increase in both $MDR_{0.11}$ and MVR_{10}, leading to a larger $D_{11}V_{10}$ is shown.
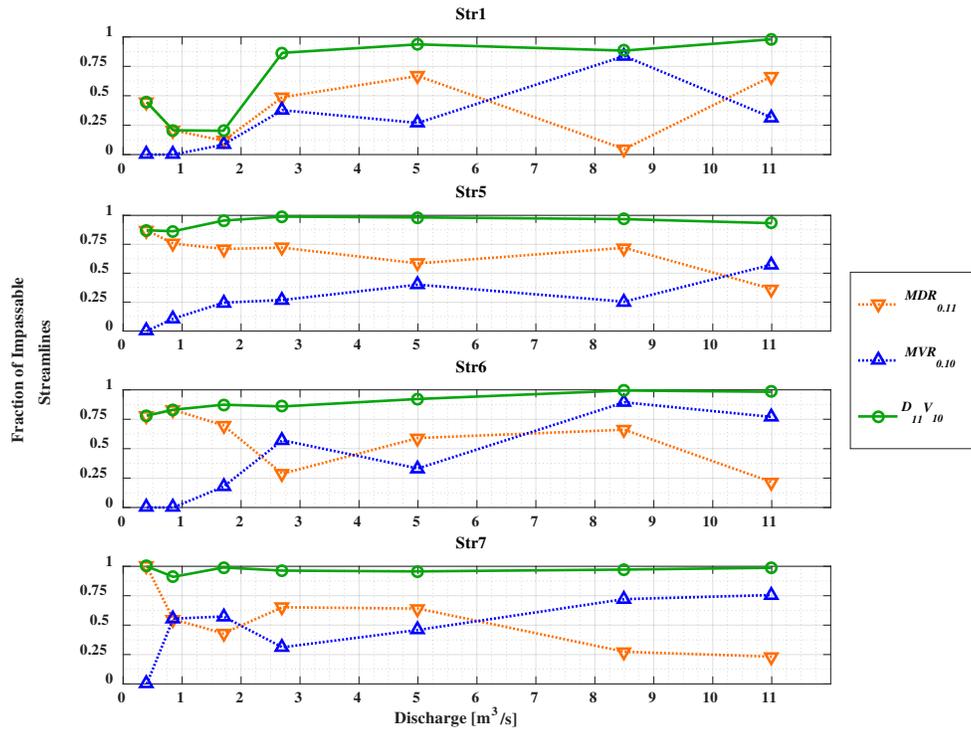
Figure 2.5. The fraction of impassable streamlines for MDR_{11} (orange dotted line with triangle marker), MVR_{10} (blue dotted line with triangle marker) and $D_{11}V_{10}$ (green solid line with circle marker) at each modeled discharge for the four WWP structures. Values range between 1 (no streamlines meet the fish swimming criteria) and 0 (all streamlines meet the fish swimming criteria).

Figure 2.6 shows the results for the passable widths computed for $MDR_{0.11}$, MVR_{10}, and $D_{11}V_{10}$. Consistent with results from Chapter 1, the passable width for $MDR_{0.11}$ tends to increase with an increase in discharge and tend to diminish from upstream (XS1) to downstream (XS5). At Str1 and Str6 the passable width for $D_{11}V_{10}$ is larger for discharges between 0.40 and 2.70 cms than for higher discharges. At Str5, the passable width is smallest for discharges of 2.7 and

5.0 cms. There appears to be no consistent overall trend to passable widths for MVR_{10} and $D_{11}V_{10}$ between structures. This may be a function of different terracing at each structure.
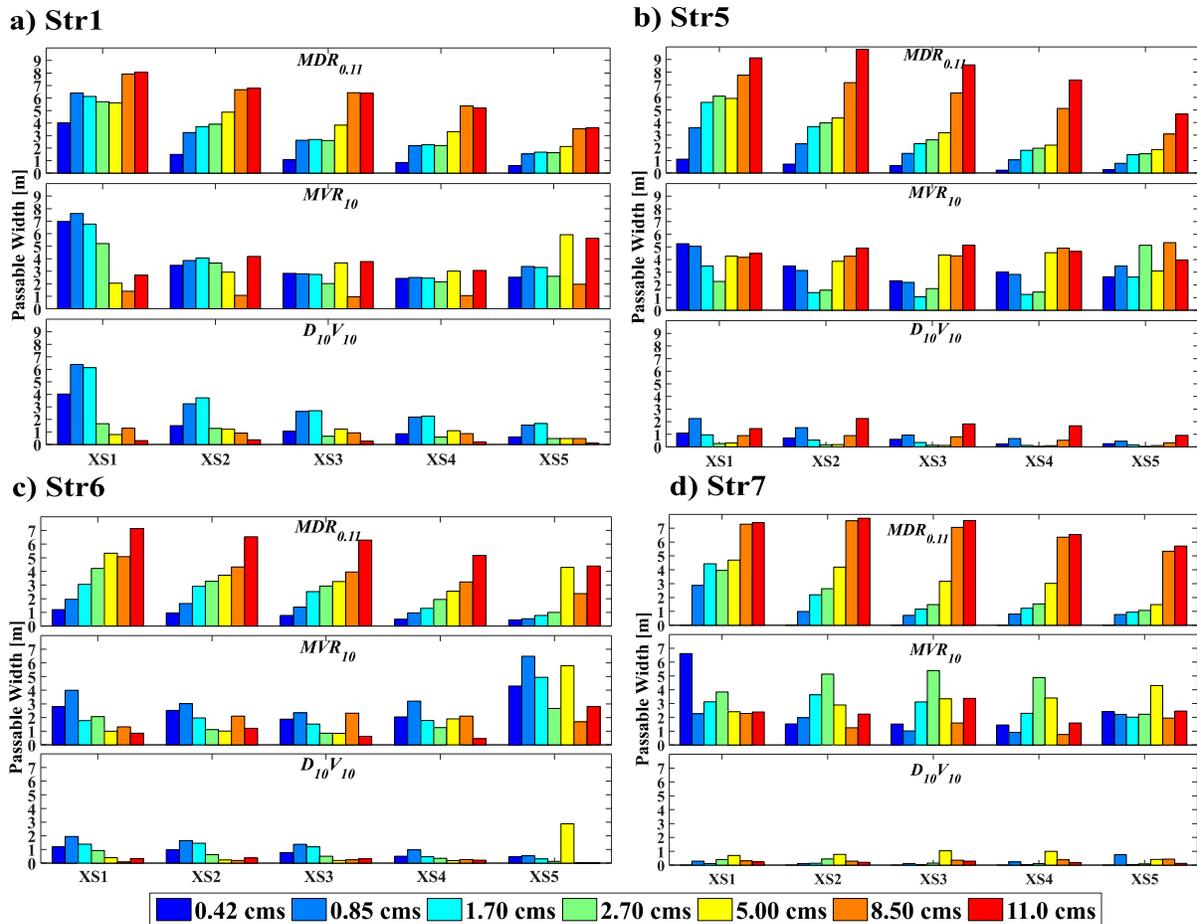
Figure 2.6. Passable widths for five equally spaced cross sections moving upstream (XS1) to downstream (XS5) based on $MDR_{0.11}$, MVR_{10}, and $D_{11}V_{10}$ for (a) Str1, (b) Str5, (c) Str6 and (d) Str7.

2.4 Discussion

The fish flows (discharges between 0.40 and 2.7 cms) are the focus for fish passage here, because observations show that the majority of upstream fish movements occur during these flows. However, investigating these WWP structures at the terrace flows (discharges between 5.0 and 11.0 cms) may provide clues into how terrace designs might be able to facilitate fish passage at these higher flows.

43

It is important to note that this analysis does not account for other possible factors commonly associated with fish passage such as turbulence (Haro et al., 2004; Hinch and Rand, 2000; Lacey et al., 2012; Lupandin, 2005; H M Tritico and Cotel, 2010) and fish behavior (Kemp et al., 2012; Santos et al., 2012). This analysis focuses solely on trout swimming performance. These metrics are easily quantifiable using 2D hydraulic modeling and are shown to be effective in predicting fish passage (Stephens et al., 2015; Chapter 1). The minimum depth criteria of 0.11 m and burst swimming speed of 2.5 m/s were developed based on brown and rainbow trout. Implications for other species, especially those of lesser swimming abilities may be more profound.

2.4.1 Chute Slope

Chute slope influences fish passage typically by creating a velocity barrier within the chute. While at the lowest discharge of 0.40 cms, velocity was not considered a barrier at of the all structures (Figure 2.5). However, at Str5 and Str6 part or all of the chute is considered impassable based on MVR_{10} (Figure F.2i-j and Figure F.3j) at 1.70 cms. Conversely, at Str1, with a low chute slope, almost the entire main chute is still passable based on MVR_{10} until 2.7 cms. This suggests that while chute slope may not affect the lowest flow, subsequent higher flows within the fish flow range, maybe have less conducive to fish passage. These effects of chute slope may be ameliorated or compounded by the inclusion or design of a fish channel and terrace design

2.4.2 Fish Channel

The purpose of the fish channel is to increase fish passage at low discharges by concentrating flow into a deeper, inset channel. In Figure 2.5, the MVR_{10} is small for all the structures at low flow, suggesting velocities at low discharges are lower than the swimming burst

speed. Therefore, the minimum depth criterion is the limiting factor and increasing flow depth is necessary to improve fish passage at low discharge. The inclusion of a fish channel can provide the necessary minimum depth. Also, by designing the fish channel with a gradual slope, velocities through the fish channel at low discharges will typically be low.

Str1 has the deepest, most pronounced fish channels. Consequently, Str1 has the lowest $MDR_{0.11}$, MVR_{10}, and $D_{11}V_{10}$ and largest passable widths for discharges of 0.40, 0.85, and 1.70 cms. Figure F.1a clearly shows the passable streamlines through the two fish channels with impassable streamlines in the surrounding main chute. While MVR_{10} tends to be small at low discharges for all structures, it is the unique combination of deep flows through the fish channels (low $MDR_{0.11}$) at these low discharges that enable Str1 to create more passable streamlines than the other structures.

The slope of the fish channel may affect the velocity of flow through the fish channel, especially at low discharges. For instance, the fish channel in Str5 is steeper (slope of 0.13) than Str1's fish channels (slope of 0.09). Visual inspection of passable to impassable streamlines for MVR_{10} at Str1 from 0.40 to 2.7 cms shows that much of the fish channels are passable for Str1 until a discharge of 2.7 cms (Figure F.1). At Str5, on the other hand, shows impassable streamlines develop within the center fish channel at just 0.85 cms (Figure F.2i). Furthermore, this is important because at Str1, the fish channels are passable whether considering $MDR_{0.11}$, MVR_{10}, or $D_{11}V_{1}$.

All three structures with fish channels perform better at lower discharges than Str7, which has no fish channel. This is highlighted by comparing Str1 and Str7 since they have similar chute slopes. With no fish channel, flow at Str7 is spread out over a larger area and are too shallow for fish passage. At Str1, flow is concentrated and deeper in the two fish channels. as highlighted by

examining the streamlines MVR_{10} at structures with relatively equal chute slopes; Str1 with fish channels (Figure F.1h-k) versus Str7 without a fish channel (Figure F.4h-i). Str1 as noted above is almost completely passable up to 2.7 cms whereas much of the chute at Str7 is considered impassable, even at 0.85 cms. Further compounding this issue is that Str7 only receives 60-70% of the total discharge. So, of all the structures, Str7 could benefit the most from a fish channel.

2.4.3   Sidewall Terrace

Sidewall terraces function to maintain the reduction of channel width at higher discharges. This effect can still be accomplished by using terracing. Terracing develops a dynamic nature of how flow is distributed laterally at higher discharges. These effects are highlighted as the incremental increase in discharge is able to activate a new terrace level. When a new terrace is first activated, the flow is distributed at low depths over much of the terrace, allowing for the opportunity to create new, potentially passable flow paths.

In Str1, the symmetrical terrace levels are only activated at 2.7 and 11.0 cms, meaning flows are somewhat channelized between the two terrace levels. This reduces the ability of activated terraces to increase fish passage at higher discharges. Conversely, because Str5 and Str6 utilize offset terracing, they activate four and three different terraces at varying discharges, including low discharges. By activating terraces at several levels, there is a greater chance of overlapping areas passable for both width and depth.

This study does not examine the slope, lateral width, or height of terracing. However, these could affect flow depth and velocity as new terrace levels are activated and at what discharges activate a given terrace.

2.4.4 Design Recommendations

Below are several design features that may improve fish passage at WWP structures based on this analysis:

- The chute slope is critical in creating the hydraulic jump desired by boaters. A high chute slope creates high velocities and low depths to maintain adequate hydraulic conditions necessary for a hydraulic jump. The minimum chute slope necessary to create the desired wave should be used.

- The presence of a fish channel appears to create more passable streamlines, especially at low discharges. Also, the slope of the fish channel may be as important as the slope of the main chute.

- Sidewall terraces are important for fish passage at higher flows. Offsetting terraces to induce terrace activation at a variety of flows, especially at flows relevant to fish passage, can help increase fish passage.

- Designing a separate, high flow fish channel located on a terrace may provide additional passable areas as the terrace is activated at higher discharges.

- Using plan designs, a sensitivity analysis can be conducted prior to construction to optimize fish passage.

Overall, I suggest future WWP designs look to minimize chute slope for the desired hydraulic jump, include a low flow fish channel, and include offset terracing for low discharges with a separate fish channel inset into one of the terraces.

2.5 Conclusions

This study investigates the effects of WWP structure design with regards to upstream fish movement by evaluating 2D CFD model results along streamlines. Evaluating along streamlines

allows for a spatially explicit approach to understanding the hydraulics at scales relevant to potential fish swimming paths. Future WWP designs can be evaluated prior to construction to best optimize the design relating to chute slope, fish channels, and sidewall terracing. Further research investigating the slope and dimensions of terraces, effects of a terrace fish channel, and dimensions of the fish channel can help refine design recommendations. A detailed study using observations of actual fish movement would be critical in quantifying actual fish passage at these WWP structures. Also, more research is necessary to better develop fish swimming criteria to investigate fish passage for a wide range of species.

REFERENCES

Boavida, I., Santos, J.M., Katopodis, C., Ferreira, M.T., Pinheiro, A., 2013. Uncertainty in

predicting the fish-response to two-dimensional habitat modeling using field data. River

Res. Appl. 29, 1164–1174. doi:10.1002/rra.2603

Bonetti, R.M., Reinfelds, I. V., Butler, G.L., Walsh, C.T., Broderick, T.J., Chisholm, L.A., 2016.

A multi-scale GIS and hydrodynamic modelling approach to fish passage assessment:

Clarence and Shoalhaven Rivers, NSW Australia. Geomorphology 260, 79–90.

doi:10.1016/j.geomorph.2015.06.015

Branco, P., Boavida, I., Santos, J.M., Pinheiro, A., Ferreira, M.T., 2013. Boulders as building

blocks: Improving habitat and river connectivity for stream fish. Ecohydrology 6.

doi:10.1002/eco.1290

Fausch, K.D.., Torgersen, C.E.., Baxter, C.V.., Li, H.W., 2002. Landscapes to Riverscapse:

Bridging the Gap between Research and Conservation of Stream Fishes. Bioscience 52,

483–498.

Fox, B.D., Bledsoe, B.P., Kolden, E., Kondratieff, M.C., Myrick, C.A., 2016. Eco-hydraulic

evaluation of a whitewater park as a fish passage barrier. J. Am. Water Resour. Assoc. 52,

420–442. doi:10.1111/1752-1688.12397

Grantham, T.E., 2013. Use of hydraulic modelling to assess passage flow connectivity for

salmon in streams. River Res. Appl. 29, 250–267. doi:10.1002/rra.1591

Haro, A., Castro-Santos, T., Noreika, J., Odeh, M., 2004. Swimming performance of upstream

migrant fishes in open-channel flow: a new approach to predicting passage through velocity

barriers. Can. J. Fish. Aquat. Sci. 61, 1590–1601. doi:10.1139/f04-093

Hinch, S.G., Rand, P.S., 2000. Optimal swimming speeds and forward-assisted propulsion:

energy-conserving behaviours of upriver-migrating adult salmon. Can. J. Fish. Aquat. Sci. 57, 2470–2478. doi:10.1139/f00-238

Holmes, R.W., Rankin, D.E., Ballard, E., Gard, M., 2016. Evaluation of Steelhead passage flows using hydraulic modeling on an unregulated coastal California river. River Res. Appl. 32, 697–710. doi:10.1002/rra.2884

Kemp, P.S., Anderson, J.J., Vowles, A.S., 2012. Quantifying behaviour of migratory fish: Application of signal detection theory to fisheries engineering. Ecol. Eng. 41, 22–31. doi:10.1016/j.ecoleng.2011.12.013

Lacey, J.R.W., Neary, V.S., Liao, J.C., Enders, E.C., Tritico, H.M., 2012. The IPOS framework: linking fish swimming performance in altered flows from laboratory experiments to rivers. River Res. Appl. 28, 429–443. doi:10.1002/rra.1584

Lacey, R.W.J., Millar, R.G., 2004. Reach scale hydraulic assessment of instream salmonid habitat restoration. J. Am. Water Resour. Assoc. 4, 1631–1644. doi:10.1111/j.1752-1688.2004.tb01611.x

Lee, J.H., Kil, J.T., Jeong, S., 2010. Evaluation of physical fish habitat quality enhancement designs in urban streams using a 2D hydrodynamic model. Ecol. Eng. 36, 1251–1259. doi:10.1016/j.ecoleng.2010.05.004

Lupandin, A.I., 2005. Effect of flow turbulence on swimming speed of fish. Biol. Bull. 32, 461–466. doi:10.1007/s10525-005-0125-z

Nelson, J.M., Shimizu, Y., Abe, T., Asahi, K., Gamou, M., Inoue, T., Iwasaki, T., Kakinuma, T., Kawamura, S., Kimura, I., Kyuka, T., McDonald, R.R., Nabi, M., Nakatsugawa, M., Simoes, F.R., Takebayashi, H., Watanabe, Y., 2016. The international river interface cooperative: Public domain flow and morphodynamics software for education and

applications. Adv. Water Resour. 93, 62–74. doi:10.1016/j.advwatres.2015.09.017

Poff, N.L., Allan, J.D., Bain, M.B., Karr, J.R., Prestegaard, K.L., Richter, B.D., Sparks, R.E., Stromberg, J.C., 1997. The Natural flow regime. Bioscience 47, 769–784. doi:10.2307/1313099

Reinfelds, I. V., Lincoln-Smith, M., Haeusler, T., Ryan, D., Growns, I., 2010. Hydraulic assessmtent of environmental flow regimes to facilitate fish passage through natural riffles: Shoalhaven River below Tallowa Dam, New South Wales, Australia. River Res. Appl. 26, 589–604. doi:10.1002/rra.1262

Santos, J.M., Silva, A., Katopodis, C., Pinheiro, P., Pinheiro, A., Bochechas, J., Ferreira, M.T., 2012. Ecohydraulics of pool-type fishways: Getting past the barriers. Ecol. Eng. 48, 38–50. doi:10.1016/j.ecoleng.2011.03.006

Schlosser, I.J., Angermeier, P.L., 1995. Spatial variation in demographic processes of lotic fishes: conceptual models, empirical evidence, and implications for conservation. Am. Fish. Soc. Symp. 17, 392–401.

Stephens, T.A., Bledsoe, B.P., Fox, B.D., Kolden, E., Kondratieff, M.C., 2015. Effects of whitewater parks on fish passage: A spatially explicit hydraulic analysis. Ecol. Eng. 83, 305–318. doi:10.1016/j.ecoleng.2015.06.032

Takebayashi, H., Shimizu, Y., 2014. iRIC Software Nays2DH Solver Manual.

Tritico, H.M., Cotel, A.J., 2010. The effects of turbulent eddies on the stability and critical swimming speed of creek chub (*Semotilus atromaculatus*). J. Exp. Biol. 213, 2284–2293. doi:10.1242/jeb.041806

Waddle, T., 2010. Field evaluation of a two-dimensional hydrodynamic model near boulders for habitat calculation. River Res. Appl. 26, 730–741. doi:10.1002/rra.1278

CHAPTER 3: SPATIALLY EXPLICIT FISH PASSAGE EVALUATION AT WHITEWATER PARKS USING 2D HYDRAULIC MODELING: A GUIDE

3.1 Introduction

In-stream whitewater park structures (WWPs), which create waves for kayakers and other recreationalists, are becoming increasingly popular recreational attractions. These structures typically constrict the flow of rivers by decreasing the width of flow into a chute. The chute usually exhibits a locally steeper slope and a steep drop off into a plunge pool (Figure 3.1). These physical constraints create supercritical hydraulic conditions (shallow flow depths and high flow velocities) within the chute. These conditions are necessary to form a hydraulic jump, or wave, which is used by recreationalists. While these flows may be ideal for recreationalists, WWPs have been known to partially inhibit upstream fish movement (Fox et al., 2016). By limiting a fish's ability to move upstream, a WWP has the potential to become a barrier to longitudinal connectivity.

Figure 3.1. Photo of a WWP structure looking upstream during low discharge.

There are many factors that affect a fish's ability and/or willingness to successfully move upstream including flow depth, velocity, turbulence, temperature, plunge pool depth, and available width of swimming paths. However, flow depth and velocity have been shown to be dominant factors.

Stephens et al. (2015) developed a spatially explicit methodology utilizing results from a three-dimensional computational fluid dynamic (CFD) model to evaluate fish passage at three WWP structures. This methodology was then adapted for use with two-dimensional (2D) CFD models. In comparison to 3D CFD modeling, utilizing 2D CFD modeling greatly reduces computational costs and times.

This document is a guide to aid practitioners and water resource managers in evaluating fish passage of existing or proposed WWP structures. This guide will follow the work flow of the methodology as described in Figure B (Appendix B). Some sections (e.g. Field Data Collection and Hydraulic Modeling) have relatively standard protocol and thus focus on the general approach and highlight considerations to evaluating WWPs with regards to fish passage. Other sections (e.g. Streamline Development and Streamline Analysis) guide a user through each necessary task.

3.2   Field Data Collection

When evaluating existing WWP structures, field data collection is fundamental to accurately representing a WWP structure. Typically, field data collection comprises three main tasks: topographic survey, hydraulic validation measurements, and fish assemblage identification. First, topographic surveys inform the 2D hydraulic model. Second, hydraulic validation measurements, typically consisting of water surface elevation (WSE) point measurements and velocity point measurements, are necessary for validating the 2D hydraulic

model to ensure it accurately predicts actual hydraulic conditions. These point measurements should be geographically consistent with the topographic data. Knowing the discharge, either by measurement or reliable stream gage information, at the time of hydraulic validation measurements is essential. Third, identification of the fish species present and their life stages is used to determine the appropriate fish swimming criteria.

For proposed WPP structures, topographic data could be obtained from a combination of pre-implementation topographic survey and the proposed WWP structure design. Depending on the project design, hydraulic calibration measurements could be estimated from existing conditions.

The following sections describe the general approach and provide specific guidance to obtain adequate field data to evaluate fish passage of WWPs. The methodology may vary with project requirements and constraints and standard field protocol should be researched and applied.

3.2.1 Topographic Survey

2D hydraulic models depend heavily on an accurate representation of the channel bathymetry. Therefore, high resolution topographic surveys are recommended. Topographic data should be obtained at least 4-5 channel widths upstream and downstream of the WWP structure. This distance is used as guidance to minimize the effects of model boundary conditions on the area of interest. Conducting surveys during low flow periods will likely provide the optimal safety conditions for wading and maximum channel bed exposure for higher resolution surveying.

There are two main methods for surveying channel topography: traditional and high-resolution. Traditional topographic methods using a total station or real time kinetic GPS (RTK-

GPS) are ideal for obtaining a high number of surveyed points. Channel bathymetry is typically obtained by surveying cross sections. An alternate method is to survey longitudinal break lines (i.e. top of bank, bottom of bank, edge of water, thalweg, etc.). Longitudinal surveys can also be used in conjunction with surveyed cross sections. Spacing between survey points and cross sections will be constrained by project area size and time available. In-channel features, such as boulders and large wood, should be surveyed in detail. The use of high resolution methods, such as terrestrial laser scanning (TLS), airborne laser scanning, structure-from-motion (SfM), acoustic Doppler depth soundings or other methods, are also highly recommended. These high-resolution methods can be used in conjunction with traditional survey methods. It should be noted that most high-resolution methods do not penetrate the water column. In such cases, extra care should be taken to capture submerged features using traditional methods.

3.2.2 *Hydraulic Validation Measurements*

Hydraulic validation data should be collected at flows representative of those to be modeled. If possible, the upper and lower limits of the modeled flows should be measured as validation data. It is important to correlate these hydraulic validation measurements with known discharge data.

It is common practice to measure water surface elevations at the edge of water. However, the intersection between surveyed topographic data and measured water surface is the area most prone to error in 2D hydraulic models. Therefore, it is recommended to collect water surface elevations approximately 1 m towards the center of the channel from the edge of water.

Velocity point measurements should be taken at various locations surrounding the WWP structure. When flows permit, it is advisable to obtain measurements in and around the chute as these are the most important areas to consider when evaluating fish passage.

3.2.3 Fish Assemblage

It is important to know the species of fish present or expected to be present in the stream and their life stages. These data will inform the fish swimming criteria necessary for evaluating a WWP structure for fish passage. This may be determined by electrofishing methods or by consulting the local fish and wildlife authorities.

3.3 2D Hydraulic Modeling

This section will highlight aspects of creating a steady state 2D hydraulic model relevant to modeling WWP structures. Here we use the Nays2DH solver included in the International River Interface Cooperative (iRIC) software package (Nelson et al., 2016; Takebayashi and Shimizu, 2014). Tutorials on how to create a working model can be found on the iRIC downloads page (http://i-ric.org/en/downloads). As stated above, these methods for evaluating WWP structures are not limited to the Nays2DH solver. There are several solvers within iRIC and other well-established solvers outside of iRIC that may be suitable to solve the complex flows of WWP structures. While the following subsections are specific to modeling in Nays2DH, some of the principles are transferrable to other solvers.

3.3.1 Nays2DH

Nays2DH utilizes the cubic interpolated polynomial (CIP) method, which is a high-order finite differencing method that increases local precision, especially in areas of local unsteadiness and flow separation. It is for these reasons that Nays2DH was chosen for this instructional guide. However, any industry-standard 2D solver that can adequately resolve the complex flows at WWP structures will suffice. This guide also lists the file formats for each step so that the methodology can be adapted to use model results from any solver.

3.3.2   Input Topographic Data

Topographic data is input into iRIC as ".tpo" files. These are tab separated files consisting of the number of points in the file entered on the first line followed by the coordinates of each point on each successive line.

3.3.3   Create Computational Mesh

Once the topographic data file is entered, a computational mesh can be created. There are several options in Nays2DH for creating a mesh. The "grid from polygonal line and width" option is typically sufficient for the relatively short reaches of interest when modeling WWP structures. Mesh grid size should be minimized based on computer processing capabilities. Some models are capable of non-uniform or unstructured meshes that allow the user to create denser meshes in areas of interest, such as the chute of a WWP structure, while leaving the exterior areas sparser.

3.3.4   Set Calculation Conditions

Within Nays2DH, there are several important calculation conditions, which should be considered when modeling WWP structures. Here, we will highlight some of these conditions:

3.3.4.1   <u>Solver Type Options</u>

To optimize model accuracy and ability to adequately resolve complex flows typical of WWP structures, select the following options as shown in Figure 3.3:

 - Select solver type: +Advanced

 - Select finite differential method of advection terms: CIP method

- Select turbulent model: zero equation model or K-epsilon method
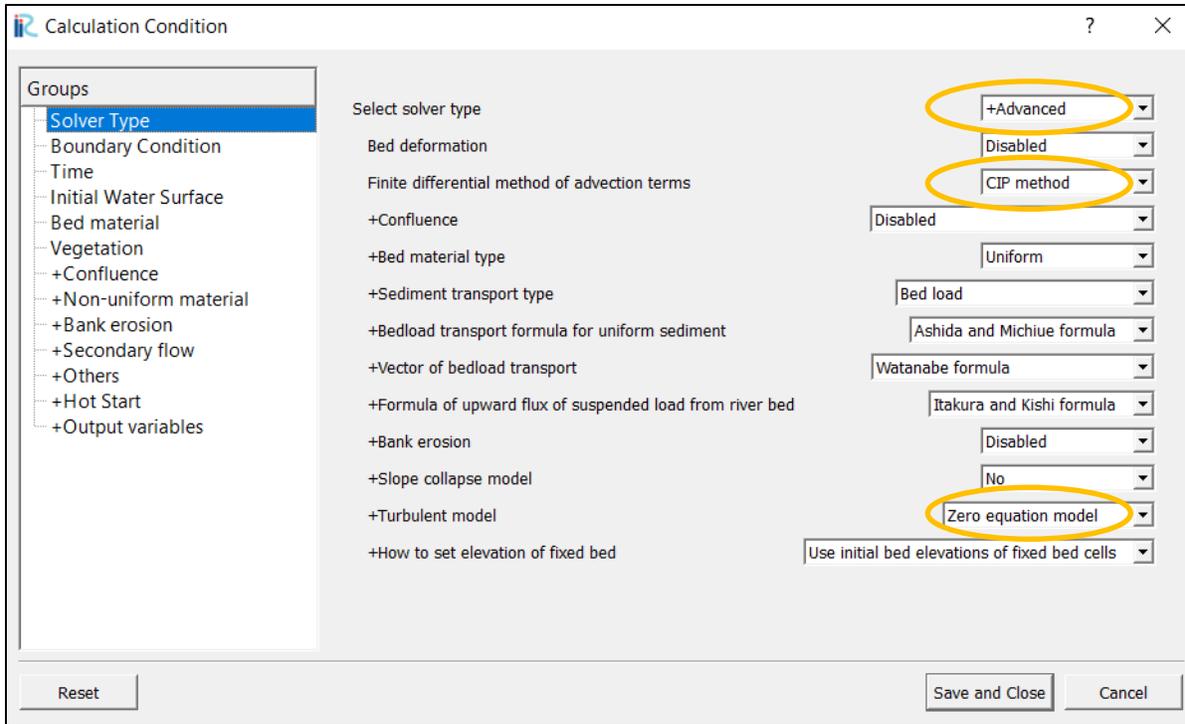
Figure 3.3. Nays2DH menu to select "Solver Type" options. Important considerations are highlighted.

3.3.4.2 <u>Boundary Condition Options</u>

The boundary conditions are dependent on the data available to the user. In Nays2DH, required boundary conditions are: water surface elevation at downstream, velocity at upstream, and discharge at upstream (Figure 3.4). In the example below, water surface at the downstream and the velocity at the upstream are both estimated from the uniform flow approximation, which is calculated internally from geographic data. The discharge at the upstream was entered as a constant value over the duration of the desired model. Be sure to model using a time unit of seconds and to ensure your units of discharge (m^3/s) are consistent.
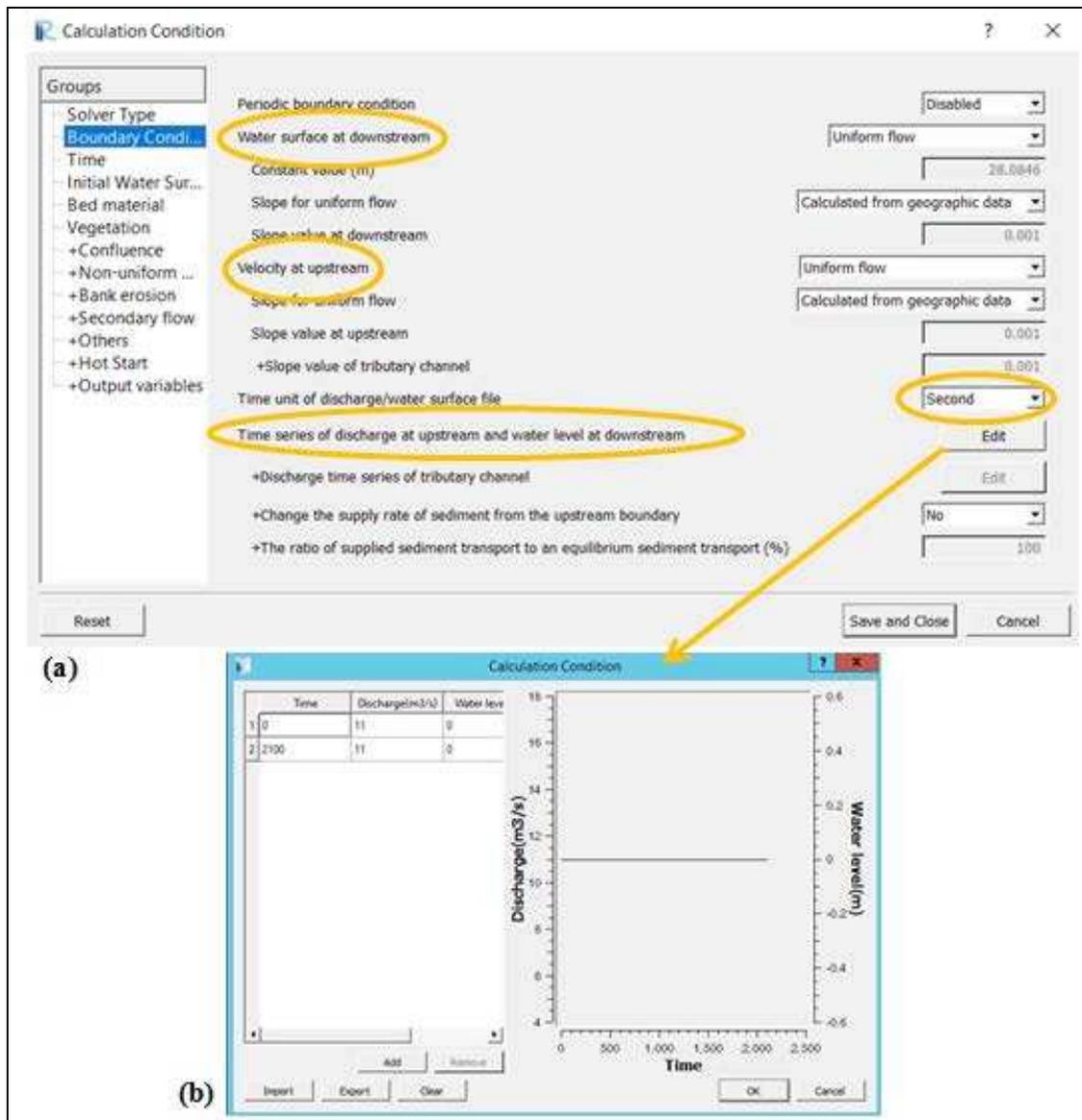
Figure 3.4. The "Boundary Conditions" options menu (a) in Nays2DH and (b) the window to enter discharge at upstream boundary by clicking "edit".

3.3.4.3   Time Options

Fundamental numerical analysis, based on the Courant-Friedrichs-Lewy (CFL) condition, tells us that for given spatial dimensions (i.e. mesh spacing) and flow condition (velocity) there is a maximum allowable time step necessary for the numerical model to converge. In essence, the CFL condition states that as the mesh spacing of a model decreases, the calculation time step must also decrease. This is important when modeling WWP structures because mesh spacing is

minimized in the creation of the computational mesh (see Section 3.3). Therefore, the

computational time step must also be small for the model to converge. For example, when

modeling a small WWP with uniform mesh spacing of 0.05 m a calculation time step of 0.0001

seconds was used as shown in Figure 3.5.
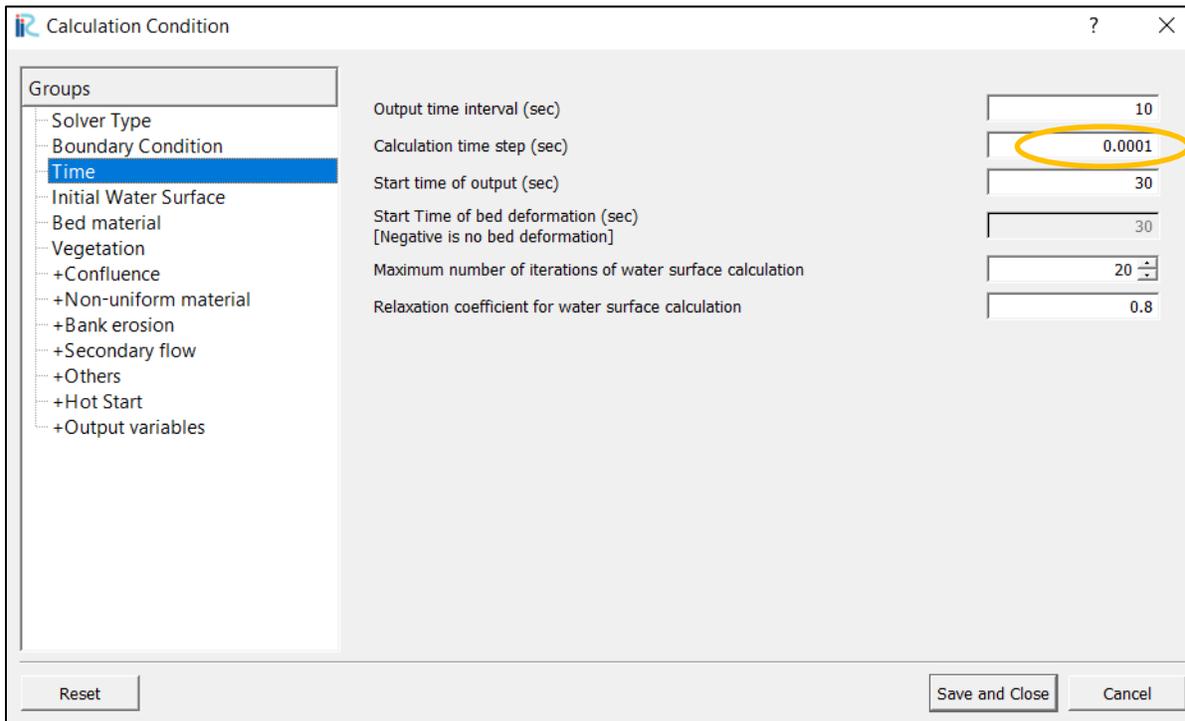
Figure 3.5. Nays2DH options for defining the "Time" constraints. The circle highlights the calculation time step.

3.3.4.4 Time Options

Roughness values are user assigned and typically used to validate hydraulic models. In

Nays2DH the roughness value is assigned to mesh nodes by drawing a polygon encompassing

the model space. If necessary, assigning a spatially varied roughness can be achieved using

multiple polygons. Nays2DH uses Manning's n values to compute roughness characteristics.

3.3.4.5 Exporting Results

Once the model has converged (i.e. the solution has become stable), model results are

exported as an unstructured grid file (.VTK) for each time step.

3.4 Streamline Development

This section provides the steps necessary to create streamlines from the 2D hydraulic model results. The 2D hydraulic model results are imported as unstructured grid files (.VTK) into the free, open-source data analysis and visualization software ParaView (Ayachit et al., 2015). Specifically, Paraview processes the model results by integrating the velocity vector field to create streamlines. Each individual streamline created will be analyzed with respect to the fish swimming criteria (flow depth and velocity). For more information on Paraview and its capabilities see the guide developed by Ayachit et al. (2015) or other online resources (http://Paraview.org).

The area of interest (AoI) is defined as the area most critical to fish passage where channel constriction and increase in local slope cause low flow depths and high velocities. To identify the AoI, we first locate the chute by identifying the four key zones in the water surface profile through the WWP structure: the gradual slope upstream, steep slope of the chute, the hydraulic jump, and the gradual slope downstream (Figure 3.6). We define the top of the chute (BL_{US}) as the location the water surface profile transitions from the gradual upstream slope to the steep slope in the chute. The bottom of the chute (BL_{DS}) is located downstream of the hydraulic jump as the water surface profile returns to a gradual slope. Hence, the longitudinal length of the chute (L_c) is defined as

$$L_c = BL_{US} - BL_{DS}.$$

The longitudinal length of the AoI (L_{AoI}) is then determined by the L_c with the addition of a buffer of half the L_c or,

$$L_{AoI} = L_c + (0.5)L_c.$$

The upstream and downstream longitudinal coordinates of the L_{AoI}, pt_{us} and pt_{DS}, respectively are used as a guide for ensuring streamlines are created outside of the AoI (Section 4.2) and in processing streamlines (Section 5).
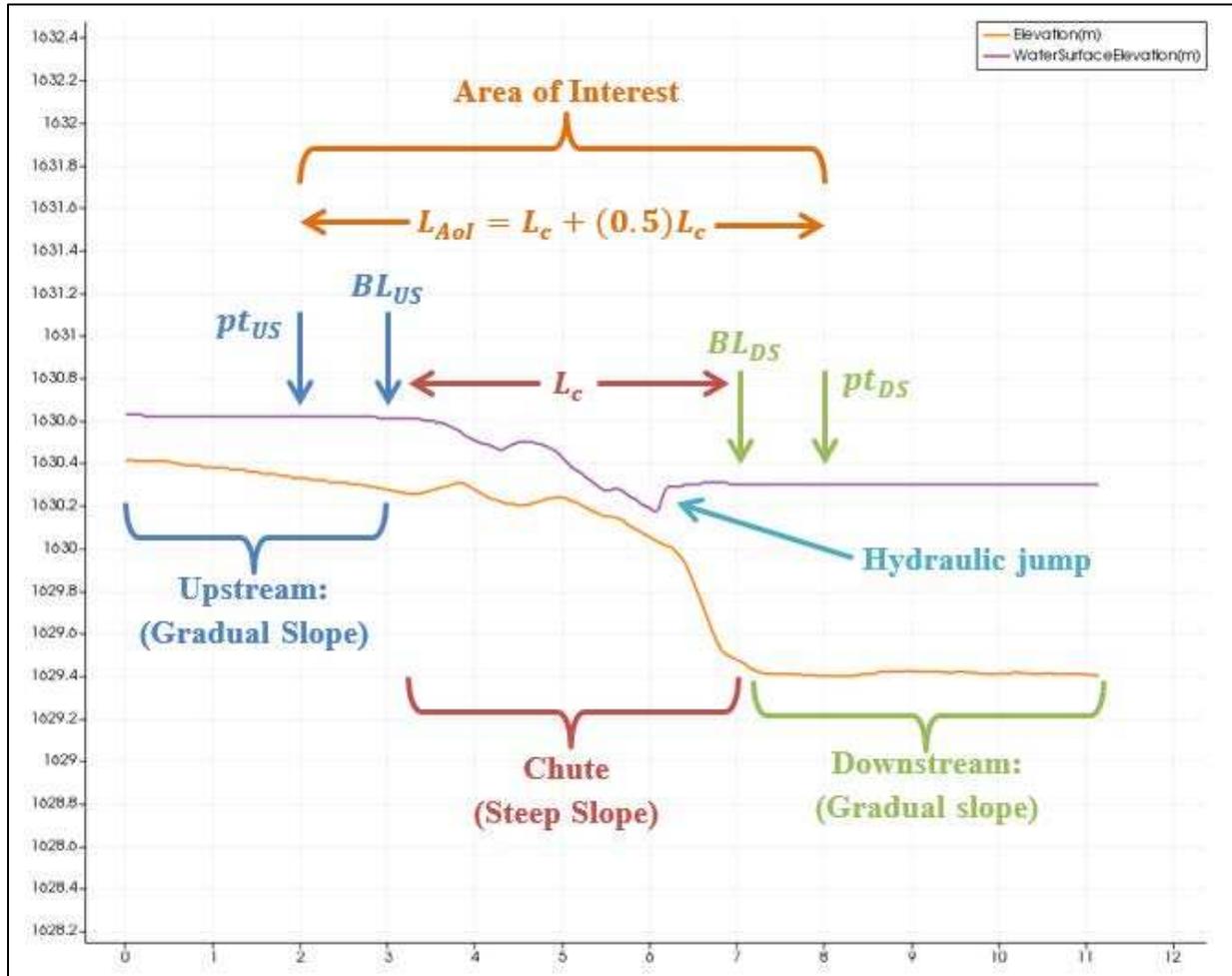
Figure 3.6. Schematic showing sample WSE and bed elevations of a WWP structure. Upstream and downstream of the WWP structure, the water surface slope varies gradually in contrast to the slope in the chute. The transition points (BL_{US}) and (BL_{DS}) are located upstream of the steep sloping chute and downstream of the hydraulic jump.

3.4.1 Import 2D Hydraulic Model Results

The following steps present the steps required to import the hydraulic steps into Paraview.

- Import the .VTK hydraulic results into the Pipeline Browser by clicking the open folder

  and selecting the desired file. This will load the file into the Pipeline Browser

  window (Figure 3.7a).

- With the file highlighted in the Pipeline Browser, click [Apply] in the properties

  window to bring the data into the Layout window (Figure 3.7b). (Note: for large files this

  may take some time and Paraview does not indicate it is applying the data). Notice that

  the hydraulic results show up as a solid color.

- To view scalar values of the hydraulic results, ensure the file is selected in the Pipeline

  Browser. Under the "coloring" section in the properties window, select the scalar value to

  be displayed. For now, view the elevation as a backdrop by selecting "Elevation" from

  the drop down list (Figure 3.7c). *Note: your color scheme may be different than shown

  here. To change your color scheme, see the "Coloring" section of the properties in your

  .VTK results file.

- It is often helpful to view results by overlaying the hydraulic data on top of the elevation

  data. To accomplish this, repeat the first two steps to add the same .VTK file to the layout

  view a second time. With the second instance of the .VTK file selected, choose "Depth"

  from the drop down box for Coloring in the properties window. The second results file

  added that is colored according to depth will be displayed on top (Figure 3.8).
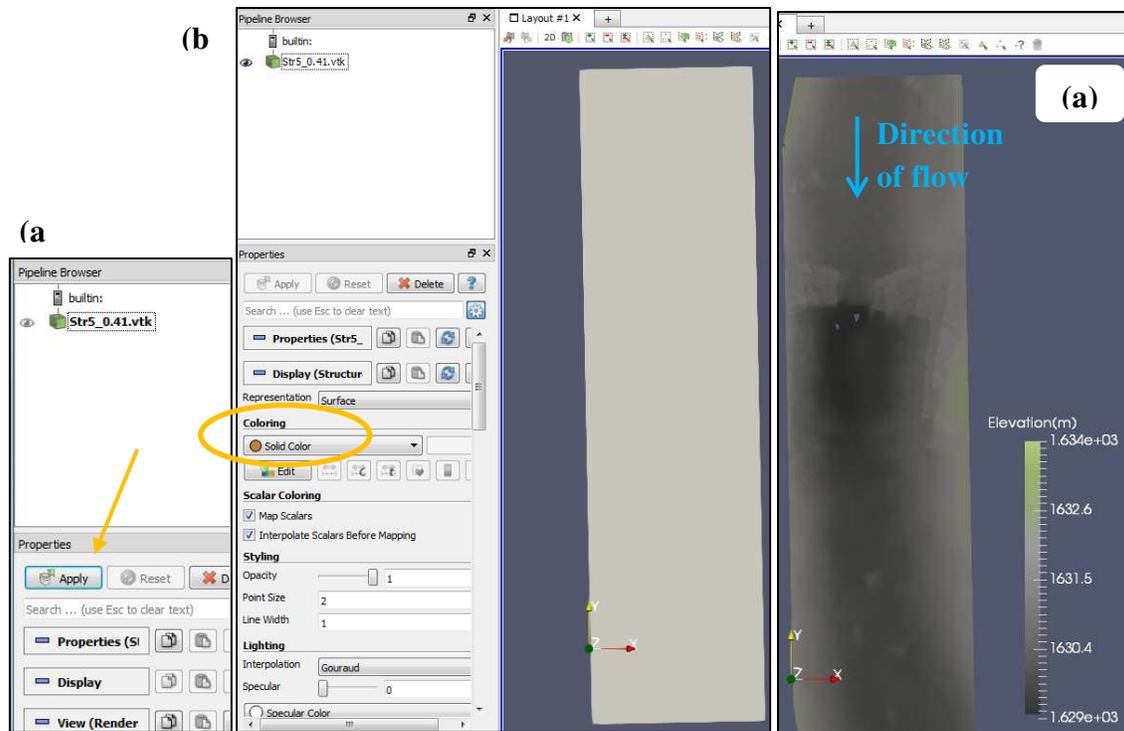
Figure 3.7. (a) Pipeline Browser window showing .VTK results file prior to "applying" data and (b) the .VTK results applied to the "LayoutView." The "Coloring" setting (circled) is set to solid color by default and (c) shown with scalar value elevation selected.
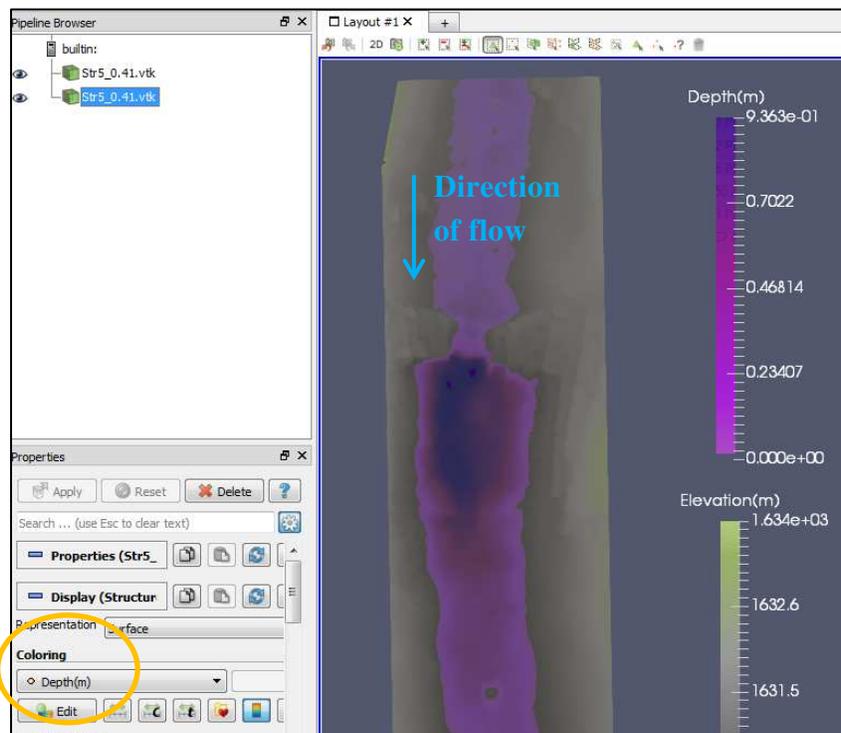
Figure 3.8. A second results file shown in the Pipeline Browser with the depth scalar selected, and displayed in the LayoutView.

3.4.2 Define the Area of Interest

The AoI is defined by using the "Plot Over Line" function in Paraview which returns scalar values along a plotted line at defined intervals.

- To create a "Plot Over Line," select the hydraulic results file in the Pipeline Browser as the source file and click [icon]. This will load a PlotOverLine object in the Pipeline Browser and a line spanning the extent of the results file in the LayoutView. *Note: the line shows up automatically and is often found only by zooming out to see the endpoints.*

- Place the start of the PlotOverLine (the end with the sphere) 5 – 10 meters upstream from the chute and the endpoint (the end with the arrow) 5-10 meters downstream of chute (Figure 3.9). Ensure that the Z-value for both endpoints on the line you create are equal to zero. The coordinates of the line endpoints can be seen and edited in the "Properties" tab (Figure 3.9).

- Click [Apply]. This will split the LayoutView with an added LineChartView window (Figure 3.9). *Note: default LineChartView plots all variables of the source file.*

- Clicking on the chart area in LineChartView will bring up the chart properties in the Properties window. Under "Series Parameters" select only water surface elevation and bed elevation. Leave the default X Array Name as arc_length, which is the longitudinal value of the Plot Over Line. The LineChartView should now only show the water surface elevation and bed elevation as seen in Figure 3.10.

- Adjust the axes scales by clicking and holding the right mouse button in the chart area. Drag up and down to adjust the y-axis or left and right to adjust the x-axis. Adjust the axes until the WSE and Elevation plots are easier to read (Figure 3.11). Now, determine the locations of the chute and AoI following the schematic in Figure HH. Once, pt_{US}

and pt_{DS} are located, record the corresponding arc_length value by rolling the mouse over the location in LineChartView1.
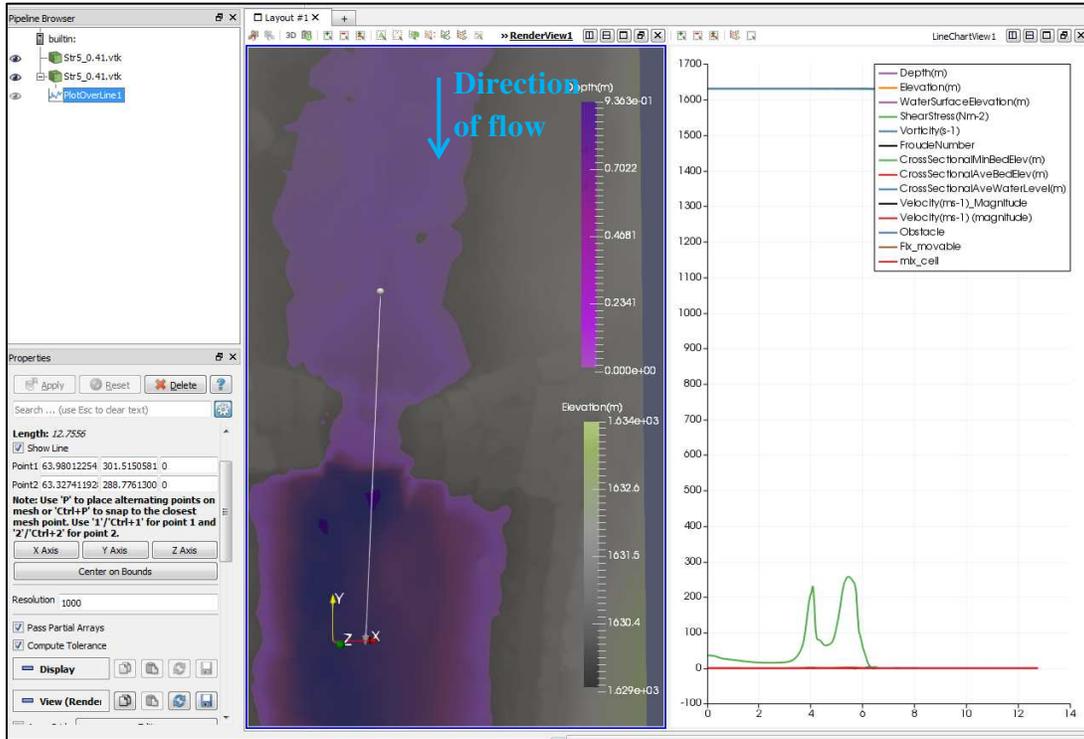
Figure 3.9. Screenshot showing "PlotOverLine" through the center of the chute alongside the "LineChartView" plotting all the scalar values included in the source file.
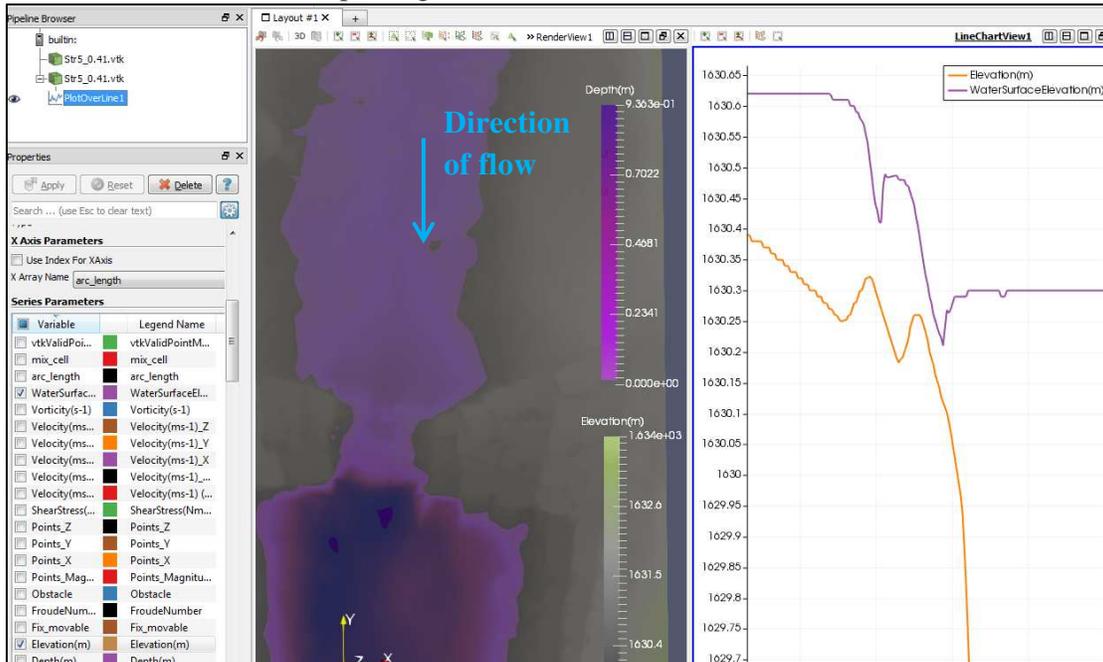
Figure 3.10. Screenshot showing water surface elevation and bed elevation selected as PlotOverLine parameters in the Properties window and the corresponding LineChartView.

- Next, show only the PlotOverLine1 object in the RenderView1 window by deselecting

 the two results files in the Pipeline Browser window (👁 → 👁).
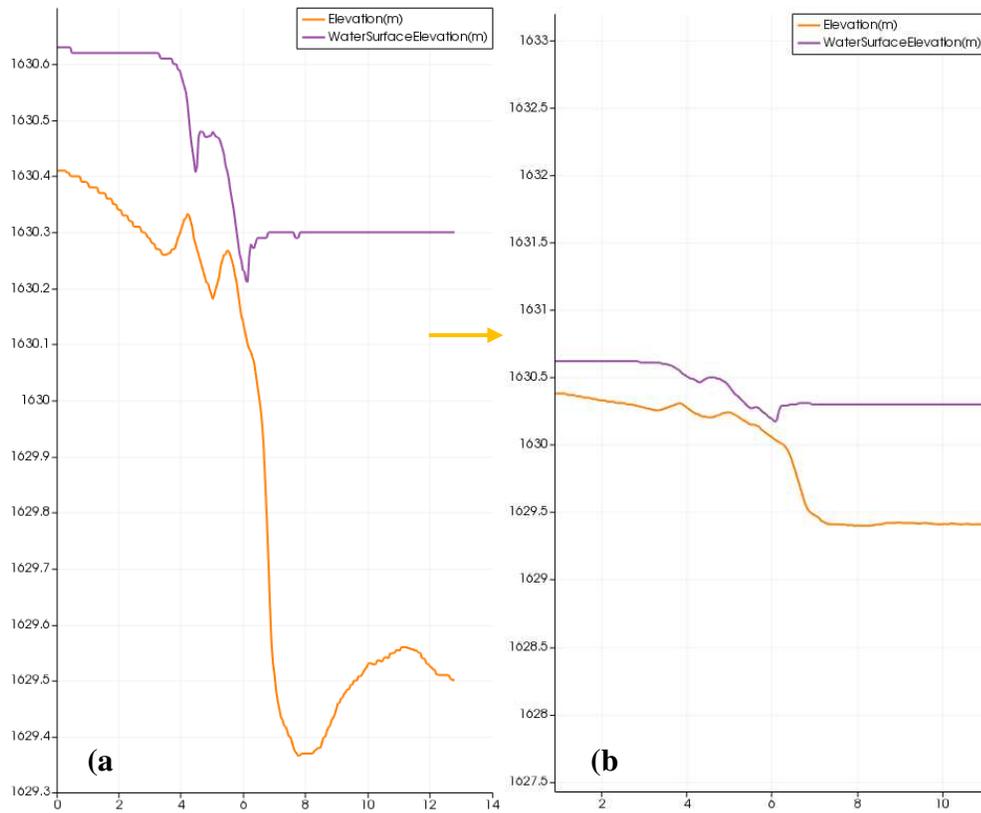
Figure 3.11. LineChartView (a) before and (b) after axes adjustment.

- On the top toolbar in RenderView1, click the "Hover Points On" ·? tool.

- While hovering over the PlotOverLine1, identify pt_{US} and pt_{DS} using the arc_length

 value and record the geographic coordinates (X,Y) from the "Coords" variable displayed

 (Figure 3.12). These values will be used in the next steps to place the streamlines. *Note:

 the "Hover Points On" tool can be somewhat imprecise. If it is difficult to identify the

 exact location, always err to the direction away from the AoI.*
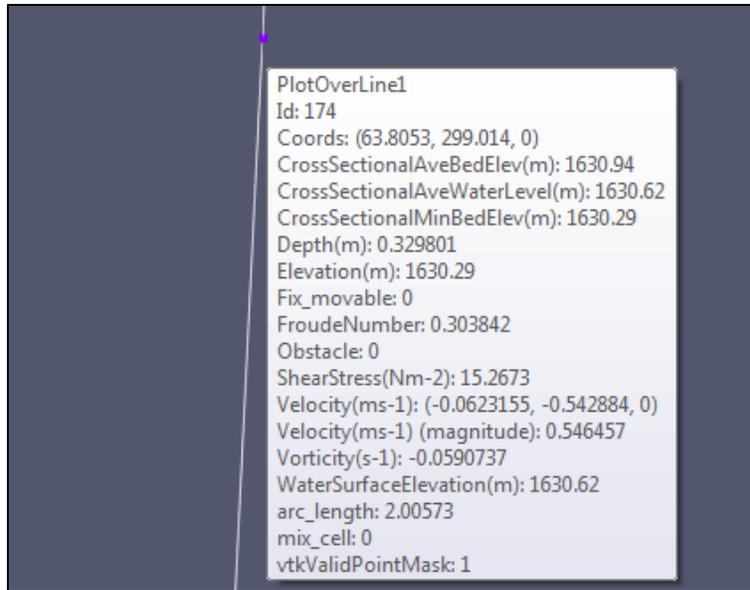
Figure 3.12. Screenshot of the "Hover Points On" tool to locate the arc_length to obtain the geographic coordinates.

3.4.3   Create Streamlines

The preparation is now completed so that streamlines can be created. As a general guideline, create streamlines with 0.01 m spacing (resolution = 100 streamlines per 1 m length). This value may depend on the size of the WWP structure, the size of model results files, and computing capabilities. It is suggested to add another layer of the results data into the Pipeline on which to compute the streamlines.

Upstream and downstream streamlines will be computed separately. The upstream streamlines will be created first:

- Click the "Stream Tracer" filter on the toolbar ![icon] . This brings a StreamTracer1 object into the Pipeline Browser window. *Note: the StreamTracer object may not immediately become visible in the LayoutView. The default mode typically creates a point source (seeds created from a single point, however it may show up as a line source as well. It may help to zoom out to locate the StreamTracer.*

68

- Under "Integration Parameters" in the Properties window, change the integration direction for the upstream streamlines to FORWARD.

- Under "Seeds" in the Properties window, select "High Resolution Line Source." This brings up a line over the results in the LayoutView Adjust the endpoints of the line so that they are approximately perpendicular to the flow directly upstream of the AoI and approximately 0.5 m upstream of the pt_{US} (Figure 3.13). *Note: The additional 0.5 m buffer extension beyond the pt_{US} will ensure the streamlines are processed properly.*

- Extend the endpoints of the line to the modeled edge of water or slightly beyond to include the entire flow field (Figure 3.13). To compute the streamlines, click [Apply] and the streamlines should plot in the LayoutView. *Note: Creating streamlines may be an iterative process with the goal of covering as much of the modeled flow field with streamlines. Any changes must be re-computed by clicking* [Apply] .

- Under "Streamline Parameters", decrease the maximum streamline length so that all streamlines created pass through the downstream extent of the AoI but not far beyond. This length will depend on the specific project, but a good starting point is 20 m. This will avoid computing excess data outside of the AoI and help minimize file sizes. Determining an appropriate streamline length may require several iterations. *Note: The StreamTracer object will likely resemble a surface, but zooming in will allow individual streamlines to come into focus.*

- For computing streamlines at one WWP structure for multiple flows, use the same StreamTracer source object. To do so, import all modeled hydraulic results files using the open folder button. Right click on the StreamTracer object in the Pipeline Browser,

select "Change Input…" Select the new results file. Minor adjustments to the endpoints might be required to capture the new flow field.
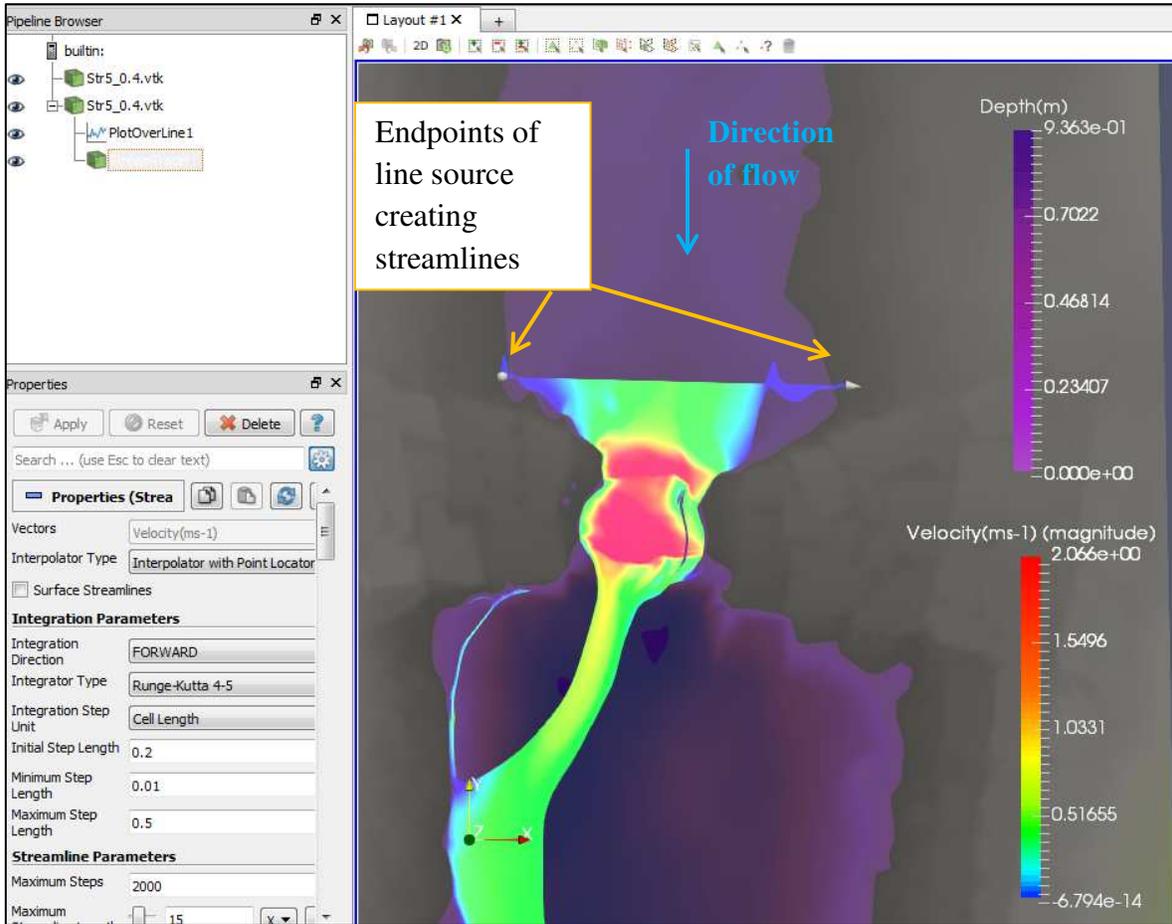
Figure 3.13. Completed upstream streamlines displaying velocity scalar. The endpoints are highlighted by arrows. The line source is perpendicular to the main direction of flow.

Next, create the downstream streamlines by following the above steps with minor alterations:

- Click the "Stream Tracer" filter on the toolbar ⌇. This brings a StreamTracer2 object into the Pipeline Browser window.

- Under "Integration Parameters" in the Properties window, change the integration direction for the upstream streamlines to BACKWARD.

- Under "Seeds" in the Properties window, select "High Resolution Line Source." This brings up a line over the results in the LayoutView Adjust the endpoints of the line so that they are

70

approximately perpendicular to the main flow direction (parallel to the upstream line source) of the AoI and approximately 0.5 m downstream of the pt_{DS} .

- Extend the endpoints of the line to the modeled edge of water or slightly beyond to include the entire flow field. To compute the streamlines, click [Apply] and the streamlines should plot in the LayoutView. *Note: Creating streamlines may be an iterative process with the goal of covering as much of the modeled flow field with streamlines. Any changes must be re-computed by clicking* [Apply] *.*
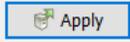
- Under "Streamline Parameters", decrease the maximum streamline length so that streamlines created pass through the upstream extent of the AoI, but not far beyond. Again, 20 m is a good starting point and this may require several iterations.

3.4.4   Compiling the Streamline Data

The streamlines created have information for individual points along the streamlines (called "Point Data") and for individual streamlines (called "Cell Data"). These data will be combined to determine which points belong to which streamline. To illustrate this, each type of dataset will be examined in the Spreadsheet View in Paraview:

- Examine the streamline data in spreadsheet view by clicking the split screen icon next to "RenderView1" RenderView1 ☐ . This will bring up a "Create View" menu list.

- Click SpreadSheet View. When "Point Data" is selected under "Attribute," a large table with hydraulic results data associated with each point along each streamline is displayed.

- Switch the "Attribute" to select "Cell Data" to display information about individual streamlines. Notice each streamline has a SeedId.

Now, combine the point data and cell data.

- Press Crtl + Spacebar to open a search for "Sources." Type "Cell Data to Point Data," select it from the menu, and press Enter.

- This will bring up a "CellDatatoPointData1" object in the Pipeline Browser window. Under Properties, click .

- To view the newly created dataset, ensure that "CellDatatoPointData1" is selected under the "Showing" drop down menu in the Spreadsheet View window. The same hydraulic results data as the Point Data are displayed, except that now the Cell Data (including SeedId) are included as well. This SeedId is used to separate the point data by individual streamlines.

3.4.5 Saving the Two Streamlines Files

Save the streamline data as two comma-separated (.csv) files: one for the upstream and one for the downstream.

- Select the streamline file in the Pipeline Browser and click the save button .

- Select a directory, and name each file using the following naming scheme: Str1_0.40_US.csv and Str1_0.40_DS.csv where Str1 corresponds to an individual WWP structure, 0.40 is the modeled flow, and US/DS represents whether the dataset is from upstream or downstream of the structure.

- A "Configure Writer" window will appear. Leave the default settings and click "OK."

  Note: This may take a few minutes if the file size is large.

3.5 Streamline Analysis (using Matlab)

The upstream and downstream streamline files are analyzed based on selected fish swimming criteria for flow depth and velocity. A script was written in Matlab, which first imports the streamline files (.csv) from Paraview. The script then isolates the individual streamlines and crops them to include only streamlines within the AoI. Streamlines are then split

between complete (start and end at opposite ends of the AoI) and incomplete streamlines (start at

one end of the AoI and never reach the opposite end) (Figure 3.14).
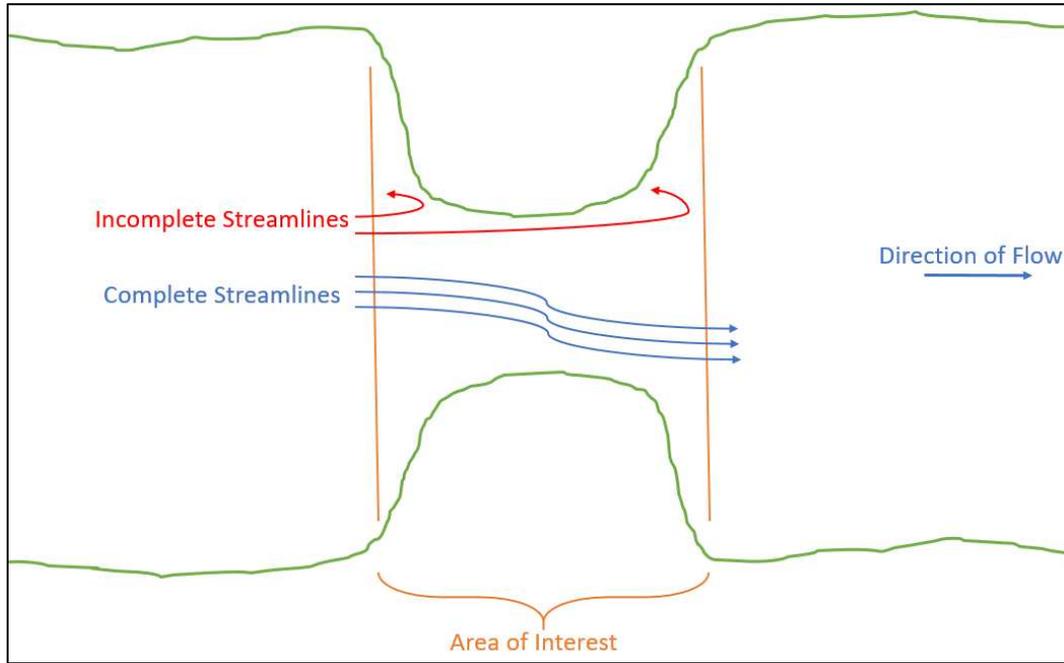
Figure 3.14. A schematic of WWP structure (green) shows incomplete (red) and complete (blue) streamlines originating from upstream of the AoI (orange), with the direction of flow to the right.

Incomplete streamlines are connected to the closest complete streamline. The maximum

distance between connection points is a user designated input (default set at 0.15 cm).

3.5.1 The Matlab Script

The streamline analysis is conducted within the "StreamlineAnalysis.m" Matlab script.

This script is written to analyze one user-selected WWP structure for any number of user-

designated flows in m^3/s. The script loops through each flow.

The points on each streamline are isolated and cropped to include only points within the

AoI. Complete streamlines are defined as those that cross both upstream and downstream

boundaries. Incomplete streamlines are those that do not reach the opposite boundary, either

stopping prematurely (velocity approached 0 m/s), recirculating back to the same boundary, or

reaching the specified length limit. Incomplete streamlines that recirculated back to their original

73

boundaries are split at the inflection point to create two separate incomplete streamlines. All incomplete streamlines are connected from the terminal point to the closest point of a complete streamline, provided that the distance between the terminal point and the closest complete streamline does not exceed a user-specified distance (default value = 0.15 m). This process is conducted iteratively so that a newly connected streamline becomes a complete streamline to which an incomplete streamline can be connected. Any incomplete streamlines that remain after this process are removed, so that only complete streamlines are used in this analysis.

Complete streamlines are processed based on user-designated fish swimming criteria. The script also creates summary plots showing streamlines and how they as well as summary files (saved as Matlab files).

3.5.2 The Matlab Script

Each streamline is evaluated based on fish swimming criteria for minimum flow depth and maximum velocity. If any point on a streamline does not meet one of the criteria, it is determined to be impassable. For a given structure at a given flow, the fraction of the impassable streamlines is computed.

Streamlines are evaluated through the AoI at five equally spaced cross sections. The point of intersection between a cross section and passable streamlines are recorded. The distance between intersections of consecutive passable streamlines were calculated and summed to determine the passable width across each cross-section.

Please refer to Chapter 1 and Stephens et al. (2015) for more information on streamline evaluation variables.

3.5.3   User Tutorial

The script is set up to load Paraview streamline files created in Section 4, given that they are in the same directory as the Matlab script file. The following is a list of all required user inputs organized by their corresponding script line:

Line 8– Select the structure to be modeled

Line 11– Enter a vector of the modeled flows in units of m^3/s

Line 15 – Enter the maximum allowable distance to connect incomplete streamlines to complete streamlines

Line 19 – Enter the desired buffer to apply outside of AoI. Default value = 0.3 m (recommended)

Line 22/24 – Define minimum swimming depth criteria (this is based on fish assemblage present in stream). Default values are selected for salmonid species (Rainbow and Brown trout).

Line 28 – select the desired fish lengths to be analyzed. This vector value divides the range of fish lengths to be analyzed into size classes.

Line 31/32 – Define the burst swimming speed for fish assemblage. Default values of 10 body lengths per second and 25 body lengths per second. **Note: These values are based on salmonid species (Rainbow and Brown trout).*

Line 36 – Initialize the 3-dimensional results matrix:

- Rows: number of modeled flows

- Columns: number of size fish size classes

- Depth: number of streamline evaluation variables being analyzed. The script is set up for 8 variables as described above.

The script then loops through each modeled flow defined on L*ine 11*. Paraview streamline files are For each structure in the switch function (*Line 54 – 88*) there are several user inputs:

pt_us – refers to the (X,Y) point defined as pt_{US} from Section 4.2

pt_ds - refers to the (X,Y) point defined as pt_{DS} from Section 4.2

rot – defined as the counter-clockwise angle necessary to rotate the hydraulic results data so that the main flow axis is in the +x direction.

There are also several plotting specifications that are relevant to each structure. These values can be obtained either iteratively by visualizing results or in analyzing the hydraulic results data.

3.5.4 Visualizing Results

A results matrix is created to report the fraction of impassable streamlines for each structure, at each flow modeled, and for all the streamline evaluation variables (*lines 690 – 697*). This is saved as a Matlab file (.m) for further summary. A streamline summary matrix records the number of streamlines at various steps throughout the script (*lines 701 – 706*). The script plots the streamlines used in the analysis (named "Figures 1-3" in the script, Figure 3.15). Passable streamlines are colored blue and impassable streamlines are colored red. These plots also include passable width cross sections for all flows used in the analysis. Figure 1.3 summarizes the passable widths for each of the variables (Figure 3.16).
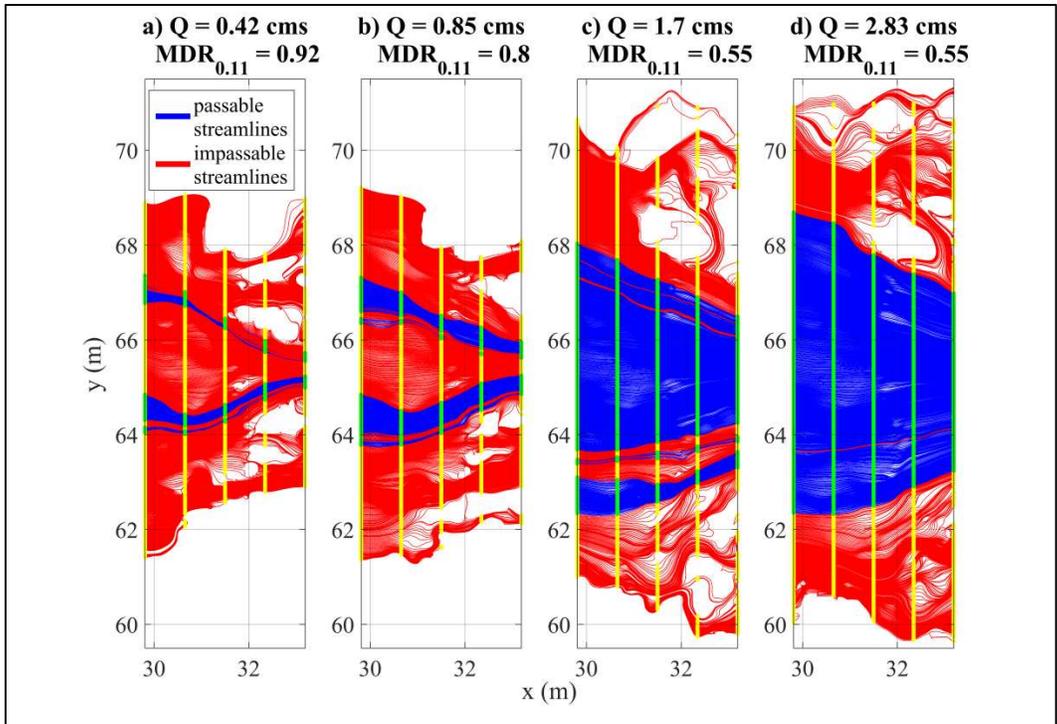
Figure 3.15. Example of streamline summary plots for one structure at 4 different discharges showing passable streamlines (blue) and impassable streamlines (red). Cross section intersection points are plotted for passable (green) and impassable (yellow).
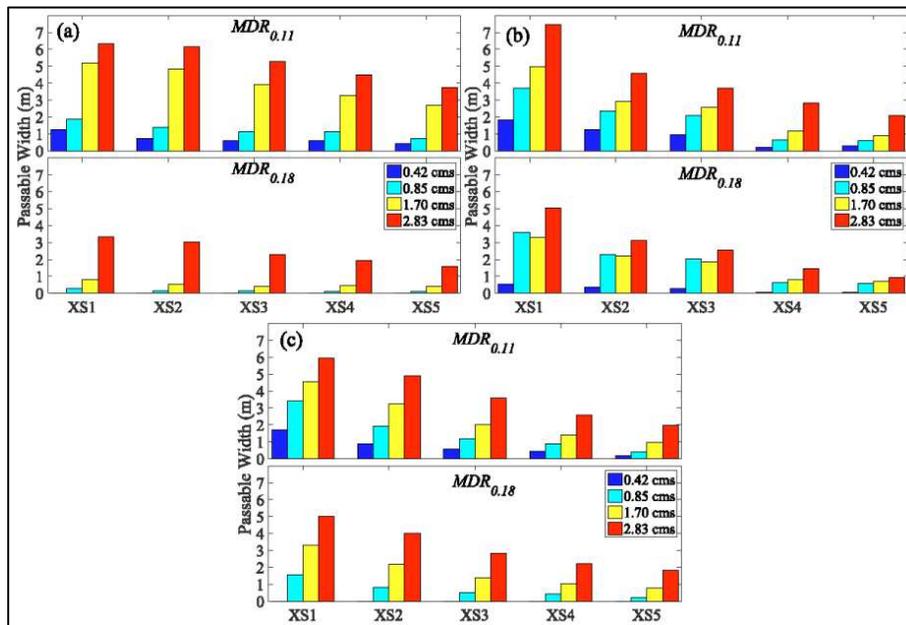
Figure 3.16. Example output of Figure 1.3 summarizing passable widths for two depth criteria at three different structures.

REFERENCES

Ayachit, U., Bauer, A., Chaudhary, A., DeMarle, D., Geveci, B., Jourdain, S., Lutz, K., Marion, P., Maynard, R., Shetty, N., Yuan, Y., 2015. The ParaView Guide. Kitware. Kitware Inc. doi:10.1017/CBO9781107415324.004

Fox, B.D., Bledsoe, B.P., Kolden, E., Kondratieff, M.C., Myrick, C.A., 2016. Eco-hydraulic evaluation of a whitewater park as a fish passage barrier. J. Am. Water Resour. Assoc. 52, 420–442. doi:10.1111/1752-1688.12397

Nelson, J.M., Shimizu, Y., Abe, T., Asahi, K., Gamou, M., Inoue, T., Iwasaki, T., Kakinuma, T., Kawamura, S., Kimura, I., Kyuka, T., McDonald, R.R., Nabi, M., Nakatsugawa, M., Simoes, F.R., Takebayashi, H., Watanabe, Y., 2016. The international river interface cooperative: Public domain flow and morphodynamics software for education and applications. Adv. Water Resour. 93, 62–74. doi:10.1016/j.advwatres.2015.09.017

Stephens, T.A., Bledsoe, B.P., Fox, B.D., Kolden, E., Kondratieff, M.C., 2015. Effects of whitewater parks on fish passage: A spatially explicit hydraulic analysis. Ecol. Eng. 83, 305–318. doi:10.1016/j.ecoleng.2015.06.032

Takebayashi, H., Shimizu, Y., 2014. iRIC Software Nays2DH Solver Manual.

APPENDIX A: 2D APPROACH DIFFERENCES

Erin Ryan (2015) conducted a 2D comparative analysis similar to the study discussed here. One key difference is that Ryan's study analyzed only one of the three WWP structures studied in the Stephens et al. (2015) 3D study. This study utilized some of the methods put forth in Ryan's initial study, however some alterations were made. The following is a list distinguishing factors between Ryan's initial study and the study described here, with the reasons changes were made

Table A1. Outline of the differences between Ryan's study and the current study.

Difference	Ryan (2015)	Current Study	Reasoning for alteration
# of structures studied	1	3	Time availability
CFD model used	River2D	Nays2DH (in iRIC)	- The iRIC software supports a wide array of different CFD and morphodynamic model solvers. This allows for modelers to switch between solvers with ease, based on project needs. Nays2DH has the optional CIP method solves complex flows with better accuracy in areas of locally unsteady flow conditions, like steep slopes through a WWP structure (Nelson et al., 2016; Takebayashi and Shimizu, 2014). - River2D, on the other hand, is not recommended for steep slopes (Steffler and Blackburn, 2002)
Model Results Visualization Software	Blue Kenue (2011)	Paraview (Ayachit et al., 2015)	- Paraview is a widely used software program for complex flow visualization projects.
Statistical Analysis	JMP Pro 11	R	- This study performed the statistical analysis using the free programming scripting language R (JMP Pro is proprietary and requires a license) - By developing a structured script using a free software package, the aim is to develop an inexpensive, fully-transferrable methodology

APPENDIX B: WORKFLOW FOR EVALUATING WWPS USING 2D APPROACH
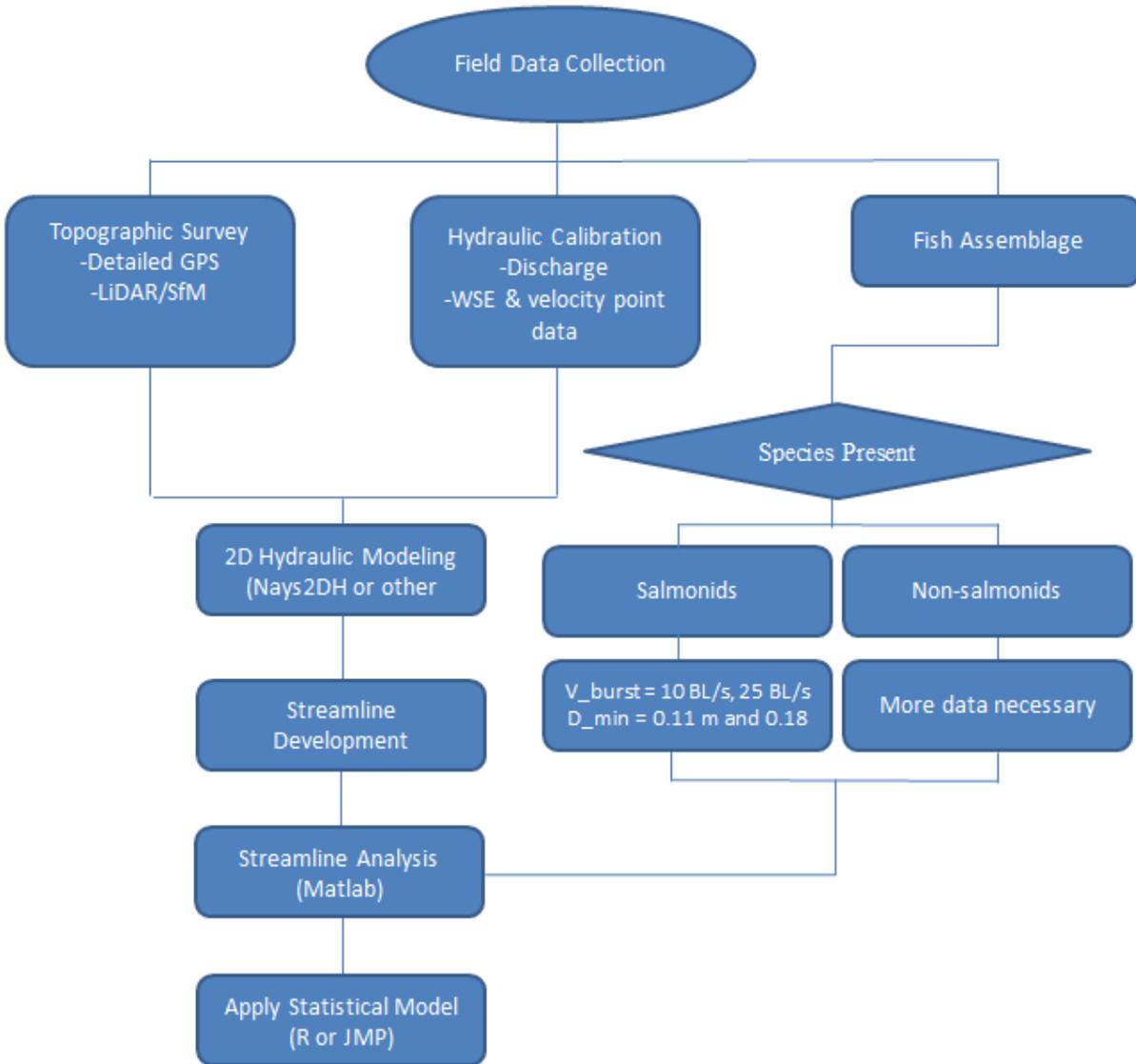
Fig B. A diagram of the workflow required for evaluating WWP using a spatially explicit, 2D CFD modeling approach.

APPENDIX C: HYDRAULIC RESULTS SHOWN AS STREAMLINES

Appendix C presents Figures C1 – C3 showing example hydraulic model results shown as streamlines.
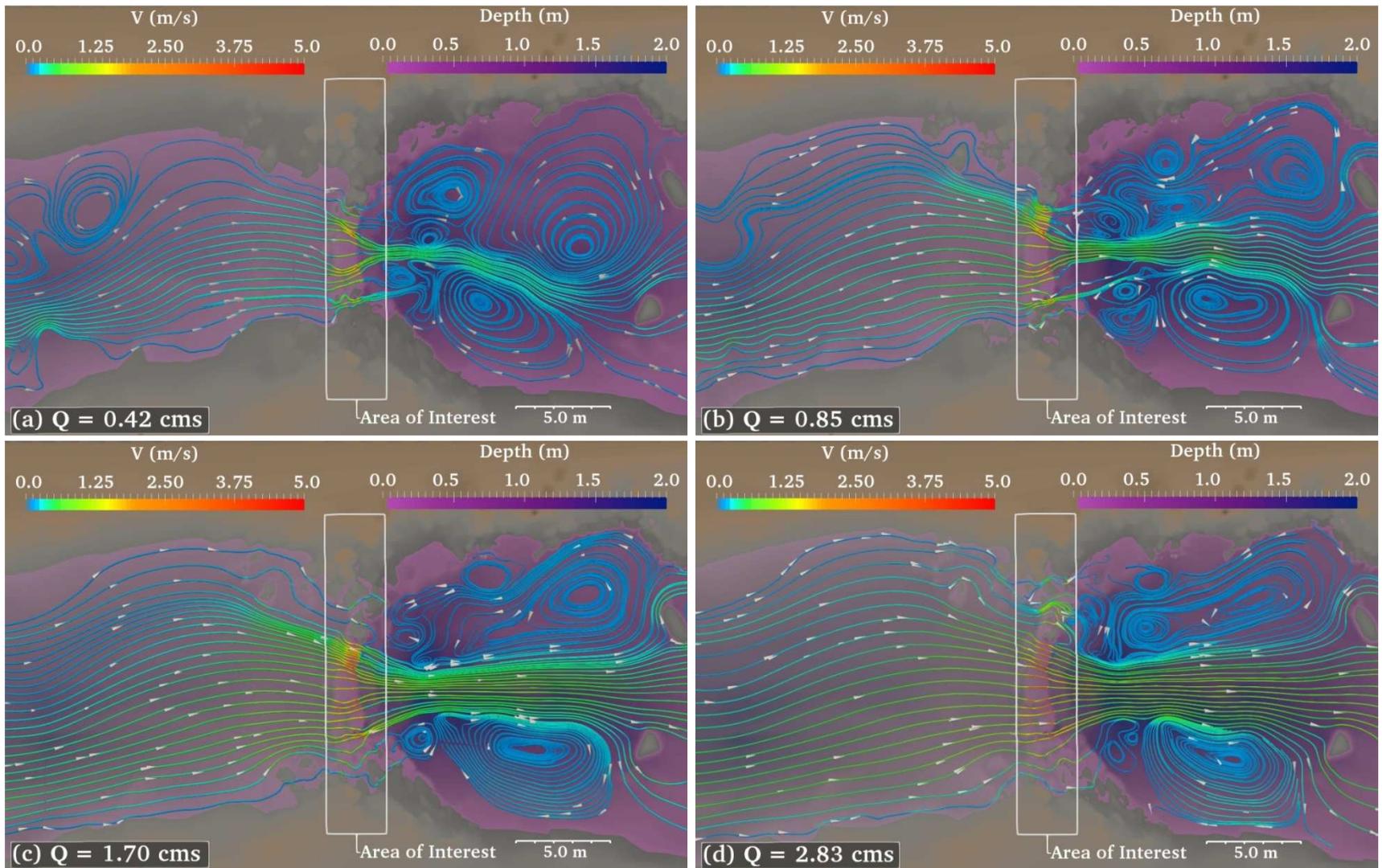
Figure C1. Example results at WWP1 showing depth and velocity along streamlines for (a) Q = 0.42 cms, (b) Q = 0.85 cms, (c) Q = 1.70 cms, and (d) Q = 2.83 cms. **Note:** Actual numbers of streamlines shown are approximately 3% of number of streamlines used in analysis.
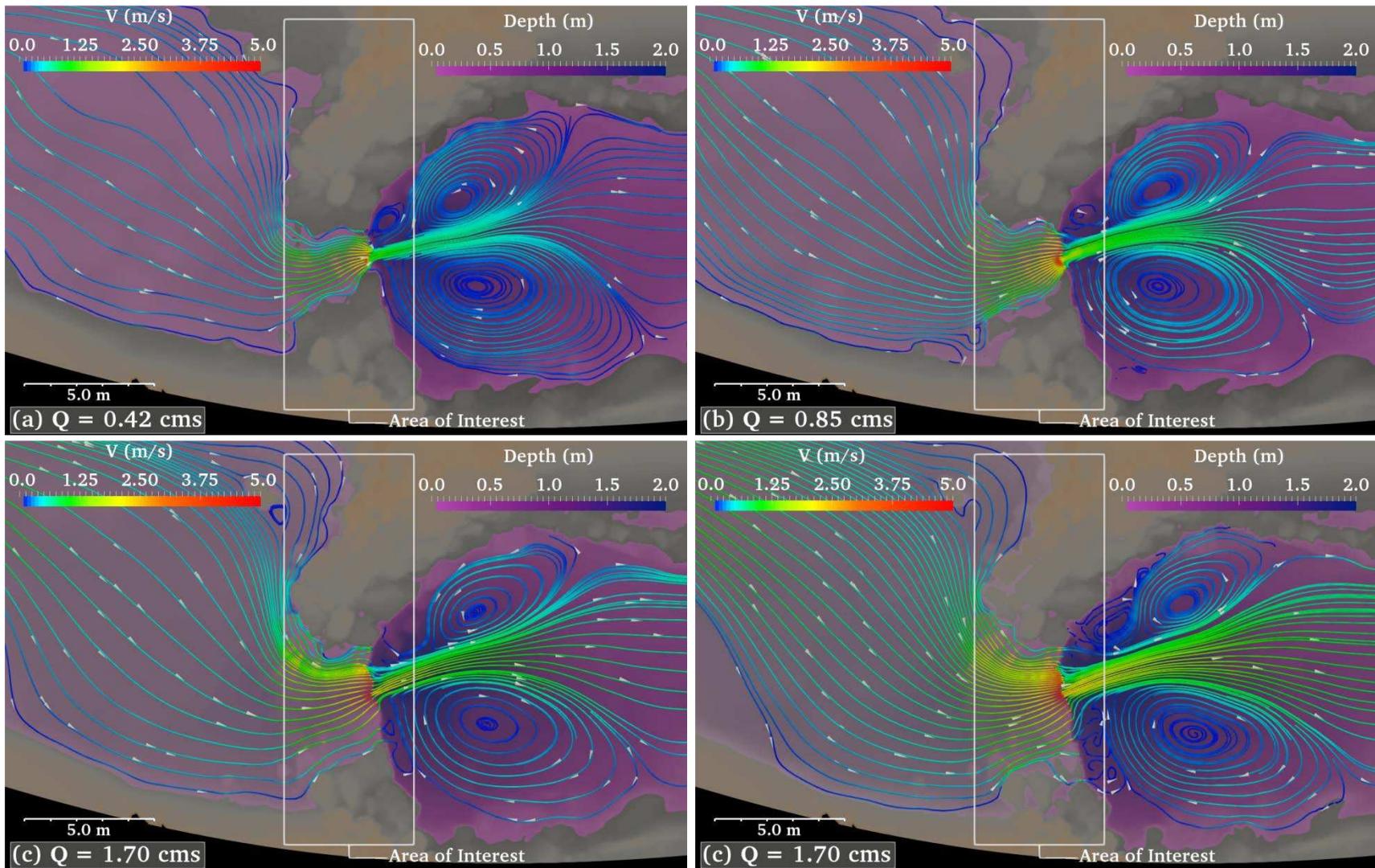
Figure C2. Example results at WWP2 showing depth and velocity along streamlines for (a) Q = 0.42 cms, (b) Q = 0.85 cms, (c) Q = 1.70 cms, and (d) Q = 2.83 cms. **Note:** Actual numbers of streamlines shown are approximately 3% of number of streamlines used in analysis.
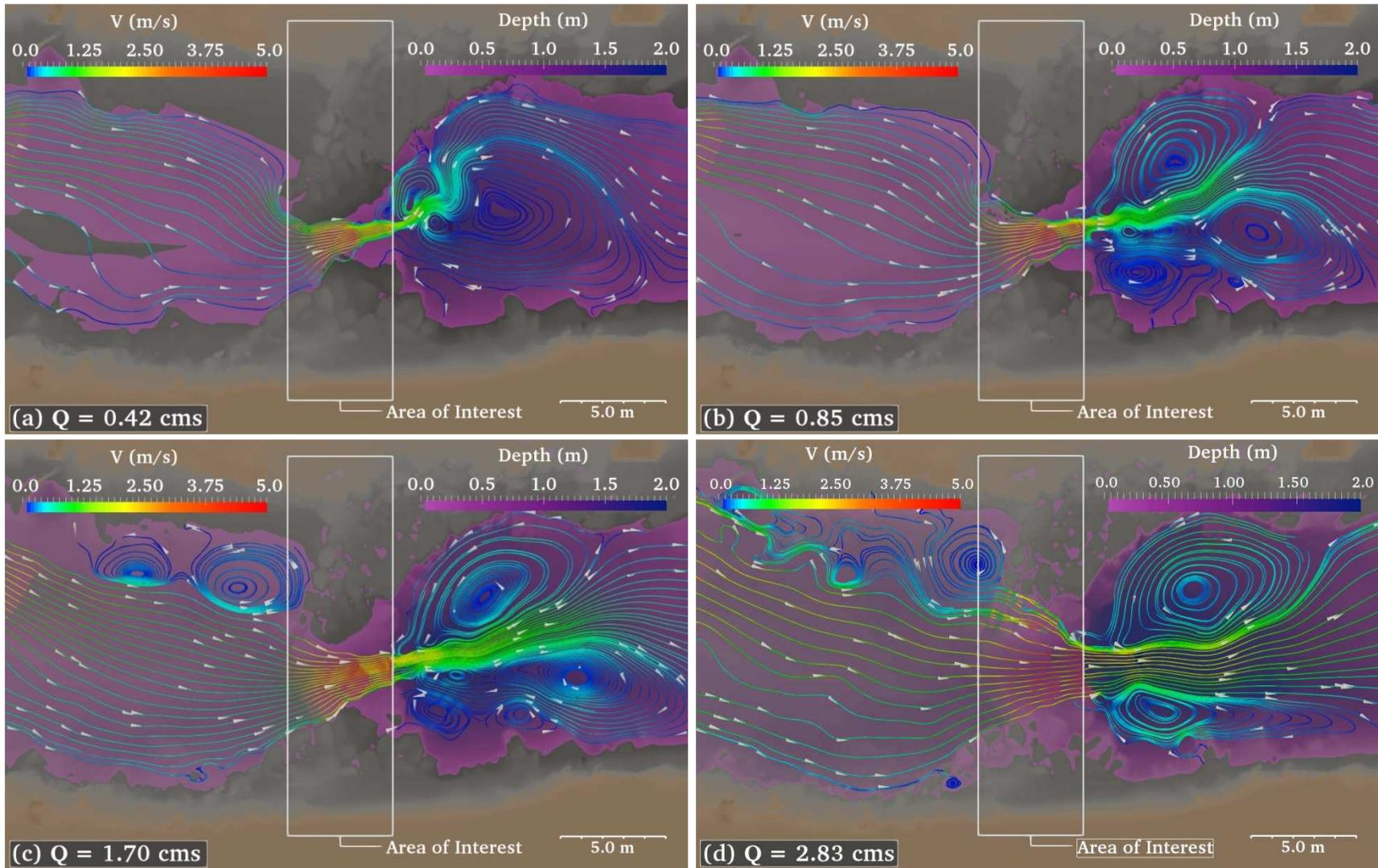
Figure C3. Example results at WWP3 showing depth and velocity along streamlines for (a) Q = 0.42 cms, (b) Q = 0.85 cms, (c) Q = 1.70 cms, and (d) Q = 2.83 cms. **Note:** Actual numbers of streamlines shown are approximately 3% of number of streamlines used in analysis.

84

APPENDIX D: FRACTION OF IMPASSABLE STREAMLINES

Appendix D presents Tables D1 – D18 showing the fraction of impassable streamlines for every WWP structure, at every modeled discharge, and for every fish size class.

Table D1. MVR_{10} from 2D model

	Discharge (cms)	Fish Lengths (m)												
		0.1	0.125	0.15	0.175	0.2	0.225	0.25	0.275	0.3	0.325	0.35	0.375	0.4
WWP1	0.42	0.61	0.26	0.18	0.12	0.07	0.01	0	0	0	0	0	0	0
	0.85	0.81	0.68	0.40	0.31	0.20	0.10	0.01	0	0	0	0	0	0
	1.7	0.66	0.63	0.61	0.53	0.33	0.21	0.14	0.07	0.03	0.01	0	0	0
	2.83	0.80	0.53	0.50	0.47	0.44	0.38	0.19	0.10	0.05	0.02	0	0	0
WWP2	0.42	0.74	0.42	0.38	0.32	0.18	0.14	0.10	0.08	0.03	0	0	0	0
	0.85	0.76	0.74	0.72	0.56	0.46	0.34	0.27	0.19	0.14	0.11	0.06	0	0
	1.7	1	0.96	0.69	0.65	0.57	0.54	0.45	0.29	0.25	0.17	0.15	0.10	0.05
	2.83	1	0.99	0.97	0.96	0.94	0.81	0.68	0.58	0.46	0.33	0.28	0.21	0.10
WWP3	0.42	0.47	0.35	0.23	0.21	0.17	0.12	0.08	0	0	0	0	0	0
	0.85	1	0.95	0.92	0.72	0.65	0.57	0.42	0.29	0.13	0	0	0	0
	1.7	1	1	1	0.96	0.95	0.93	0.84	0.70	0.51	0.27	0.13	0.05	0.01
	2.83	1	1	1	1	1	0.96	0.82	0.66	0.57	0.48	0.38	0.20	0.08

Table D2. MVR_{10} from 3D model

	Discharge (cms)	Fish Lengths (m)												
		0.1	0.125	0.15	0.175	0.2	0.225	0.25	0.275	0.3	0.325	0.35	0.375	0.4
WWP1	0.42	1	1	1	1	1	0.93	0.89	0.75	0.53	0.16	0.12	0.12	0.11
	0.85	1	1	1	1	1	1	1	0.75	0.58	0.39	0.2	0.12	0.09
	1.7	1	1	1	1	1	1	1	0.99	0.96	0.26	0.17	0.13	0.12
	2.83	1	1	1	1	1	1	1	1	0.96	0.93	0.62	0.21	0.12
WWP2	0.42	1	1	1	1	1	1	1	1	0.88	0.25	0.15	0.11	0.06
	0.85	1	1	1	1	1	1	1	1	1	1	0.45	0.39	0.28
	1.7	1	1	1	1	1	1	1	1	1	1	1	1	0.88
	2.83	1	1	1	1	1	1	1	0.99	0.98	0.71	0.69	0.62	0.47
WWP3	0.42	1	1	1	1	1	1	1	0.51	0.14	0.01	0	0	0
	0.85	1	1	1	1	1	1	1	0.96	0.61	0	0	0	0
	1.7	1	1	1	1	1	1	1	0.68	0.65	0.04	0.01	0	0
	2.83	1	1	1	1	1	1	1	0.87	0.84	0.76	0.57	0.36	0.26

Table D3. MVR_{10} from 2D minus 3D model results

	Discharge (cms)	Fish Lengths (m)												
		0.1	0.125	0.15	0.175	0.2	0.225	0.25	0.275	0.3	0.325	0.35	0.375	0.4
WWP1	0.42	0.39	-0.74	-0.82	-0.88	-0.93	-0.92	-0.89	-0.75	-0.53	-0.16	-0.12	-0.12	-0.11
	0.85	-0.19	-0.32	-0.60	-0.69	-0.80	-0.90	-0.99	-0.75	-0.58	-0.39	-0.20	-0.12	-0.09
	1.7	-0.34	-0.37	-0.39	-0.47	-0.67	-0.79	-0.86	-0.92	-0.93	-0.25	-0.17	-0.13	-0.12
	2.83	-0.20	-0.47	-0.50	-0.53	-0.56	-0.62	-0.81	-0.90	-0.91	-0.91	-0.62	-0.21	-0.12
WWP2	0.42	-0.26	-0.58	-0.62	-0.68	-0.82	-0.86	-0.90	-0.92	-0.85	-0.25	-0.15	-0.11	-0.06
	0.85	-0.24	-0.26	-0.28	-0.44	-0.54	-0.66	-0.73	-0.81	-0.86	-0.89	-0.39	-0.39	-0.28
	1.7	0	-0.04	-0.31	-0.35	-0.43	-0.46	-0.55	-0.71	-0.75	-0.83	-0.85	-0.90	-0.83
	2.83	0	-0.01	-0.03	-0.04	-0.06	-0.19	-0.32	-0.41	-0.52	-0.38	-0.41	-0.41	-0.37
WWP3	0.42	-0.53	-0.65	-0.77	-0.79	-0.83	-0.88	-0.92	-0.51	-0.14	-0.01	0	0	0
	0.85	0	-0.05	-0.08	-0.28	-0.35	-0.43	-0.58	-0.67	-0.48	0	0	0	0
	1.7	0	0	0	-0.04	-0.05	-0.07	-0.16	0.02	-0.14	0.23	0.12	0.05	0.01
	2.83	0	0	0	0	0	-0.04	-0.18	-0.21	-0.27	-0.28	-0.19	-0.16	-0.18

Table D4. MVR25 from 2D Model

	Discharge (cms)	Fish Lengths (m)												
		0.1	0.125	0.1	0.175	0.2	0.225	0.25	0.275	0.3	0.325	0.5	0.375	0.4
WWP1	0.42	0	0	0	0	0	0	0	0	0	0	0	0	0
	0.85	0.01	0	0	0	0	0	0	0	0	0	0	0	0
	1.7	0.14	0.02	0	0	0	0	0	0	0	0	0	0	0
	2.83	0.19	0.03	0	0	0	0	0	0	0	0	0	0	0
WWP2	0.42	0.10	0.01	0	0	0	0	0	0	0	0	0	0	0
	0.85	0.27	0.12	0	0	0	0	0	0	0	0	0	0	0
	1.7	0.45	0.20	0.10	0	0	0	0	0	0	0	0	0	0
	2.83	0.68	0.38	0.21	0.03	0	0	0	0	0	0	0	0	0
WWP3	0.42	0.08	0	0	0	0	0	0	0	0	0	0	0	0
	0.85	0.42	0.04	0	0	0	0	0	0	0	0	0	0	0
	1.7	0.84	0.34	0.05	0	0	0	0	0	0	0	0	0	0
	2.83	0.82	0.51	0.20	0.01	0	0	0	0	0	0	0	0	0

Table D5. MVR_{25} from 3D Model

	Discharge (cms)	Fish Lengths (m)												
		0.1	0.125	0.15	0.175	0.2	0.225	0.25	0.275	0.3	0.325	0.35	0.375	0.4
WWP1	0.42	0.89	0.2	0.12	0.07	0.02	0.02	0	0	0	0	0	0	0
	0.85	1	0.44	0.12	0.08	0.01	0	0	0	0	0	0	0	0
	1.7	1	0.28	0.13	0.06	0.05	0	0	0	0	0	0	0	0
	2.83	1	0.95	0.21	0.07	0	0	0	0	0	0	0	0	0
WWP2	0.42	1	0.85	0.11	0	0	0	0	0	0	0	0	0	0
	0.85	1	1	0.39	0.25	0.23	0.23	0.23	0.23	0.23	0.03	0.03	0.03	0
	1.7	1	1	1	0.19	0.01	0	0	0	0	0	0	0	0
	2.83	1	0.97	0.62	0.28	0.17	0	0	0	0	0	0	0	0
WWP3	0.42	1	0.07	0	0	0	0	0	0	0	0	0	0	0
	0.85	1	0.07	0	0	0	0	0	0	0	0	0	0	0
	1.7	1	0.27	0	0	0	0	0	0	0	0	0	0	0
	2.83	1	0.83	0.36	0.01	0	0	0	0	0	0	0	0	0

Table D6. MVR_{25} from 2D minus 3D Model Results

	Discharge (cms)	Fish Lengths (m)												
		0.1	0.125	0.15	0.175	0.2	0.225	0.25	0.275	0.3	0.325	0.35	0.375	0.4
WWP1	0.42	-0.89	-0.20	-0.12	-0.07	-0.02	-0.02	0	0	0	0	0	0	0
	0.85	-0.99	-0.44	-0.12	-0.08	-0.01	0	0	0	0	0	0	0	0
	1.7	-0.86	-0.26	-0.13	-0.06	-0.05	0	0	0	0	0	0	0	0
	2.83	-0.81	-0.92	-0.21	-0.07	0	0	0	0	0	0	0	0	0
WWP2	0.42	-0.90	-0.84	-0.11	0	0	0	0	0	0	0	0	0	0
	0.85	-0.73	-0.88	-0.39	-0.25	-0.23	-0.23	-0.23	-0.23	-0.23	-0.03	-0.03	-0.03	0
	1.7	-0.55	-0.80	-0.90	-0.19	-0.01	0	0	0	0	0	0	0	0
	2.83	-0.32	-0.59	-0.41	-0.25	-0.17	0	0	0	0	0	0	0	0
WWP3	0.42	-0.92	-0.07	0	0	0	0	0	0	0	0	0	0	0
	0.85	-0.58	-0.03	0	0	0	0	0	0	0	0	0	0	0
	1.7	-0.16	0.07	0.05	0	0	0	0	0	0	0	0	0	0
	2.83	-0.18	-0.32	-0.16	0	0	0	0	0	0	0	0	0	0

Table D7. $D_{0.11}V_{10}$ from 2D model

	Discharge (cms)	Fish Lengths (m)												
		0.1	0.125	0.15	0.175	0.2	0.225	0.25	0.275	0.3	0.325	0.35	0.375	0.4
WWP1	0.42	1	1	1	0.99	0.97	0.92	0.92	0.92	0.92	0.92	0.92	0.92	0.92
WWP1	0.85	1	1	1	0.99	0.97	0.90	0.82	0.80	0.80	0.80	0.80	0.80	0.80
WWP1	1.7	1	1	1	0.98	0.85	0.76	0.68	0.61	0.57	0.56	0.55	0.55	0.55
WWP1	2.83	1	1	1	1	0.99	0.93	0.74	0.64	0.60	0.56	0.55	0.55	0.55
WWP2	0.42	1	1	1	1	0.98	0.95	0.92	0.90	0.86	0.83	0.83	0.83	0.83
WWP2	0.85	1	1	1	1	0.97	0.88	0.81	0.73	0.68	0.65	0.60	0.54	0.54
WWP2	1.7	1	1	1	1	0.95	0.93	0.85	0.68	0.65	0.56	0.54	0.49	0.44
WWP2	2.83	1	1	1	1	0.99	0.94	0.82	0.72	0.60	0.47	0.42	0.36	0.24
WWP3	0.42	1	1	1	1	1	1	0.99	0.90	0.90	0.90	0.90	0.90	0.90
WWP3	0.85	1	1	1	1	1	1	0.90	0.77	0.61	0.48	0.48	0.48	0.48
WWP3	1.7	1	1	1	1	1	1	0.99	0.90	0.72	0.48	0.34	0.25	0.21
WWP3	2.83	1	1	1	1	1	1	1	1	0.93	0.84	0.74	0.56	0.44

Table D8. $D_{0.11}V_{10}$ from 3D model

	Discharge (cms)	Fish Lengths (m)												
		0.1	0.125	0.15	0.175	0.2	0.225	0.25	0.275	0.3	0.325	0.35	0.375	0.4
WWP1	0.42	1	1	1	1	1	0.98	0.98	0.95	0.82	0.69	0.68	0.68	0.68
WWP1	0.85	1	1	1	1	1	1	1	0.98	0.94	0.79	0.65	0.62	0.61
WWP1	1.7	1	1	1	1	1	1	1	1	0.98	0.96	0.89	0.88	0.87
WWP1	2.83	1	1	1	1	1	1	1	1	0.97	0.94	0.75	0.45	0.37
WWP2	0.42	1	1	1	1	1	1	1	1	0.92	0.31	0.21	0.18	0.16
WWP2	0.85	1	1	1	1	1	1	1	1	1	1	0.92	0.86	0.81
WWP2	1.7	1	1	1	1	1	1	1	1	1	1	1	1	0.95
WWP2	2.83	1	1	1	1	1	1	1	0.99	0.99	0.94	0.92	0.88	0.73
WWP3	0.42	1	1	1	1	1	1	1	1	1	0.97	0.96	0.96	0.96
WWP3	0.85	1	1	1	1	1	1	1	1	0.83	0.26	0.26	0.26	0.26
WWP3	1.7	1	1	1	1	1	1	1	1	1	0.69	0.65	0.65	0.65
WWP3	2.83	1	1	1	1	1	1	1	1	0.99	0.96	0.93	0.73	0.63

Table D9. $D_{0.11}V_{10}$ from 2D minus 3D model results

	Discharge (cms)	Fish Lengths (m)												
		0.1	0.125	0.15	0.175	0.2	0.225	0.25	0.275	0.3	0.325	0.35	0.375	0.4
WWP1	0.42	0	0	0	-0.01	-0.03	-0.06	-0.06	-0.04	0.10	0.23	0.23	0.23	0.23
WWP1	0.85	0	0	0	-0.01	-0.03	-0.10	-0.18	-0.18	-0.14	0.01	0.15	0.19	0.19
WWP1	1.7	0	0	0	-0.02	-0.15	-0.24	-0.32	-0.39	-0.41	-0.40	-0.35	-0.33	-0.33
WWP1	2.83	0	0	0	0	-0.01	-0.07	-0.26	-0.36	-0.37	-0.38	-0.20	0.10	0.17
WWP2	0.42	0	0	0	0	-0.02	-0.05	-0.08	-0.10	-0.06	0.53	0.62	0.66	0.67
WWP2	0.85	0	0	0	0	-0.03	-0.12	-0.19	-0.27	-0.32	-0.35	-0.32	-0.32	-0.27
WWP2	1.7	0	0	0	0	-0.05	-0.07	-0.15	-0.32	-0.35	-0.44	-0.46	-0.51	-0.51
WWP2	2.83	0	0	0	0	-0.01	-0.06	-0.18	-0.28	-0.39	-0.47	-0.51	-0.53	-0.49
WWP3	0.42	0	0	0	0	0	0	-0.01	-0.10	-0.10	-0.07	-0.06	-0.06	-0.06
WWP3	0.85	0	0	0	0	0	0	-0.10	-0.23	-0.22	0.22	0.22	0.22	0.22
WWP3	1.7	0	0	0	0	0	0	-0.01	-0.10	-0.28	-0.21	-0.32	-0.40	-0.44
WWP3	2.83	0	0	0	0	0	0	0	0	-0.06	-0.12	-0.19	-0.17	-0.19

Table D10. $D_{0.11}V_{25}$ **from 2D model**

	Discharge (cms)	Fish Lengths (m)												
		0.1	**0.125**	**0.15**	**0.175**	**0.2**	**0.225**	**0.25**	**0.275**	**0.3**	**0.325**	**0.35**	**0.375**	**0.4**
WWP1	**0.42**	0.92	0.92	0.92	0.92	0.92	0.92	0.92	0.92	0.92	0.92	0.92	0.92	0.92
	0.85	0.82	0.80	0.80	0.80	0.80	0.80	0.80	0.80	0.80	0.80	0.80	0.80	0.80
	1.7	0.68	0.57	0.55	0.55	0.55	0.55	0.55	0.55	0.55	0.55	0.55	0.55	0.55
	2.83	0.74	0.57	0.55	0.55	0.55	0.55	0.55	0.55	0.55	0.55	0.55	0.55	0.55
WWP2	**0.42**	0.92	0.84	0.83	0.83	0.83	0.83	0.83	0.83	0.83	0.83	0.83	0.83	0.83
	0.85	0.81	0.66	0.54	0.54	0.54	0.54	0.54	0.54	0.54	0.54	0.54	0.54	0.54
	1.7	0.85	0.59	0.49	0.39	0.39	0.39	0.39	0.39	0.39	0.39	0.39	0.39	0.39
	2.83	0.82	0.52	0.36	0.17	0.14	0.14	0.14	0.14	0.14	0.14	0.14	0.14	0.14
WWP3	**0.42**	0.99	0.90	0.90	0.90	0.90	0.90	0.90	0.90	0.90	0.90	0.90	0.90	0.90
	0.85	0.90	0.52	0.48	0.48	0.48	0.48	0.48	0.48	0.48	0.48	0.48	0.48	0.48
	1.7	0.99	0.54	0.25	0.20	0.20	0.20	0.20	0.20	0.20	0.20	0.20	0.20	0.20
	2.83	1	0.87	0.56	0.37	0.36	0.36	0.36	0.36	0.36	0.36	0.36	0.36	0.36

Table D11. $D_{0.11}V_{25}$ **from 3D model**

	Discharge (cms)	Fish Lengths (m)												
		0.1	**0.125**	**0.15**	**0.175**	**0.2**	**0.225**	**0.25**	**0.275**	**0.3**	**0.325**	**0.35**	**0.375**	**0.4**
WWP1	**0.42**	0.98	0.72	0.68	0.68	0.68	0.68	0.68	0.68	0.68	0.68	0.68	0.68	0.68
	0.85	1	0.83	0.62	0.60	0.56	0.55	0.55	0.55	0.55	0.55	0.55	0.55	0.55
	1.7	1	0.98	0.88	0.87	0.86	0.86	0.86	0.86	0.86	0.86	0.86	0.86	0.86
	2.83	1	0.96	0.45	0.34	0.29	0.29	0.29	0.29	0.29	0.29	0.29	0.29	0.29
WWP2	**0.42**	1	0.91	0.18	0.16	0.16	0.16	0.16	0.16	0.16	0.16	0.16	0.16	0.16
	0.85	1	1	0.86	0.78	0.76	0.76	0.76	0.76	0.76	0.76	0.76	0.76	0.76
	1.7	1	1	1	0.84	0.77	0.77	0.77	0.77	0.77	0.77	0.77	0.77	0.77
	2.83	1	0.98	0.88	0.54	0.43	0.26	0.26	0.26	0.26	0.26	0.26	0.26	0.26
WWP3	**0.42**	1	0.99	0.96	0.96	0.96	0.96	0.96	0.96	0.96	0.96	0.96	0.96	0.96
	0.85	1	0.31	0.26	0.26	0.26	0.26	0.26	0.26	0.26	0.26	0.26	0.26	0.26
	1.7	1	0.89	0.65	0.65	0.65	0.65	0.65	0.65	0.65	0.65	0.65	0.65	0.65
	2.83	1	0.97	0.73	0.40	0.39	0.39	0.39	0.39	0.39	0.39	0.39	0.39	0.39

Table D12. $D_{0.11}V_{25}$ **from 2D minus 3D model results**

	Discharge (cms)	Fish Lengths (m)												
		0.1	**0.125**	**0.15**	**0.175**	**0.2**	**0.225**	**0.25**	**0.275**	**0.3**	**0.325**	**0.35**	**0.375**	**0.4**
WWP1	**0.42**	-0.06	0.20	0.23	0.23	0.23	0.23	0.23	0.23	0.23	0.23	0.23	0.23	0.23
	0.85	-0.18	-0.03	0.19	0.20	0.24	0.25	0.25	0.25	0.25	0.25	0.25	0.25	0.25
	1.7	-0.32	-0.41	-0.33	-0.32	-0.32	-0.32	-0.32	-0.32	-0.32	-0.32	-0.32	-0.32	-0.32
	2.83	-0.26	-0.39	0.10	0.20	0.26	0.26	0.26	0.26	0.26	0.26	0.26	0.26	0.26
WWP2	**0.42**	-0.08	-0.06	0.66	0.67	0.67	0.67	0.67	0.67	0.67	0.67	0.67	0.67	0.67
	0.85	-0.19	-0.34	-0.32	-0.24	-0.22	-0.22	-0.22	-0.22	-0.22	-0.22	-0.22	-0.22	-0.22
	1.7	-0.15	-0.41	-0.51	-0.45	-0.38	-0.37	-0.37	-0.37	-0.37	-0.37	-0.37	-0.37	-0.37
	2.83	-0.18	-0.47	-0.53	-0.37	-0.29	-0.12	-0.12	-0.12	-0.12	-0.12	-0.12	-0.12	-0.12
WWP3	**0.42**	-0.01	-0.09	-0.06	-0.06	-0.06	-0.06	-0.06	-0.06	-0.06	-0.06	-0.06	-0.06	-0.06
	0.85	-0.10	0.21	0.22	0.22	0.22	0.22	0.22	0.22	0.22	0.22	0.22	0.22	0.22
	1.7	-0.01	-0.35	-0.40	-0.45	-0.45	-0.45	-0.45	-0.45	-0.45	-0.45	-0.45	-0.45	-0.45
	2.83	0	-0.10	-0.17	-0.04	-0.03	-0.03	-0.03	-0.03	-0.03	-0.03	-0.03	-0.03	-0.03

Table D13. $D_{0.18}V_{10}$ from 2D model

	Discharge (cms)	Fish Lengths (m)												
		0.1	0.125	0.15	0.175	0.2	0.225	0.25	0.275	0.3	0.325	0.35	0.375	0.4
WWP1	0.42	1	1	1	1	1	1	1	1	1	1	1	1	1
WWP1	0.85	1	1	1	1	1	1	0.98	0.97	0.97	0.97	0.97	0.97	0.97
WWP1	1.7	1	1	1	1	1	1	0.99	0.95	0.93	0.92	0.92	0.92	0.92
WWP1	2.83	1	1	1	1	1	1	0.93	0.88	0.84	0.80	0.79	0.79	0.79
WWP2	0.42	1	1	1	1	1	1	0.98	0.96	0.96	0.96	0.96	0.96	0.96
WWP2	0.85	1	1	1	1	1	0.91	0.85	0.77	0.72	0.69	0.64	0.58	0.58
WWP2	1.7	1	1	1	1	1	1	1	0.97	0.94	0.86	0.83	0.79	0.74
WWP2	2.83	1	1	1	1	1	1	1	0.93	0.83	0.71	0.65	0.59	0.48
WWP3	0.42	0.4	1	1	1	1	1	1	1	1	1	1	1	1
WWP3	0.85	1	1	1	1	1	1	1	1	0.89	0.77	0.76	0.76	0.76
WWP3	1.7	1	1	1	1	1	1	1	1	0.90	0.67	0.53	0.44	0.41
WWP3	2.83	1	1	1	1	1	1	1	1	1	0.92	0.82	0.64	0.52

Table D14. $D_{0.18}V_{10}$ from 3D model

	Discharge (cms)	Fish Lengths (m)												
		0.1	0.125	0.15	0.175	0.2	0.225	0.25	0.275	0.3	0.325	0.35	0.375	0.4
WWP1	0.42	1	1	1	1	1	1	1	1	0.96	0.95	0.95	0.95	0.95
WWP1	0.85	1	1	1	1	1	1	1	1	1	0.97	0.88	0.88	0.87
WWP1	1.7	1	1	1	1	1	1	1	1	1	0.99	0.95	0.95	0.95
WWP1	2.83	1	1	1	1	1	1	1	1	0.99	0.98	0.87	0.78	0.74
WWP2	0.42	1	1	1	1	1	1	1	1	1	1	1	1	1
WWP2	0.85	1	1	1	1	1	1	1	1	1	1	0.96	0.91	0.89
WWP2	1.7	1	1	1	1	1	1	1	1	1	1	1	1	0.96
WWP2	2.83	1	1	1	1	1	1	1	1	1	1	1	1	0.89
WWP3	0.42	1	1	1	1	1	1	1	1	1	1	1	1	1
WWP3	0.85	1	1	1	1	1	1	1	1	0.96	0.88	0.87	0.87	0.87
WWP3	1.7	1	1	1	1	1	1	1	1	1	0.75	0.72	0.72	0.72
WWP3	2.83	1	1	1	1	1	1	1	1	1	0.99	0.97	0.78	0.68

Table D15. $D_{0.18}V_{10}$ from 2D minus 3D model results

	Discharge (cms)	Fish Lengths (m)												
		0.1	0.125	0.15	0.175	0.2	0.225	0.25	0.275	0.3	0.325	0.35	0.375	0.4
WWP1	0.42	0	0	0	0	0	0	0	0	0.04	0.05	0.05	0.05	0.05
WWP1	0.85	0	0	0	0	0	0	-0.02	-0.03	-0.03	0	0.09	0.09	0.10
WWP1	1.7	0	0	0	0	0	0	-0.01	-0.05	-0.07	-0.07	-0.03	-0.03	-0.03
WWP1	2.83	0	0	0	0	0	0	-0.07	-0.12	-0.15	-0.18	-0.08	0.01	0.05
WWP2	0.42	0	0	0	0	0	0	-0.02	-0.04	-0.04	-0.04	-0.04	-0.04	-0.04
WWP2	0.85	0	0	0	0	0	-0.09	-0.15	-0.23	-0.28	-0.31	-0.32	-0.33	-0.31
WWP2	1.7	0	0	0	0	0	0	0	-0.03	-0.06	-0.14	-0.17	-0.21	-0.22
WWP2	2.83	0	0	0	0	0	0	0	-0.07	-0.17	-0.29	-0.35	-0.41	-0.41
WWP3	0.42	0	0	0	0	0	0	0	0	0	0	0	0	0
WWP3	0.85	0	0	0	0	0	0	0	0	-0.07	-0.11	-0.11	-0.11	-0.11
WWP3	1.7	0	0	0	0	0	0	0	0	-0.10	-0.08	-0.19	-0.28	-0.31
WWP3	2.83	0	0	0	0	0	0	0	0	0	-0.07	-0.15	-0.14	-0.16

Table D16. $D_{0.18}V_{25}$ from 2D model

	Discharge (cms)	Fish Lengths (m)											
		0.1	0.125	0.15	0.175	0.2	0.225	0.25	0.275	0.3	0.325	0.35	0.375	0.4
WWP1	0.42	1	1	1	1	1	1	1	1	1	1	1	1	1
WWP1	0.85	0.98	0.97	0.97	0.97	0.97	0.97	0.97	0.97	0.97	0.97	0.97	0.97	0.97
WWP1	1.7	0.99	0.93	0.92	0.92	0.92	0.92	0.92	0.92	0.92	0.92	0.92	0.92	0.92
WWP1	2.83	0.93	0.82	0.79	0.79	0.79	0.79	0.79	0.79	0.79	0.79	0.79	0.79	0.79
WWP2	0.42	0.98	0.96	0.96	0.96	0.96	0.96	0.96	0.96	0.96	0.96	0.96	0.96	0.96
WWP2	0.85	0.85	0.70	0.58	0.58	0.58	0.58	0.58	0.58	0.58	0.58	0.58	0.58	0.58
WWP2	1.7	1	0.89	0.79	0.69	0.69	0.69	0.69	0.69	0.69	0.69	0.69	0.69	0.69
WWP2	2.83	1	0.75	0.59	0.40	0.38	0.38	0.38	0.38	0.38	0.38	0.38	0.38	0.38
WWP3	0.42	1	1	1	1	1	1	1	1	1	1	1	1	1
WWP3	0.85	1	0.80	0.76	0.76	0.76	0.76	0.76	0.76	0.76	0.76	0.76	0.76	0.76
WWP3	1.7	1	0.74	0.44	0.40	0.40	0.40	0.40	0.40	0.40	0.40	0.40	0.40	0.40
WWP3	2.83	1	0.95	0.64	0.44	0.44	0.44	0.44	0.44	0.44	0.44	0.44	0.44	0.44

Table D17. $D_{0.18}V_{25}$ from 3D model

	Discharge (cms)	Fish Lengths (m)											
		0.1	0.125	0.15	0.175	0.2	0.225	0.25	0.275	0.3	0.325	0.35	0.375	0.4
WWP1	0.42	1	0.95	0.95	0.95	0.95	0.95	0.95	0.95	0.95	0.95	0.95	0.95	0.95
WWP1	0.85	1	0.98	0.88	0.87	0.83	0.83	0.83	0.83	0.83	0.83	0.83	0.83	0.83
WWP1	1.7	1	1	0.95	0.95	0.95	0.95	0.95	0.95	0.94	0.94	0.94	0.94	0.94
WWP1	2.83	1	0.99	0.78	0.73	0.73	0.73	0.73	0.73	0.73	0.73	0.73	0.73	0.73
WWP2	0.42	1	1	1	1	1	1	1	1	1	1	1	1	1
WWP2	0.85	1	1	0.91	0.86	0.85	0.85	0.85	0.85	0.85	0.85	0.85	0.85	0.85
WWP2	1.7	1	1	1	0.89	0.85	0.84	0.84	0.84	0.84	0.84	0.84	0.84	0.84
WWP2	2.83	1	1	1	0.72	0.64	0.47	0.47	0.47	0.47	0.47	0.47	0.47	0.47
WWP3	0.42	1	1	1	1	1	1	1	1	1	1	1	1	1
WWP3	0.85	1	0.88	0.87	0.87	0.87	0.87	0.87	0.87	0.87	0.87	0.87	0.87	0.87
WWP3	1.7	1	0.92	0.72	0.72	0.72	0.72	0.72	0.72	0.72	0.72	0.72	0.72	0.72
WWP3	2.83	1	1	0.78	0.45	0.44	0.44	0.44	0.44	0.44	0.44	0.44	0.44	0.44

Table D18. $D_{0.18}V_{25}$ from 2D minus 3D model results

	Discharge (cms)	Fish Lengths (m)											
		0.1	0.125	0.15	0.175	0.2	0.225	0.25	0.275	0.3	0.325	0.35	0.375	0.4
WWP1	0.42	0	0.05	0.05	0.05	0.05	0.05	0.05	0.05	0.05	0.05	0.05	0.05	0.05
WWP1	0.85	-0.02	-0.01	0.09	0.10	0.14	0.14	0.14	0.14	0.14	0.14	0.14	0.14	0.14
WWP1	1.7	-0.01	-0.07	-0.03	-0.03	-0.03	-0.03	-0.03	-0.03	-0.02	-0.02	-0.02	-0.02	-0.02
WWP1	2.83	-0.07	-0.17	0.01	0.06	0.06	0.06	0.06	0.06	0.06	0.06	0.06	0.06	0.06
WWP2	0.42	-0.02	-0.04	-0.04	-0.04	-0.04	-0.04	-0.04	-0.04	-0.04	-0.04	-0.04	-0.04	-0.04
WWP2	0.85	-0.15	-0.30	-0.33	-0.28	-0.27	-0.27	-0.27	-0.27	-0.27	-0.27	-0.27	-0.27	-0.27
WWP2	1.7	0	-0.11	-0.21	-0.20	-0.16	-0.15	-0.15	-0.15	-0.15	-0.15	-0.15	-0.15	-0.15
WWP2	2.83	0	-0.25	-0.41	-0.32	-0.26	-0.09	-0.09	-0.09	-0.09	-0.09	-0.09	-0.09	-0.09
WWP3	0.42	0	0	0	0	0	0	0	0	0	0	0	0	0
WWP3	0.85	0	-0.08	-0.11	-0.11	-0.11	-0.11	-0.11	-0.11	-0.11	-0.11	-0.11	-0.11	-0.11
WWP3	1.7	0	-0.18	-0.28	-0.32	-0.32	-0.32	-0.32	-0.32	-0.32	-0.32	-0.32	-0.32	-0.32
WWP3	2.83	0	-0.05	-0.14	-0.01	0	0	0	0	0	0	0	0	0
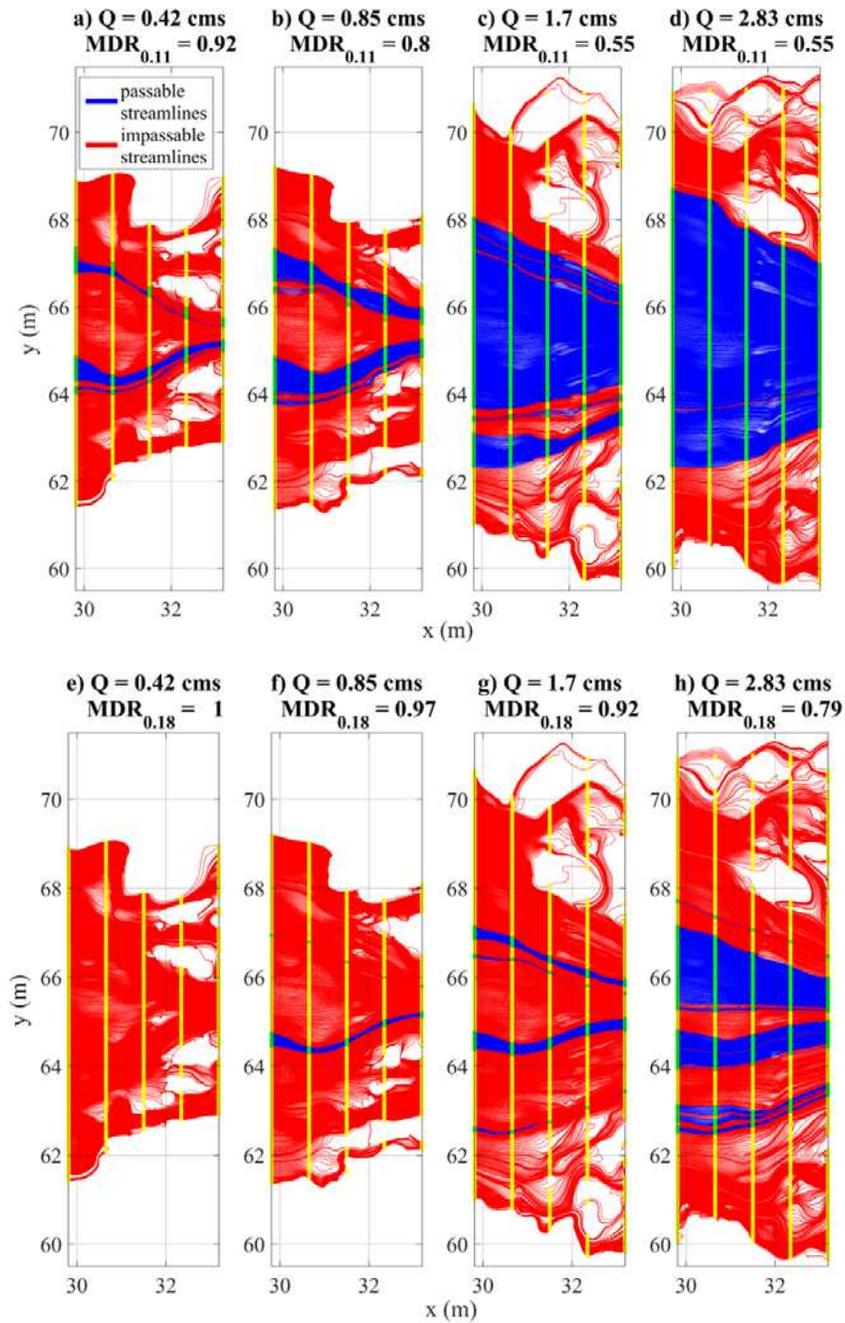
Figure E1. Depth limited streamlines for *MDR₁₁* (a – d) and *MDR₁₈* (e – f) with passable streamlines shown in blue and impassable streamlines shown in red. Equally spaced cross section between the upstream and downstream extents of area of interest shown as points of intersection with streamlines.
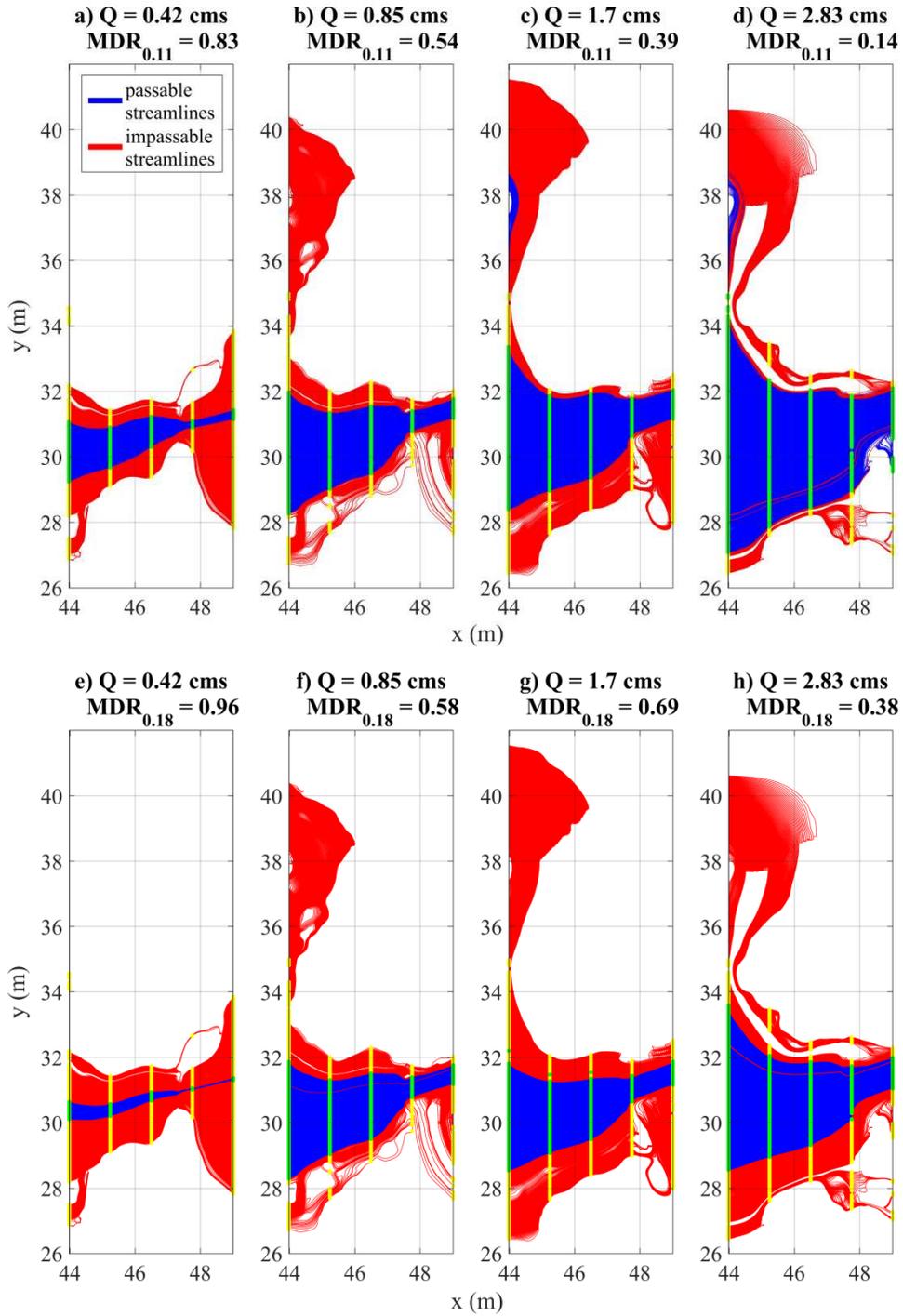
Figure E2. Depth limited streamlines for MDR_{11} (a – d) and MDR_{18} (e – f) with passable streamlines shown in blue and impassable streamlines shown in red. Equally spaced cross section between the upstream and downstream extents of area of interest shown as points of intersection with streamlines.
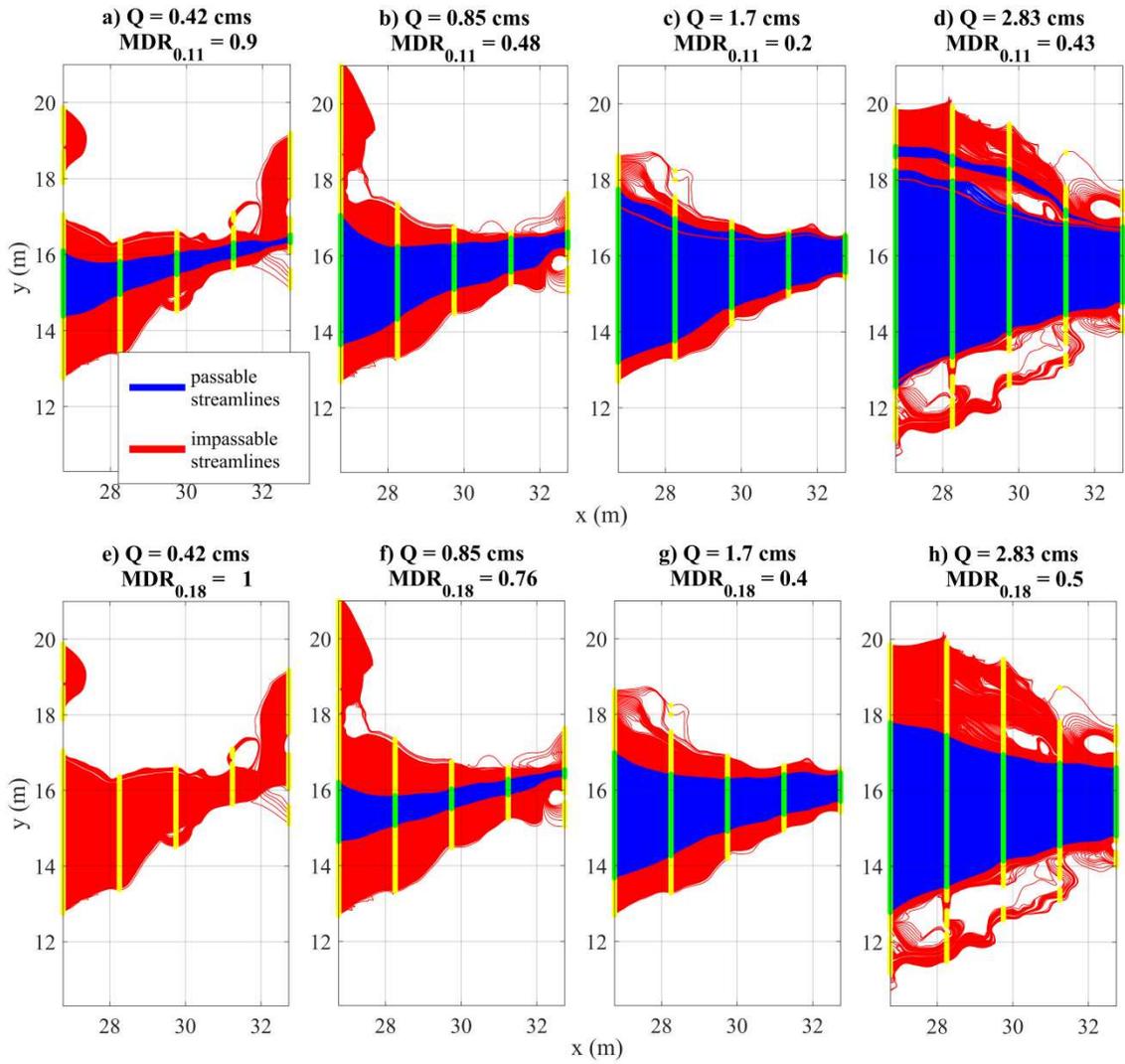
Figure E3. Depth limited streamlines for *MDR₁₁* (a – d) and *MDR₁₈* (e – f) with passable streamlines shown in blue and impassable streamlines shown in red. Equally spaced cross section between the upstream and downstream extents of area of interest shown as points of intersection with streamlines.
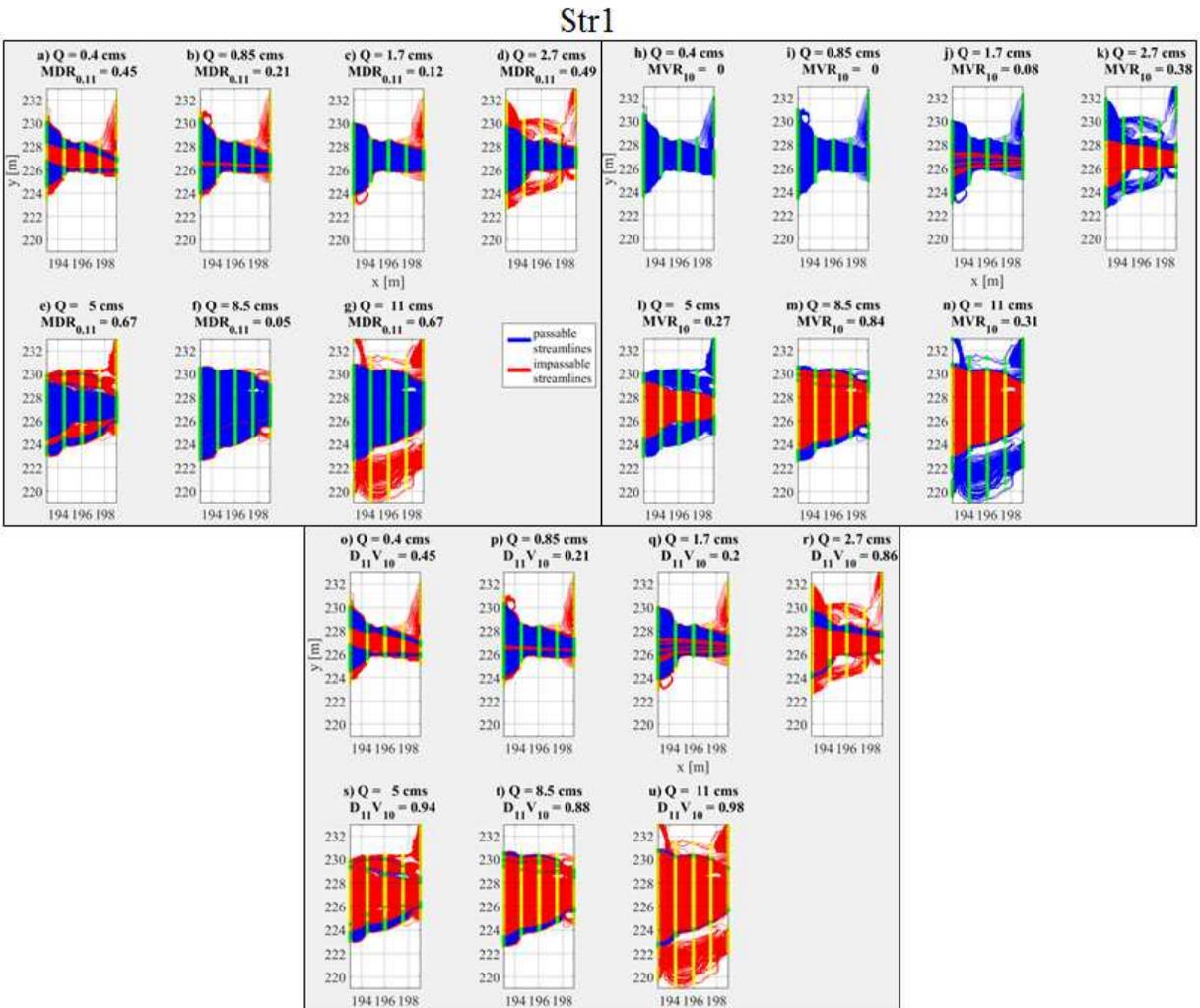
Figure F1. Passable streamlines (red) and impassable streamlines (blue) are plotted for $MDR_{0.11}$, MVR_{10}, and $D_{11}V_{10}$ at Str1. Flow is from left to right. Cross section intersections used in calculating passable width are plotted as passable (green) and impassable (yellow).
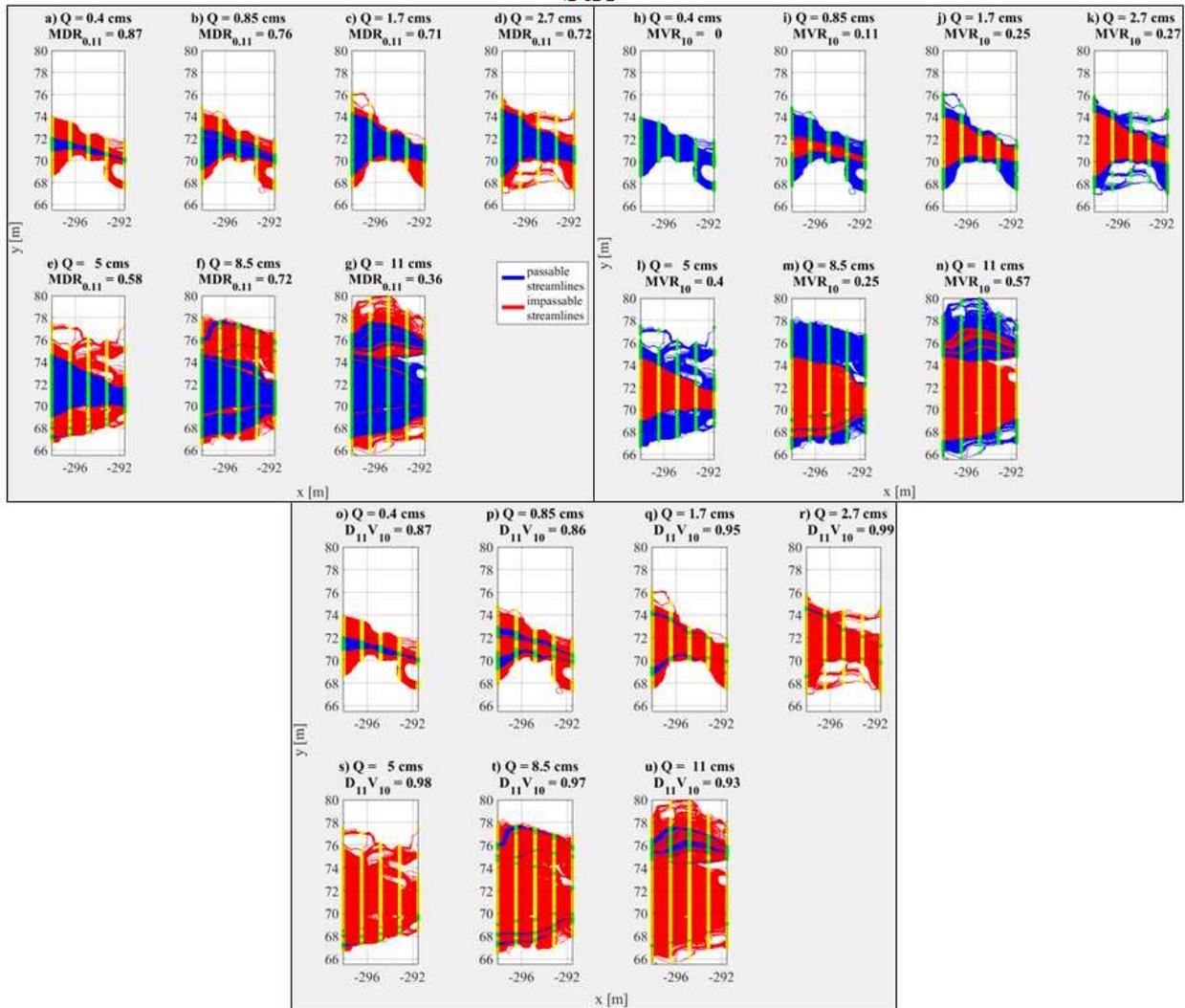
Figure F2. Passable streamlines (red) and impassable streamlines (blue) are plotted for $MDR_{0.11}$, MVR_{10}, and $D_{11}V_{10}$ at Str5. Flow is from left to right. Cross section intersections used in calculating passable width are plotted as passable (green) and impassable (yellow).

Str6
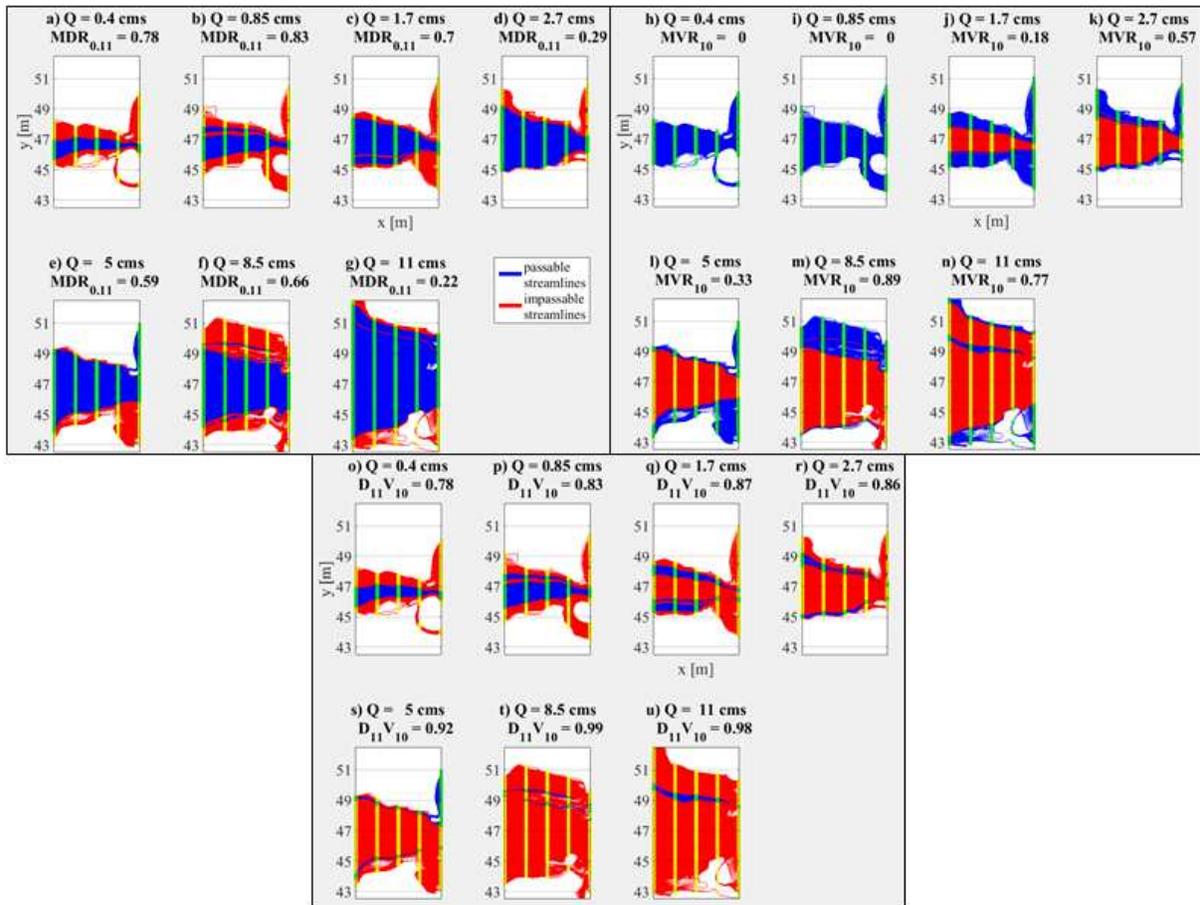
Figure F3. Passable streamlines (red) and impassable streamlines (blue) are plotted for *MDR$_{0.11}$*, *MVR$_{10}$*, and *D$_{11}$V$_{10}$* at Str6. Flow is from left to right. Cross section intersections used in calculating passable width are plotted as passable (green) and impassable (yellow).
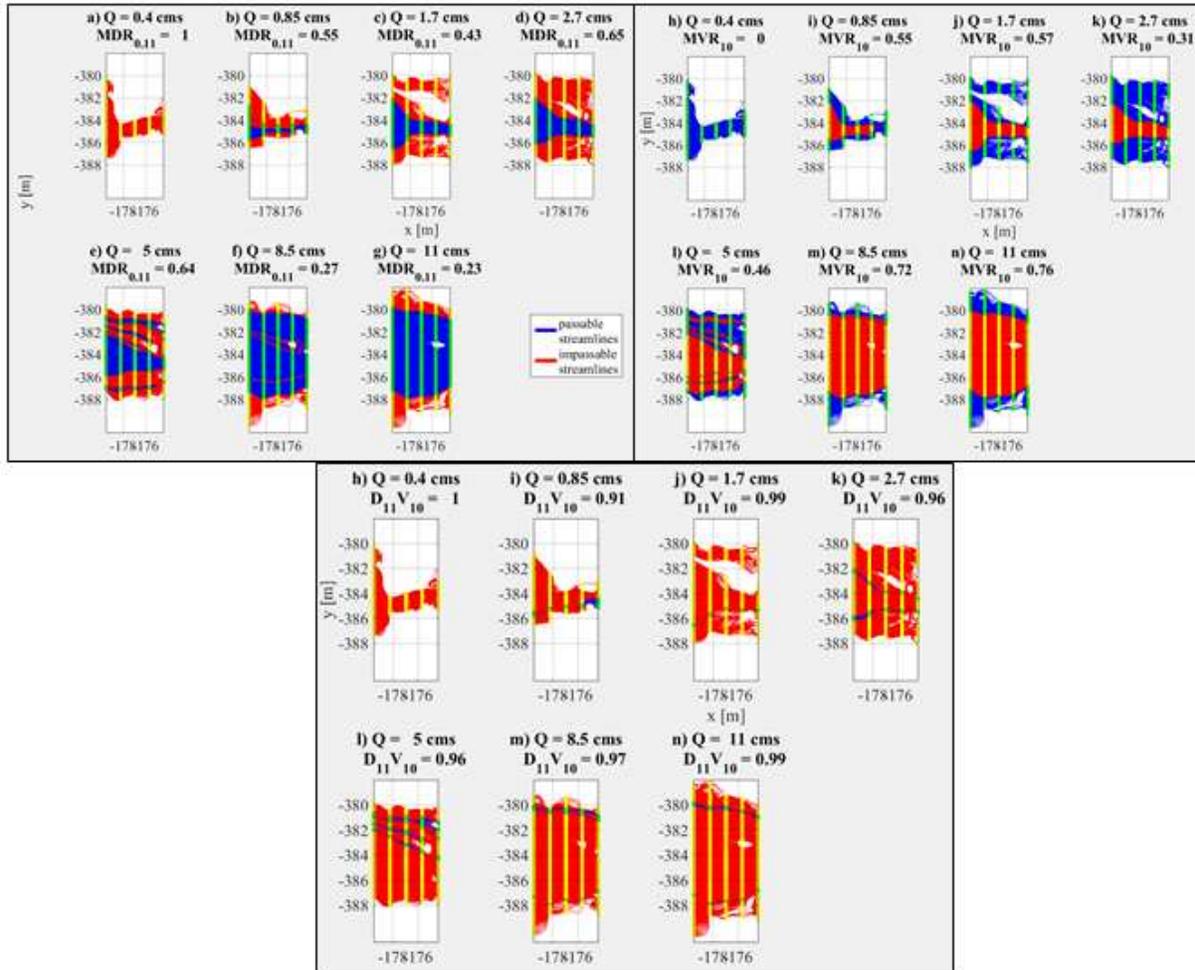
Figure F4. Passable streamlines (red) and impassable streamlines (blue) are plotted for $MDR_{0.11}$, MVR_{10}, and $D_{11}V_{10}$ at Str7. Flow is from left to right. Cross section intersections used in calculating passable width are plotted as passable (green) and impassable (yellow).